Optimal Surface Coating Distribution on a Femoral Endoprosthesis

by

Craig A. Simmons

B.Sc.(Eng.), University of Guelph
(1991)

Submitted to the Department of Mechanical Engineering
in Partial Fulfillment of the Requirements
for the Degree of

Master of Science in Mechanical Engineering

at the
Massachusetts Institute of Technology
February, 1994

Signature of Author . . . . . .
Department of Mechanical Engineering
February 1, 1994

Certified by . . . . . .
Edward J. Cheal, Thesis Advisor
Lecturer, Harvard-MIT Division of Health Sciences and Technology

Certified by . . . . . .
Myron Spector
Lecturer, Department of Mechanical Engineering

Accepted by. . . . . .
Ain A. Sonin
Chairman, Departmental Committee on Graduate Studies

Optimal Surface Coating Distribution on a Femoral Endoprosthesis

by

Craig A. Simmons

Submitted to the Department of Mechanical Engineering
on February 1, 1994
in partial fulfillment of the requirements for the
Degree of Master of Science in Mechanical Engineering

ABSTRACT

The short-term clinical failures of cementless stems, such as proximal bone resorption and thigh pain, have limited their acceptance despite the potential long-term benefits of biological fixation for younger and more active patients. The clinical problems are believed to be related to failure at the bone-stem interface. By optimizing the design of the prosthesis to prevent or minimize failure at the interface, it should be possible to reduce the clinical problems. In analytical and experimental studies, it has been shown that surface coating distribution is an important design parameter which can affect interface mechanics. The main objective of this study was to experimentally optimize the surface coating distribution, where the optimal distribution was a reasonable compromise between two of the mechanisms which are responsible for interface failure, namely proximal stress shielding and distal relative motion.

An unique experimental model was developed to study the effect of varying the surface coating distribution on stress shielding and relative motion. The experimental model consisted of a synthetic femur, a titanium alloy prosthesis and cyanoacrylate gel to simulate bone-stem bonding. Validation tests were conducted to determine the moduli of the synthetic femur components, the friction between the stem and the bone, the bonding strength of the glue and the controllability of the bonding distribution. The results of these tests confirmed that the experimental model was adequate for the purposes of this study. However, the moduli of the synthetic femur components are low compared to human bone and, therefore, the model should only be used for intercomparison studies. With this prosthesis, bonding of the distal 20%-30% of the prosthesis was not possible, because of inadequate stem-bone contact in that region.

Three synthetic femurs were tested with six bonding distributions per bone. Each bone was subjected to simulated loads of single leg stance and stair climb. Surface strains and stem-bone relative motion were measured to indicate stress shielding and relative motion, respectively. The experimental results were compared with the results of a finite element analysis.

The surface strains at the proximal and mid-stem levels of the femur varied with the bonding distribution. The maximal axial surface strains tended to decrease as the extent of the bonding was increased to 65% of the stem length. In other words, the stress shielding increased as the bond was extended distally. With bonding beyond 65%, the strains remained the same or decreased slightly.

Relative motion of the targets at the proximal level (where the stem and bone were bonded) were typically less than 20 μm. At the distal tip of the stem, the motion decreased with more distal bonding to a minimum with 81% bonding. With full coating, some relatively large motions were observed which is consistent with the absence of distal bonding. Calculated interface motions were 1.5 to 3.4 less than target motions.

There was generally good agreement between the trends observed experimentally and those predicted by the finite element analysis. As well, there was good agreement in the magnitudes of the surface strains. The most obvious discrepancies between the FEA and the experiment were the differences in strain and motion with full coating. Thus the FEA further supports the experimental observation that full bonding could not occur.

Although general trends were observed and reported, the small sample size limited the statistical power of the results. More samples are required before statistically significant conclusions can be made. Nonetheless, the trends in the data suggest that the optimal distribution (which minimizes the combination of stress shielding and relative motion) is to coat the proximal 65% to 81% of the stem length. More generally, this study experimentally demonstrated the complicated interaction between relative motion and surface strains with variation in bonding distribution. The conflicting effects of varying the surface coating distribution on these two parameters confirm that an optimization approach is necessary to determine the most suitable coating distribution, where the optimal solution corresponds to a compromise between the parameters.

Thesis Supervisor: Dr. Edward J. Cheal
Lecturer, Harvard-MIT Division of Health Sciences and Technology
Manager of Applied Research, Johnson & Johnson Orthopaedics

ACKNOWLEDGMENTS

Above all, I'd like to express my sincere thanks to my thesis advisor, Dr. Ed Cheal. Your guidance and insights made this experience intensely educational. Your patience, interest and generosity made it very enjoyable. Thank you.

Special thanks also to Dr. Tracy Orr, my "pinch hit" advisor. I'm grateful for your willingness to get so involved in my thesis so late in the game and for your invaluable input and guidance. Thank you to Dr. Myron Spector for reading my thesis and providing advise along the way.

I am grateful for the financial support I received for my studies from the Medical Research Council of Canada.

Thanks to Phil, Sarah, Bob and Balaji. I would have been lost in the lab without the machining lessons, computer tutorials and helpful suggestions that you provided. Thank you for your generosity and friendship. You made the lab cool.

And finally, thank you to Mom, Dad and Susan. By your example, you have each set a high standard to which I can aspire. And your encouragement, support and love makes it a whole lot easier to do so.

TABLE OF CONTENTS

LIST OF TABLES

LIST OF FIGURES

INTRODUCTION

Total hip arthroplasty (THA) is the most successful surgery for patients with advanced disease or dysfunction of the hip, with over 120,000 operations performed each year in the United States (Harris and Sledge 1990). The short-term success of cemented THA is well documented, particularly in older patients for whom the longevity and demand on the prosthesis are reduced (Rothman and Cohn 1990). However, the long-term results are less satisfactory due primarily to component loosening (Stauffer 1982; Sutherland *et al.* 1982; Harris and Sledge 1990; Rothman and Cohn 1990). Poor results have also been observed in younger, more active patients (Chandler *et al.* 1981; Dorr *et al.* 1983; Collis 1984; Ranawat *et al.* 1984) and after revision surgery (Kavanagh *et al.* 1985).

Improvements in cementing technique have significantly reduced the incidence of loosening of femoral components (Harris and Sledge 1990). However, for young, active patients or for some revisions, the failure of cemented stems and the potential long-term benefits of bony fixation make the use of cementless stems compelling.

Cementless femoral prostheses rely on bony ingrowth in a porous coating or bone bonding to a hydroxyapatite (HA) or tricalcium phosphate coating for fixation. Although animal studies have been promising, the short-term clinical experience with cementless stems has not been satisfactory when compared to the short-term results with cemented stems. There is a higher incidence of component loosening, thigh pain and limp; up to a quarter of patients may experience slight thigh pain even after 4 years (Engh *et al.* 1987; Callaghan *et al.* 1988; St. Ville *et al.* 1991). There is greater proximal bone atrophy with cementless stems (Engh and Bobyn 1988). The rate of revision is higher too - up to 4% after 5 years (Callaghan *et al.* 1988) as compared to no revisions with cemented stems over the same period.

1.1 FAILURE MECHANISMS

Many of the clinical problems encountered with cementless stems are believed to result from failure at the bone-prosthesis interface. Three mechanisms in particular are thought to play a significant role in interface failure: stress shielding, interface shear stresses and interfacial relative motion (micromotion).

1.1.1 Stress shielding

Stress shielding describes the redistribution of bone stresses that occurs post-arthroplasty, due to the mismatch in stiffness between the bone and the prosthesis. With a stiff stem, the load is transferred to the bone distally, essentially by-passing the proximal femur. Thus the proximal femur experiences strains that are lower than normal and atrophies. Excessive proximal bone atrophy is a local interface failure and is detrimental because it may lead to proximal loosening, stem migration and a poor environment for revision. Studies using finite element analysis (Huiskes *et al.* 1989; Huiskes 1990) and animal experiments (Turner *et al.* 1986) have shown that porous coating of only the proximal stem (thereby forcing load transfer to occur proximally) can reduce stress shielding. Using materials of lower modulus can also reduce proximal stress shielding (Huiskes *et al.* 1989; Huiskes 1990; Cheal *et al.* 1992).

1.1.2 Interface shear stresses

Shear stresses that occur at the interface of the stem and bone are the result of the stiffness mismatch between the stem and bone. Finite-element analyses have suggested that stem loosening and migration can be prevented by reducing interface shear stresses (Huiskes *et al.* 1989; Huiskes 1990; Cheal *et al.* 1992). In addition, excessive shear stresses can lead to failure at the interface.

1.1.3 Interfacial relative motion (micromotion)

Micromotion describes the movement of the stem surface relative to the adjacent bone. Typically, micromotion is elastic motion; the displacement is recoverable. Permanent displacement is referred to as migration. Excessive micromotion, due to high shear stresses or poor fixation, has been shown to correlate with a higher incidence of pain and limping (Engh *et al.* 1987; Maric and Karpman 1992). Motion of the distal tip is believed to cause local pressure and stretch which activates type-C nerve fibers (St. Ville *et al.* 1991). These fibers adhere to the basement membrane of the microvasculature and are responsible for vasomotor innervation. Their afferent conduction pathway senses deep pressure and is probably responsible for the dull and diffuse sensation of mid-thigh pain.

Minimal micromotion immediately after implantation is important for cementless stems which rely on stability for bone attachment to occur; fibrous ingrowth may be the result of excessive initial micromotion (Cameron *et al.* 1973; Pilliar *et al.* 1986; Soballe *et al.* 1992).

1.2 MECHANICAL DESIGN PARAMETERS

A successful prosthesis design will therefore attempt to minimize the stress shielding, interface shear stress and micromotion. A variety of mechanical design parameters may influence the biomechanical phenomena associated with interface failure. Among the most important are the stem geometry, the modulus of the stem material, and the parameter of interest for this study, the surface coating geometry.

1.2.1 Stem geometry

The wide variety of prosthesis designs and geometries prevents a comprehensive comparison herein. However, some general observations concerning stem geometry have been made. Walker *et al.* (1987) concluded that a stem with an "exact" fit in the canal

would provide greater stability (less micromotion) than a cementless stem without an "exact fit". A strong positive correlation between gap distance and micromotion has been demonstrated (Hayes *et al.* 1992b). Furthermore, experimental and clinical evidence suggests that maximum contact with the endosteal cortical bone surface, especially proximally, produces more normal strain values in addition to reducing the micromotion and migration of the stem (Robertson *et al.* 1988a).

1.2.2 Modulus of the stem material

The effects of the modulus of the stem material have been well documented clinically, experimentally and in finite element analyses. The high degree of proximal bone resorption experienced clinically with cementless prostheses has been attributed to their large size and high stiffness (when compared to cemented prostheses) (Engh *et al.* 1987; Engh and Bobyn 1988; Harris and Sledge 1990). The results of canine experiments by Turner *et al.* (1986) and Maistrelli *et al.* (1991) imply a greater bone loss with a stiffer stem. Finally, finite element analyses have shown that a lower modulus stem will reduce stress shielding, but also increase the interface shear stresses proximally (Huiskes *et al.* 1989; Huiskes 1990; Cheal *et al.* 1992).

1.2.3 Surface coating geometry

The geometric distribution of a porous or ceramic coating and the bonding at the interface may be a more influential factor in load transfer than is loading configuration, stem geometry or stem material (Huiskes 1990). Nonetheless, there is no clear consensus on the optimal geometric distribution of the coating, in part because the extent of surface coating is a compromise between the degree of proximal stress shielding and the amount of shear stress and shear motion at the interface. For example, a prosthesis with bonding along the entire length of the stem will have the least shear motion but will cause the most stress shielding of the proximal femur; a prosthesis bonded only proximally will cause the

least stress shielding but will have high shear motions, particularly at the distal tip. This suggests that there may be an optimal coating distribution that will minimize the combined effects of stress shielding and shear motion.

Clinically, the appropriate extent of coating is widely debated. Concerns about the loss of proximal cortical bone demonstrated in early clinical studies with fully coated prostheses (Lord and Bancel 1983) have led to the use of proximally coated stems (Bobyn *et al.* 1987; Callaghan *et al.* 1988; Engh and Bobyn 1988). With these prostheses the entire length of the prosthesis provides initial stability, and long-term stability is from bonding of the coated region alone (Jasty *et al.* 1993). Others believe that the uncoated regions cause increased distal relative motion, because smooth surfaced portions become encapsulated in fibrous tissue which provides little stability. Therefore, they advocate more fully coated prostheses which permit bonding to trabecular bone in the metaphysis and cortical bone in the diaphysis (Lord and Bancel 1983; Engh and Bobyn 1988).

The effects of varying the extent of the surface coating have been examined experimentally and by finite element analysis (FEA). The stress shielding effects of coating distribution are most commonly examined. More recently, the effects on relative motion have been studied.

Huiskes *et al.* (1989) used a two-dimensional sideplate finite element model (FEM) to examine the effects of stem material and bonding distribution on the load transfer mechanisms of uncemented femoral prostheses. They analyzed, among others, an Osteonics stem implanted with three bonding conditions - press-fit, proximal partial coating and fully coated. The implant/bone interface was considered fully bonded or not at all; friction was not accounted for. The loading condition simulated the joint force of single leg stance. A scheme for strain-adaptive bone remodeling was employed to examine the remodeling effects of stress-shielding. The fully coated stem showed severe proximal bone atrophy when remodeled. The load transfer was shown to occur distally with the proximal bone essentially being bypassed. High interface stresses were found at the distal tip of the

stem. The press-fit stem produced higher-than-normal cortical stresses in the lower proximal region. However, there was still stress shielding in the calcar region. Partial coating of the stem produced lower-than-normal stresses, but not as low as with a fully bonded stem, except in the proximal region where shielding effects were still severe. Stress concentrations were observed at the lower edge of the bond-press fit interface. When considering stress shielding, the press-fit stem did not have a large advantage over the bonded stems. However, it did increase interface shear and compressive forces which may cause relative motion and resorption.

In a study with similar objectives, Huiskes (1990) again used a two-dimensional sideplate model to study the differences in load transfer and stress patterns between cemented, fully ingrown, proximally ingrown and press-fit stems. The results of this study were consistent with other findings. Noncemented, bonded stems showed higher distal and lower proximal cortical stresses than with the cemented stem, although the stress pattern was similar. The difference is due to the relatively high rigidity of the canal-filling uncemented stem. The greatest stress shielding occurred with the fully bonded stem. The partly bonded stem showed less proximal shielding, but still more than the cemented stem. The press-fit stem showed the least resorption with only stress shielding of the calcar. The stress pattern with the press-fit stem was very different than with the bonded or cemented stems.

More recently, Engh *et al.* (1992) performed *in vitro* biomechanical tests on porous coated AML femoral prostheses recovered at autopsy. The porous coating covered either the proximal 40%, proximal 80% or entire length of the stems. The implants were recovered after 12 to 93 months of *in vivo* service. They found little relative motion between the femoral cortex and the area of porous coating on the prosthesis when the implants were subjected to simulated single leg stance and stair climbing loads for a 52 kg person. For stems with bony ingrowth, the maximum relative motion in the porous coated regions was 40 μm and the displacement was elastic. The greatest relative motion occurred

at the uncoated distal tip and was directly related to the extent of coating. The maximum relative motions at the distal tip ranged from 210 μm for the 40% coated stem to 45 μm for the 100% coated stem. Stress shielding was found to be substantial in the implanted femurs, particularly in the proximal, medial region (where longitudinal strains were 80% less than the strains in an intact femur) and in the medial and lateral midstem regions (40% decrease compared with intact). The medial strain was reduced throughout the stem length except at the tip where higher than normal strains were recorded. Although no correlation between extent of coating and stress shielding could be made, the shielding effects of the noncemented stems were similar to those of cemented stems retrieved under similar circumstances.

The findings most relevant to this study are those of Ramamurti (1992). The authors investigated the effects of varying the distribution of surface coating on interface shear stress, interface shear motion and proximal stress shielding using a three-dimensional finite element model of a human femur and femoral component. The femoral component modeled was a titanium alloy Profile stem. The model simulated three phases of gait (heel strike, mid-stance and toe-off) by applying the appropriate joint contact force and all the major muscle forces. The bonding was assumed to be ideal; there was no relative motion in the bonded regions. The bonding conditions were incrementally changed in an attempt to minimize an objective function; variation of the coating distribution in a continuous manner is unique to this study. The objective function was composed of the peak interface shear stress, peak relative shear motion at the interface and stress shielding in the proximal femur, all normalized by reference values. The optimum coating distribution was proximally coating 60% of the stem surface area (which is equivalent to 51% of the stem length), which provided contact with endosteal cortical bone (Figure 1.1). Further distal bonding reduced motion but increased shear stresses, although a slight

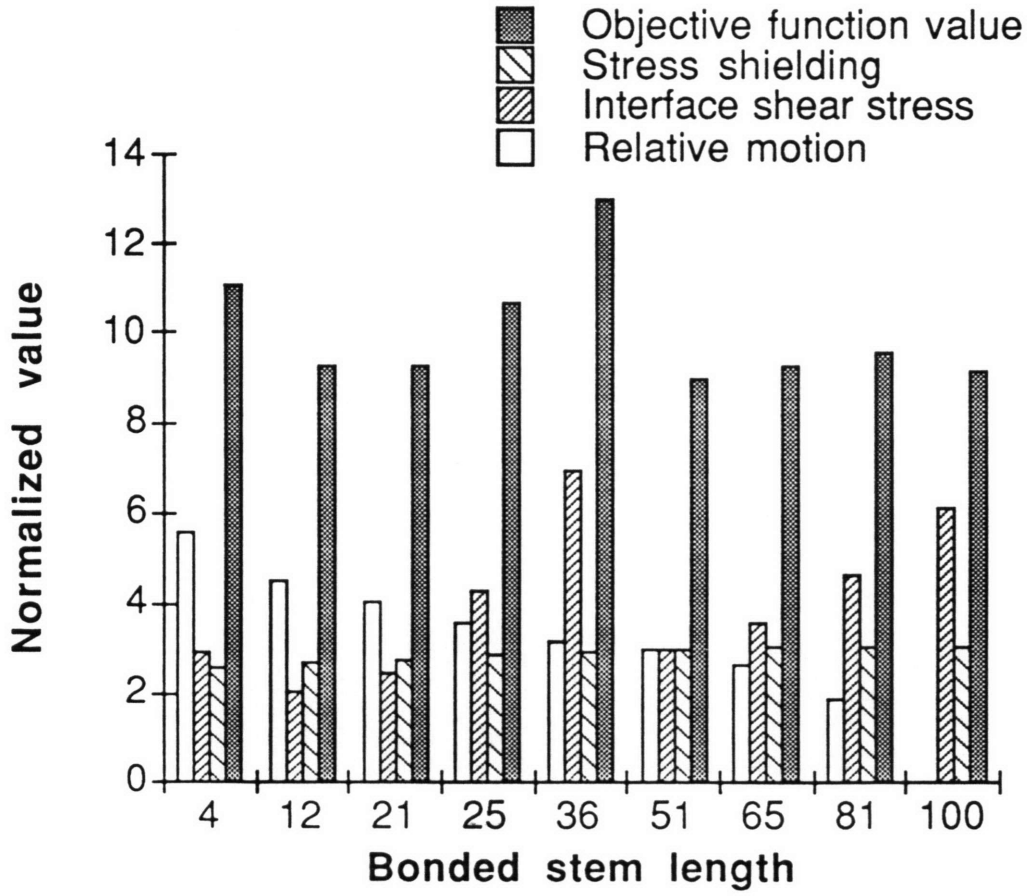

Figure 1.1 - Results of a finite element analysis to determine the effect of varying the surface coating distribution on stress shielding, interface shear stresses and relative motion at the interface (Ramamurti 1992).

extension of the bonding distally may be beneficial to ensure bonding to cortical bone. Reducing the extent of bonding caused a large increase in shear motion, but only a slight decrease in shear stresses. Stress shielding was relatively insensitive to bonding distribution, indicating that there was load transfer along the entire stem length and through sliding contact in the unbonded areas. Although the resulting optimum distribution is dependent on the objective function, the trends of shear motion and peak shear stress do agree with previous results. The reduction of stress shielding with reduction of the extent of distal coating was evident, but to a lesser degree than that reported by other studies. The lack of modeling fibrous tissue apposition may explain this finding, since a fibrous tissue layer is believed to increase proximal stresses.

The results of these studies suggest that surface bonding distribution is a critical design parameter, and that the optimal coating distribution is not easily determined. The optimization approach of Ramamurti provides the best estimate of the optimal distribution. In addition, the model demonstrates the trends in stress shielding, shear stress and shear motion with a quasi-continuous variation in coating distribution. The models of Huiskes *et al.* and the experiment by Engh *et al.* provide similar information but only for discrete distributions (Huiskes' models used no, partial or full bonding; Engh's experiment used 1/3, 4/5 or full coating). The lack of experimental evidence concerning the effects of incrementally varying coating distribution, and the need to confirm the results of the finite element analyses, indicate the necessity for validation experiments.

1.3 REVIEW OF EXPERIMENTAL METHODS AND MODELS

Research into the mechanics of post-arthroplasty load transfer and femoral component behavior has created the need for appropriate experimental models and methods to acquire the desired data. Several issues concerning the development of an appropriate model for this study were identified. The most important issues are: (i) cadaveric versus

synthetic bone; (ii) loading configuration; (iii) methods for measuring micromotion and strain; and (iv) *in vitro* bone bonding. Some work had been done on the first three issues and is reviewed in the following sections. The *in vitro* bonding issue has not previously been addressed.

1.3.1 Cadaveric versus synthetic bone

The majority of *in vitro* experiments have used fresh or embalmed cadaveric bones. Embalmed specimens are preferred because they are easier to handle and require less stringent safety precautions. Although changes in bone material properties do occur after embalming (McElhaney *et al.* 1964; Sedlin 1965; Evans 1973), consistent major changes have not been shown. It is accepted that at low strain rates, embalmed bone serves as a good model for fresh tissue (Lissner and Roberts 1966). However, embalmed bone still requires universal safety precautions, must be maintained wet and is subject to irreparable damage with repetitive use. In addition, the large anatomic variation between cadaveric samples introduces an undesirable variable. For these reasons, the use of synthetic bones as a model for living tissue is compelling.

One commercially available synthetic bone model is the composite bone (Sawbone) manufactured by Pacific Research Laboratories, Inc. (Vachon Island, WA). The bone is comprised of a fiber-reinforced epoxy cortical shell with a polyurethane foam trabecular bed. It is anatomically accurate and is designed to have the same gross mechanical behavior of living bone (Table 1.1). Szivek *et al.* (1991) performed experiments to compare the deformation response of synthetic, fresh and dry cadaveric femora by measuring cortical strains in single leg stance with an off-center body weight and abductor simulation. They found that the synthetic bone and cadaveric samples had similar amounts of interbone variation. However, in a subset of synthetic bones with similar trochanteric loading, they found low interbone strain variation and similar strain values between the synthetic and fresh samples. The synthetic bones are similar in size, have low interbone

variation - variations of 75 to 100% in strain measurements in cadaveric bone have been reported by some investigators (Szivek and Gealer 1991) - and are easier to work with. However, the synthetic bones are generally up to 30% less stiff than cadaveric bones (Szivek and Gealer 1991) and therefore are only appropriate for intercomparison studies.

Although the similarity in gross mechanical behavior between fresh and synthetic bones has been demonstrated, there has been little effort to compare these bones on a material basis. For instance, it is not known how fresh trabecular bone compares with the synthetic analog. In order to validate the synthetic bone model, parameters of interest were identified and studied. Based on a mechanical knowledge of the bone-stem interaction, the elastic modulus of the bone components and the coefficient of friction between the stem and the bone components were considered the most important parameters to be studied.

Table 1.1 - Physical properties of synthetic composite bone
(from Pacific Research Laboratories, Inc. 1992 Sawbones catalogue)

Ultimate tensile strength	170 MPa
Tensile modulus	18.6 GPa
Flexural modulus	14.2 GPa
Ultimate flexural strength	276 MPa

1.3.2 Loading configuration

The most basic loading configuration is to apply a single load to the prosthesis head with no attempt to simulate the physiological situation. The effect of a single component of the *in vivo* load (axial or torsional for instance) can be observed with this configuration (Gebauer *et al.* 1989; Nunn *et al.* 1989; Schneider *et al.* 1989; Sugiyama *et al.* 1989). Although this model provides information on micromotion, it is not appropriate for strain

measurements. Finlay *et al.* (1991) have shown that applying a load directly to the femoral head of a vertical shaft produces strains lower than those that occur with more physiologically realistic models. Rohlmann *et al.* (1983) reported that a single load to the femoral head parallel to the femoral shaft is useful if stresses in the diaphysis only are to be considered. However, proximal strains are of interest in these experiments and therefore the single load model is inadequate.

The most common in-plane loading configuration is a basic physiological loading model of single leg stance. This configuration usually has the femur aligned in 7° to 12° of adduction, which is the typical anatomical position (McLeish and Charnley 1970). A vertical load is applied to the prosthesis head through an acetabular cup (Crowninshield *et al.* 1980; Hirano 1986; Manley *et al.* 1987; Diegel *et al.* 1989; Whiteside and Easley 1989; Longo *et al.* 1992; Berzins *et al.* 1993). A simple vertical load on the head of a non-vertical femur also does not represent the physiological condition, since the resultant joint force on the femoral head is typically not vertical (McLeish and Charnley 1970).

The more realistic loading configuration is a single leg stance which considers the effect of muscle forces and an off-center body weight load. Djerf *et al.* (1987), Field *et al.* (1989), Burke *et al.* (1991), Szivek and Gealer (1991) and Engh *et al.* (1992) simulated the abductor muscles alone using straps or cables to join the bone and a simulated pelvis in the appropriate geometry. Oh and Harris (1978) accounted for the abductor muscle force by applying a load to the prosthesis head which was the resultant of the body weight and abductor muscle force. While this method applies the appropriate resultant, the stress distribution in the femur is not accurate. Rohlmann *et al.* (1983) simulated the abductors and vastus lateralis muscle using cables. Finlay *et al.* (1991) considered the effects of the abductors and the iliotibial tract separately. Both were simulated using strain-gauged cables. Finlay *et al.* found that the abductor muscle simulation alone produced excessive strains and bending moments compared with those produced by the lateral musculature. Since the effects of the iliotibial tract counteract those of the abductors and EMG studies

indicate that the iliotibial tract is active during single leg stance, they proposed that a simulation of the lateral forces is required to obtain meaningful strain data.

Numerous studies have shown that consideration of torsional loading is equally important to femoral component design and may cause increased micromotion (Gebauer *et al.* 1989; Nunn *et al.* 1989; Sugiyama *et al.* 1989; Phillips *et al.* 1990; Burke *et al.* 1991; Hayes *et al.* 1992a; Berzins *et al.* 1993). Experimentally, torsional loading has been applied through a single head load (Gebauer *et al.* 1989) or in a simulated stair climb configuration (Burke *et al.* 1991; Engh *et al.* 1992). Unfortunately, a stair climb configuration with muscle simulation is very difficult to implement and therefore is rarely attempted.

1.3.3 Micromotion measurement

The most common method to measure micromotion *in vitro* is to use a displacement transducer fixed to the bone and measure the motion of a target which is either fixed to the prosthesis or may be the prosthesis itself. Linear variable differential transformers (LVDT's) or strain gauge-based transducers are typically used to make micromotion measurements.

The measurements that are made typically fall into one of two categories: (i) site-specific uni-axial measurements, and (ii) multi-axial measurements, usually at multiple locations. The studies of Gebauer *et al.* (1989) and Nunn *et al.* (1989) used the former method. They each measured the motion of the exposed prosthesis neck with a single transducer. Measurements of this type provide only anecdotal data - the translational and rotational components of the motion cannot be resolved. Measurements of the second type, taken at multiple locations, require targets being mounted to the stem through holes in the cortical bone (Hirano 1986; Walker *et al.* 1987; Whiteside and Easley 1989; Burke *et al.* 1991; Engh *et al.* 1992; Berzins *et al.* 1993). This method is more rigorous than the uni-axial measurements, but only in a special case can it completely describe the three-

dimensional motion of the stem relative to the bone. For a rigid body, in order to resolve the translations along three orthogonal axes and the rotations about those axes (6 degrees of freedom), a minimum of six uni-axial measurements must be made at a minimum of three distinct points on the body (Hayes *et al.* 1992a). Berzins *et al.* (1993) and Hayes, Jr. *et al.* (1992a) completely described the six independent motions by using six transducers at any one level to measure the motion of three separate targets. The results are valid only for the transverse section (plane) being observed and cannot be extrapolated to the entire stem using rigid body analyses which ignore errors due to bony compliance (Hayes *et al.* 1992a). If more measurements are taken (for instance, three measurements for each of the three targets), a best-fit technique can be used to more accurately and more simply solve the components of motion (Veldpaus *et al.* 1988).

1.3.4 Strain measurement

A common technique for analyzing the stresses in bone is to use strain gauges, mounted to the cortical surface. It has been shown that strain gauge bonding techniques do not degrade the bone surface or cause enough structural damage to alter the bone's properties (Wright and Hayes 1979). However, they may produce notable reinforcement in areas of low modulus (Finlay *et al.* 1989). Nonetheless, of the available and practical techniques for assessing bone deformation, strain gauges are the least limiting and provide the most accurate data (Finlay *et al.* 1989). Consequently, this technique has been extensively applied to evaluate post-arthroplasty load transfer patterns in the femur (Oh and Harris 1978; Crowninshield *et al.* 1980; Rohlmann *et al.* 1983; Djerf and Gillquist 1987; Walker *et al.* 1987; Engelhardt and Saha 1988; Diegel *et al.* 1989; Finlay *et al.* 1989; Finlay *et al.* 1991; O'Connor *et al.* 1991; Engh *et al.* 1992).

As with micromotion measurement, the number of gauges and their positioning determine the usefulness of the data. One single-element gauge provides only anecdotal data and, where accurate determination of the principal stresses is desired, its use is not

recommended. For a general biaxial stress state, with the principal directions unknown, it can be shown that three independent strain measurements in different directions are required to determine the principal strains and stresses. This is the case when performing *in vitro* tests of implanted femurs, since the principal strain directions change post-arthroplasty (Walker *et al.* 1987; Diegel *et al.* 1989; Finlay *et al.* 1991) and are dependent on the loading configuration (Finlay *et al.* 1991). Nonetheless, some of the studies which evaluated post-arthroplasty load transfer using strain gauge techniques used only single-element gauges (Oh and Harris 1978; Crowninshield *et al.* 1980; Engelhardt and Saha 1988; Diegel *et al.* 1989). By using three-element rosette gauges, local strain environments of implanted femurs have been determined (Rohlmann *et al.* 1983; Djerf and Gillquist 1987; Walker *et al.* 1987; Finlay *et al.* 1989; Finlay *et al.* 1991; O'Connor *et al.* 1991; Engh *et al.* 1992); this analysis applies only to the point at which the gauges are mounted. By using multiple gauges mounted at the same transverse plane the normal and shear strains acting on that cross-section can be estimated, providing a better characterization of the strain distribution (Carter *et al.* 1981; Rubin and Lanyon 1982; Gross *et al.* 1992). This analysis, however, has yet to be attempted with a post-arthroplasty femur.

1.3.5 *In vitro* bone bonding

To the author's knowledge, there has been no attempt to simulate bone bonding *in vitro*. For this study, the technique required bonding of the stem to the endosteal surface with an adequate interface strength. The bonding agent should have some gap filling capability and should permit that only a portion of the stem be bonded. The stem must also be able to be de-bonded. A cyanoacrylate gel was selected as the bonding agent and validation experiments were conducted.

1.4 RESEARCH GOALS

The short-term clinical failures of cementless stems, such as thigh pain and limp, have limited their acceptance despite the potential long-term benefits of biological fixation for younger and more active patients. The clinical problems are believed to be related to failure of the bone-stem interface. By optimizing the design of the prosthesis to prevent or minimize failure at the interface, it should be possible to reduce the clinical problems. In analytical and experimental studies, it has been shown that bonding distribution is an important design parameter which can affect interface mechanics. However, there has been no attempt to experimentally optimize the surface coating distribution. These experiments are important on their own for several reasons, including: (i) They will require the development and validation of an unique experimental model that can be used for future studies; (ii) They will independently demonstrate the effect of surface coating distribution on stem mechanics; (iii) They will demonstrate sources of variation that cannot be observed with an analytical study; (iv) Experimental results are often more readily accepted by the clinical community than are results from analytical studies and, therefore, are more likely to have a clinical impact; and (v) The results can be used to validate the finite element model.

The goal of this study, therefore, is to experimentally determine the optimal surface coating distribution for a femoral prosthesis. In order to reach this goal, several research questions must be answered. Some of the questions relate to the validity of the experimental model, and must be answered before those pertaining to the main goal are answered. Specifically, the research questions related to the experimental model validation are:

1) Is the synthetic bone valid as an *in vitro* model? This requires determining how the parameters considered most important (elastic modulus and coefficient of friction) compare with published values for fresh cadaveric bone.

2) Does the cyanoacrylate gel adequately simulate bone bonding and permit removal and re-implantation? To answer this question, the interface strength, the potential for bond formation and the repeatability of the experiment with a single bone must be determined.

The research questions related to the main goal are:

3) What is the effect of varying bonding distribution on stress shielding? An indication of the degree of stress shielding can be obtained from measurement of cortical bone strains at different locations on the femur.

4) What is the effect of varying the bonding distribution on relative motion between the prosthesis and bone? Appropriate measurement of stem-bone relative motion and calculations will indicate the amount and type of micromotion.

5) Do the trends observed in the experiment correlate with those from the finite element analysis of Ramamurti (1992)? A correlation in trends will validate the finite element model.

6) What is the optimal surface coating distribution? The optimal bonding distribution will minimize the combined effects of stress shielding and micromotion.

EXPERIMENTAL METHODS

2.1 OVERVIEW OF THE EXPERIMENTS

A series of experiments were conducted to validate the synthetic bone model, including determination of material properties and the extent stem-bone contact. A simplified model, with idealized geometry, was tested to validate the model and methods.

A randomized design was used to test three synthetic human femurs with six bonding conditions per bone. Each bone was subjected to two loading cases: single leg stance and stair climb. Cortical bone surface strains and stem-bone relative motion were measured to indicate stress shielding and micromotion, respectively.

For a single treatment, the stem was implanted and bonded to the bone. The bone was tested under both loading cases. The stem was then de-bonded and removed. The bone was restored to its initial condition, re-implanted and the next treatment applied. This procedure was repeated on each bone for each of the six bonding conditions.

Finally, a finite element analysis was performed for comparison with the experimental results.

2.2 MODEL VALIDATION

Synthetic bones were ultimately selected for this study because of special requirements that could not be met by cadaveric bones. The protocol required that a single bone be tested with a variety of bonding distributions. With each test, however, the trabecular bed was damaged. The damage occurred through boiling and through repetitive insertion and removal of the prosthesis. Boiling trabecular bone can cause ultrastructural damage of the mineral phase from swelling of the collagen fibrils which results in altered mechanical properties (Borchers and Gibson 1992). Repetitive insertion

and removal of the prosthesis causes canal widening and poor fit. The advantage of synthetic bone is that the trabecular bed can be restored by filling the cortical shell with foam.

In order to test the validity of the synthetic bone model, several experiments were conducted. In order to determine the material properties of the synthetic bone three parameters were determined: bond strength, compressive modulus and coefficient of friction. The potential for bonding was assessed by examining bone-stem contact in CT scans and radiographs of the implanted bones. Finally, a simplified "ideal geometry" model was developed and experiments were conducted to validate the synthetic bone model, the bonding agent and the relative motion measurement system.

2.2.1 Tensile bond strength

In order to confirm that the cyanoacrylate was an adequate bonding agent, the strength of the bond was measured with a tensile test. Cortical bone specimens were acquired from a cadaveric femur of unknown sex and age. The femur was transversely sectioned into 4 to 7 mm thick discs at the mid-diaphysis and distal levels. Cylindrical samples were cored using a coring tool and drill press, under water irrigation and at low drill speeds (about 150 rpm). This produced samples of cortical bone that were 3 to 4 mm in diameter and 4 to 7 mm in height. Cylindrical samples of the fiber-reinforced epoxy (used in the synthetic bones to simulate cortical bone) were cored from the discarded condyles using the same technique. Attempts were made to correct any significant irregularities in the shape of the samples by refining by hand and lathing.

A servohydaulic material testing machine (Instron 8500, Instron Corp., Canton, MA) was used to conduct the test. Custom fixtures were made to hold the femoral stem and the specimen. Before bonding the specimen to the stem, both the mating surface of the specimen and the surface of the stem were pre-treated with a cyanoacrylate remover (Permabond Solvent; Permabond International, Englewood, New Jersey). Silicone

lubricant spray was applied to the exposed edges of the specimen to limit bonding to the bottom surface only.

The stem was mounted in the vise and aligned such that the specimen would rest on a flat surface of the stem. The stem was then secured with the clamps. The actuator was manually lowered under position control until the specimen and stem were just in contact. A piece of fine grain sandpaper was placed between the specimen and stem surface. The specimen was gently sanded to provide parallel surfaces between the specimen and stem. The actuator was then manually raised just enough to permit application of the cyanoacrylate gel (TruBond Super Glue Gel, True Value, Chicago, Illinois). The glue was applied to the stem surface and under load control a load of 10 N was applied while the glue cured. The curing time was one hour.

After curing the test was conducted using the Instron Series IX Automated Materials Testing System on a IBM PS/2 Model 70. Under position control the actuator was automatically advanced 0.05 mm/min. with load and position data being sampled 10 times per second. The test began from the pre-load condition and continued until the stem-specimen bond broke. The ultimate tensile strength was determined from the stress-strain curve. Five cortical bone specimens and three fiber-reinforced epoxy specimens were tested.

Although the bond strength of foam samples glued to the stem was not determined, values similar to or greater than those found in these pull-off tests were expected. Observations during stem removal also confirmed the adequacy of the bond strength using foam.

2.2.2 Compressive modulus

The compressive modulus of the synthetic bone materials was determined to characterize their mechanical behavior. Cylindrical foam specimens, approximately 6.5 mm in diameter and 7 mm in height, were removed from a block of foam using a coring

tool. Cylindrical fiber reinforced epoxy specimens were cored from the condylar region of the synthetic bones. These specimens were typically 6.5 mm in diameter and 5 mm in height. The exact specimen diameter and gauge length were measured using a micrometer. Testing was performed in the Instron with the specimen mounted between two parallel platens. The specimens were pre-conditioned by compressing to approximately 0.4% strain. This was repeated three times. The test was performed under position control at a rate of 0.5 mm/minute until the specimen yielded. The modulus was calculated as the slope of the linear portion of the stress-strain curve. The yield strength was determined from the stress-strain curve. A total of 8 foam samples and 6 epoxy samples were tested.

2.2.3 Coefficient of friction

The coefficient of friction between the titanium alloy and the polyurethane foam was measured to characterize the mechanical interaction between the smooth, unbonded portion of the prostheses and the adjacent bone components. Titanium alloy discs were machined by sectioning a prosthesis. The discs were approximately 13 mm in diameter and 6 mm thick. A block of foam was machined to a rectangular piece with approximate dimensions of 65 mm x 25 mm x 15 mm. The friction tests were performed using a custom designed wear testing apparatus. The apparatus reciprocated the titanium sample on the stationary foam block and applied a normal force of 450 N perpendicular to the interface surface. A load cell measured the normal force and the force tangential to the interface (frictional force). Four series of tests were performed: untreated samples, samples treated with silicone spray, samples treated with a silicone/cyanoacrylate glue solvent (XNMS Solvent, Loctite, Newington, CT) and samples re-treated with silicone after solvent application. Three specimens were tested.

2.2.4 Bone-prosthesis contact

In order to determine the typical potential for bonding at different sites along the length of the stem, serial transverse CT scans and radiographs in the anterior-posterior, medial-lateral and two additional mid-plane directions were taken for a single bone (Bone 2). Apposition of the prosthesis to the foam and to the fiber-reinforced epoxy was noted, as were significant gaps.

2.2.5 Simplified model

A simple rod-in-tube model was developed primarily to confirm that the bonding distribution could be controlled. A 20 cm long fiberglass tube (1" I.D.) was filled with the polyurethane foam used in the synthetic bones. A 1/2" hole was drilled into the foam along the long axis of the tube. An aluminum rod (12 cm long; 1/2" diameter) was inserted so that the implanted portion was 9 cm long. Three experiments were conducted with bonding conditions of 1/3, 2/3 and full bonding. The aluminum rod was prepared for distal micromotion measurement using the same instrumentation as was used for the prostheses. A threaded rod and target were inserted into the aluminum rod through a 5 cm round window in the tube. A mounting bracket with three orthogonally mounted LVDT's was attached to the tube to measure the relative motion of the single target. The rod-tube system was mounted in the Instron at an adduction angle of 12°. A horizontal beam connected the head of the rod to the actuator which was offset from the head and acted along a line which went through the base of the tube (the "knee"; see Figure 2.1). Loads from 0 to 1200 N in increments of 200 N were applied. The action of this load represents the body weight load. The relative motion of the distal target was measured. In order to repeat the experiment with a different bonding condition, the aluminum rod was removed by force. The spent foam was reamed out and the tube was re-filled with foam. The rod was then re-inserted with the new bonding condition.

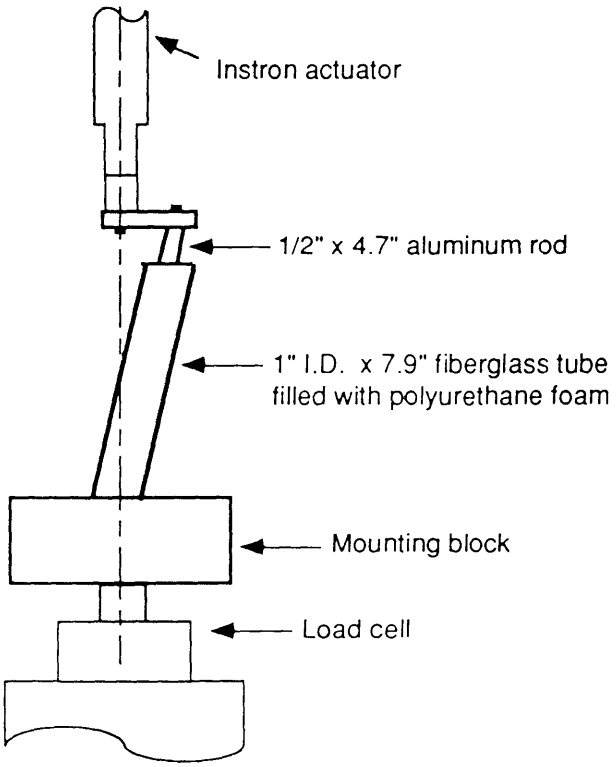

Figure 2.1 - Loading configuration for the simple rod-in-tube model.

2.3 PROSTHESIS AND BONE PREPARATION

Three smooth, titanium alloy, anatomic femoral prostheses (Profile, DePuy, Inc., Warsaw, IN) were used in this study (Figure 2.2). Size 4 prostheses were used to match that of the finite-element model (Ramamurti 1992). Three composite synthetic femora were custom manufactured by Pacific Research Labs, Inc. (Vashon Island, WA) for use in this investigation (Figure 2.2). A composite femur consists of an outer "cortical" shell of fiber reinforced epoxy which is filled with a polyurethane foam that simulates the trabecular bone. The femora were manufactured to minimize variability between bones. The medullary canal diameter was sized to provide a good fit with a size 4 prosthesis.

All three femora were initially implanted by an orthopaedic surgeon using standard surgical techniques and equipment. A steel cable was attached to the trochanteric region of each bone to simulate the abductor musculature. The condyles and distal shaft of each bone were removed to facilitate potting with bone cement (Fastray, Harry J. Bosworth Co., Skokie, IL) and mounting in the loading fixture.

Each bone was instrumented for micromotion and strain measurements. To measure the relative motion of the stem with respect to the bone, #3-48 threaded rod markers were screwed into the stem through 5 mm diameter holes in the femur. Tapped cubes were attached to the rods and served as targets. Fixtures to hold the displacement transducers were press-fit and fixed with epoxy to the bone (Figure 2.3). Linear variable differential transformers (LVDT's, Schaevitz Engineering, Pennsuaken, NJ) were attached to the fixtures and aligned to contact the target. Each bone had a total of six targets; three mounted at the distal tip of the prosthesis and three mounted at the proximal end (Figure 2.4). The targets were spaced circumferentially (Figure 2.5) and defined two micromotion planes. The circumferential positions of the targets were determined from transverse CT scans. The three LVDT's mounted orthogonally in each fixture provided

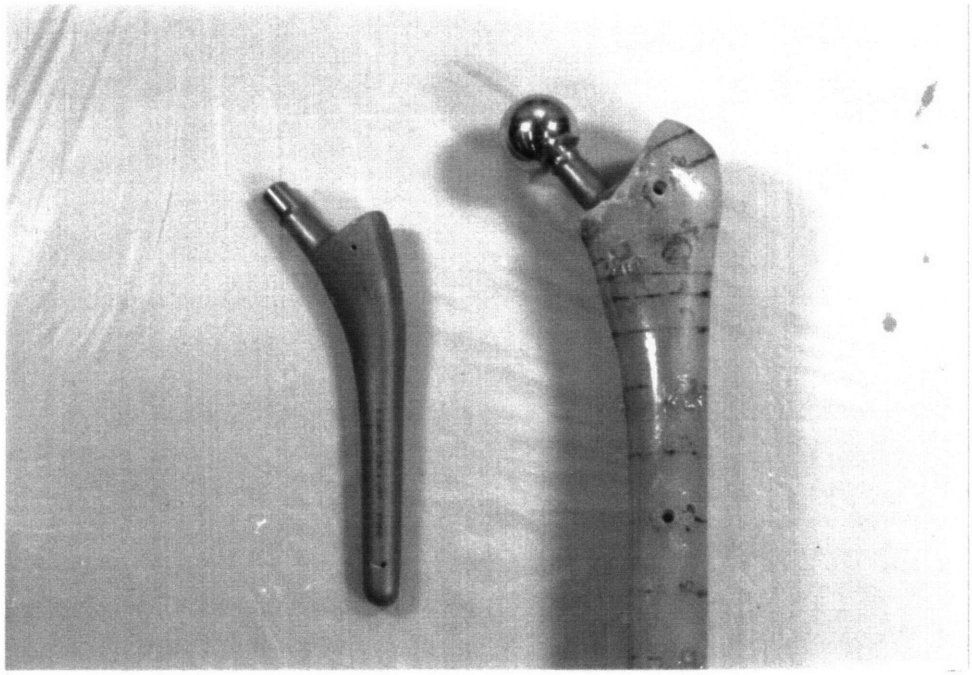

Figure 2.2 - A synthetic femur and Profile® titanium alloy prosthesis used in the experiment.

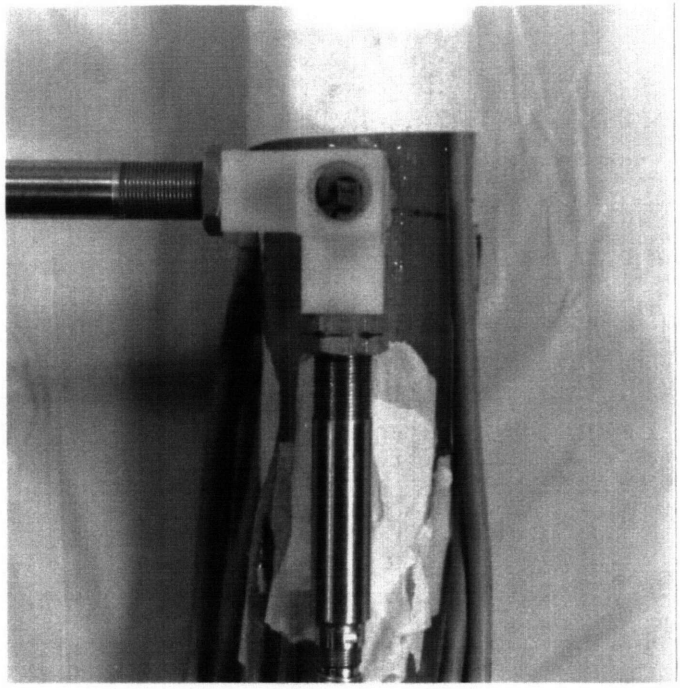

Figure 2.3 - Bracket used to fix the LVDT's to the bone

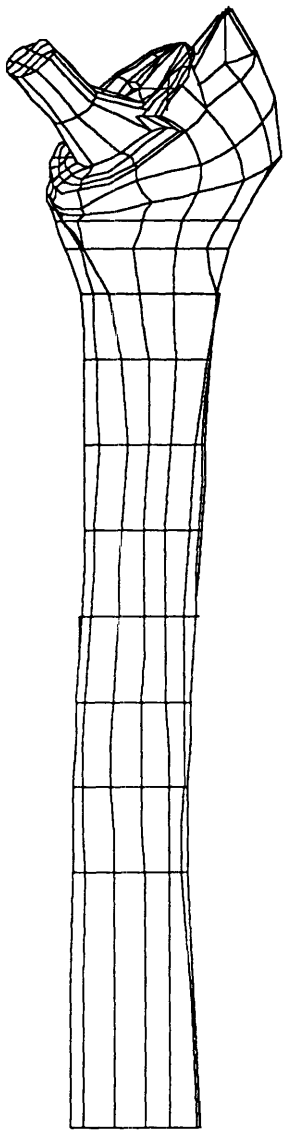

LEVEL	% STEM LENGTH	TRANSDUCER
14	0	NONE
13	-	LVDT
12	-	STRAIN
11	21	NONE
10	26	NONE
9	36	NONE
8	51	STRAIN
7	65	NONE
6	81	LVDT
5	100	NONE
4	-	STRAIN
3	-	NONE
2	-	(POTTED)
1	-	(POTTED)

Figure 2.4 - Schematic of a femur with the strain gauge and LVDT locations identified.

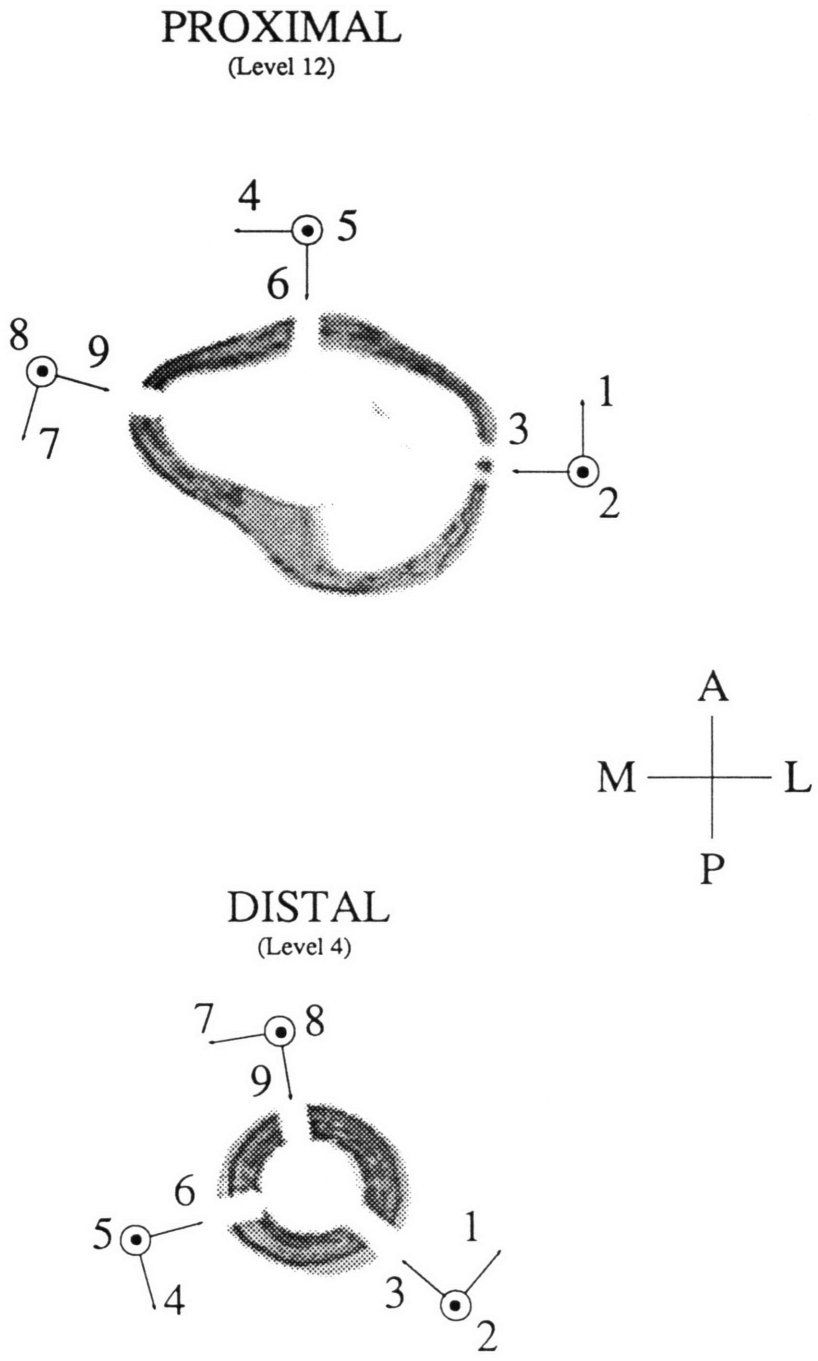

Figure 2.5 - Circumferential position and labels for the LVDT's.

three measurements of displacement at each of three separate locations on each micromotion plane (a total of nine per plane).

Each bone was also instrumented with nine rectangular rosette surface strain gauges (Type WA-13-060WR-120, MicroMeasurements Group, Inc., Raleigh, NC). Three gauges were placed circumferentially around each bone at each of three levels: proximal, mid-stem, and distal, beyond the stem tip (Figure 2.4). The three sets of gauges defined three strain planes. Transverse CT scans were taken at each level to accurately determine the gauge's circumferential positions (Figure 2.6). The gauges were mounted so that the center gauge was aligned with the longitudinal axis for the cross-section. The gauges were fixed to the bone with epoxy (M-Bond AE-10, MicroMeasurements Group, Inc., Raleigh, NC).

2.4 EXPERIMENTAL APPARATUSES

2.4.1 Single leg stance

Since simple loading cases fail to accurately characterize the deformation response of the femur (Rohlmann *et al.* 1983; Finlay *et al.* 1991), a loading apparatus was designed to simulate the in-plane body weight and muscle loads encountered at the hip in single leg stance (Figure 2.7). The anatomical orientation and muscle loads were determined from published data (McLeish and Charnley 1970; Rohlmann *et al.* 1983; Finlay *et al.* 1991). The Instron was used to apply and measure the body weight load. The potted femur was mounted to the load cell at an adduction angle of 12°. A simulated pelvis was attached to the actuator of the Instron. A polyethylene acetabular cup transmitted a compressive load to the head of the prosthesis. The abductor cable was attached to the pelvis through a turnbuckle which could be adjusted to vary the abductor load. An uniaxial strain gauge mounted to the turnbuckle measured the magnitude of the abductor load. The angle of the abductor with respect to the vertical was 15° to 20°. The

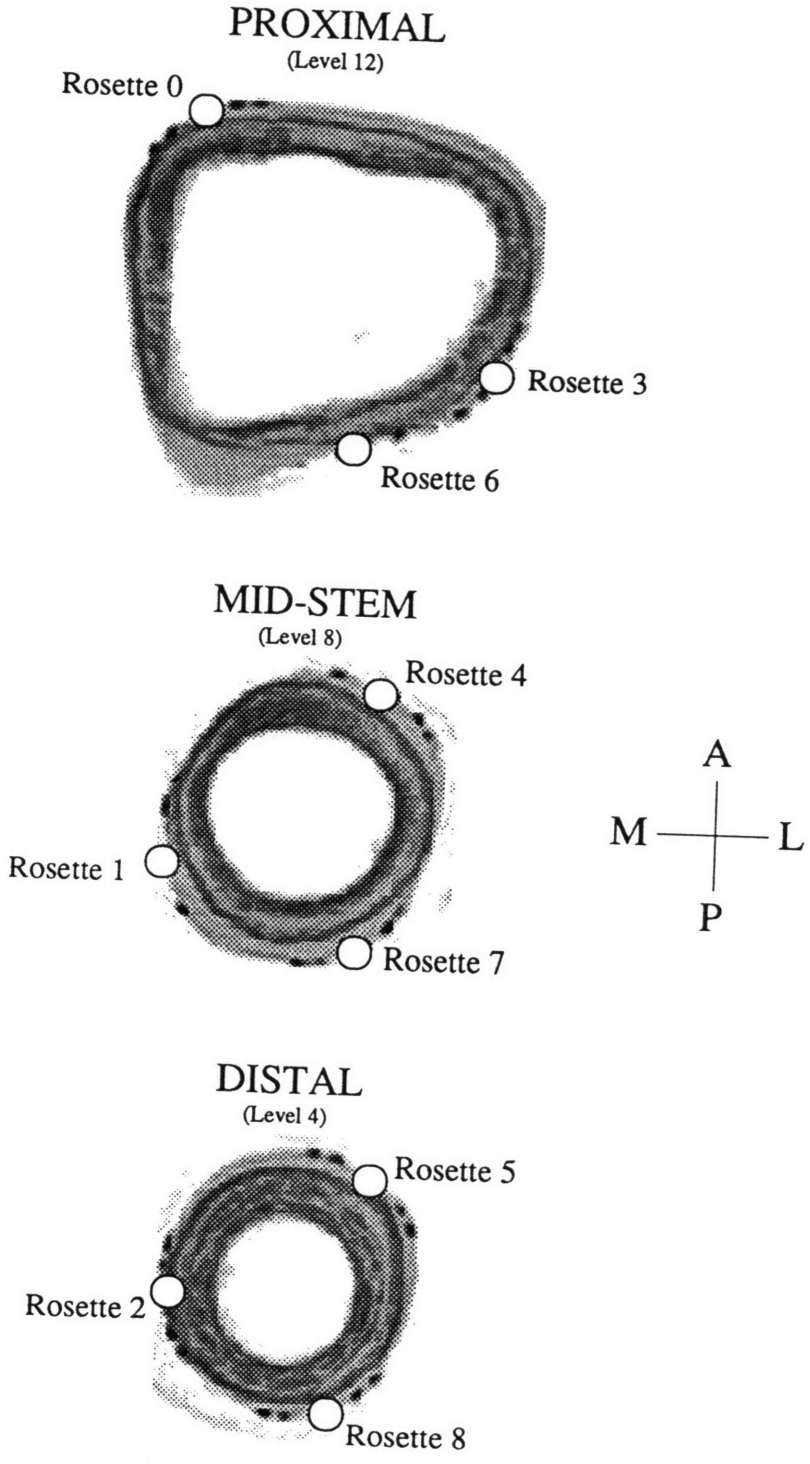

Figure 2.6 - Circumferential position and labels for the strain gauge rosettes.

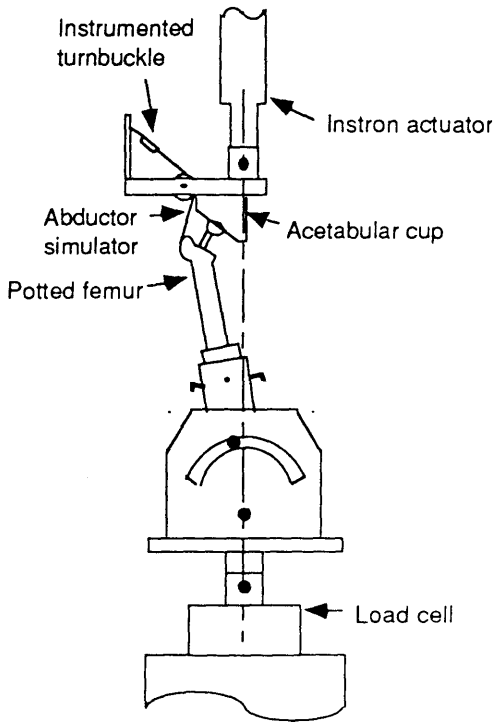

Figure 2.7 - Loading apparatus to simulate single leg stance with abductor muscle simulation.

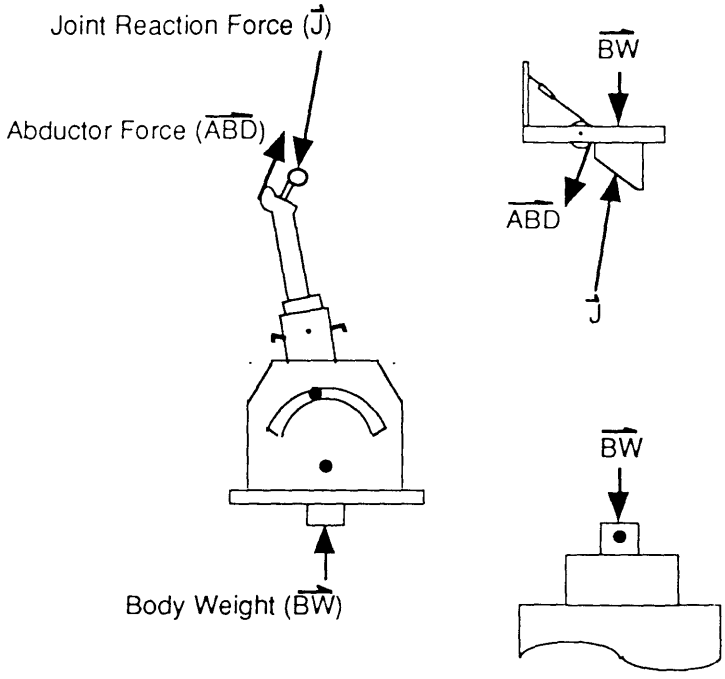

Figure 2.8 - Free body diagram showing the measured forces and the calculated joint reaction force.

bone was positioned so that the line of action of the body weight force would act through the medial femoral condyle. From the geometry and the known forces (body weight and abductor), the joint reaction force could be calculated (Figure 2.8).

2.4.2 Stair climbing

Accurate stair climb loading is difficult to simulate, but the importance of out-of-plane loading on micromotion necessitates this loading case. An apparatus was designed to provide out-of-plane loads, but without muscle simulation. The femur was oriented such that the force applied by the Instron acted on the femoral head 35 degrees anterior to the coronal plane of the femur (Figure 2.9). This is the orientation of the contact load when forces on the femoral head are maximal during stair ascent (Andriacchi *et al.* 1980).

The single leg stance and stair climbing loads were applied sequentially. For the single leg stance case, the bones were statically loaded to a final load body weight load of 650 N, which represents an 80 kg subject. The abductor force was adjusted to be 1.5 times body weight. The resultant on the head at the final body weight load of 650 N was approximately 1550 N at an angle of about 22° from the long axis of the bone in the coronal plane. By pausing the loading at intervals of 100 N for 10 to 20 seconds, data for multiple static body weight loads (150, 250, 350, 450, 550, and 650 N) were obtained. In stair climbing configuration, head loads of 250, 500, 750 and 1000 N were applied. To prevent damage to the bones, the head load did not exceed 1000 N. The data from the nine LVDT's, the Instron load cell, the Instron actuator extensometer and the elapsed time (12 channels) were acquired on a PC-based data acquisition system using LabTech Notebook software (Laboratory Technologies Corp., Wilmington, MA). These data were sampled at 10 Hz and stored to disk. The strain gauge data, abductor load, body weight load and elapsed time (30 channels total) were acquired using an Apple Macintosh IIci with National Instruments SCXI instrumentation and custom programs written using

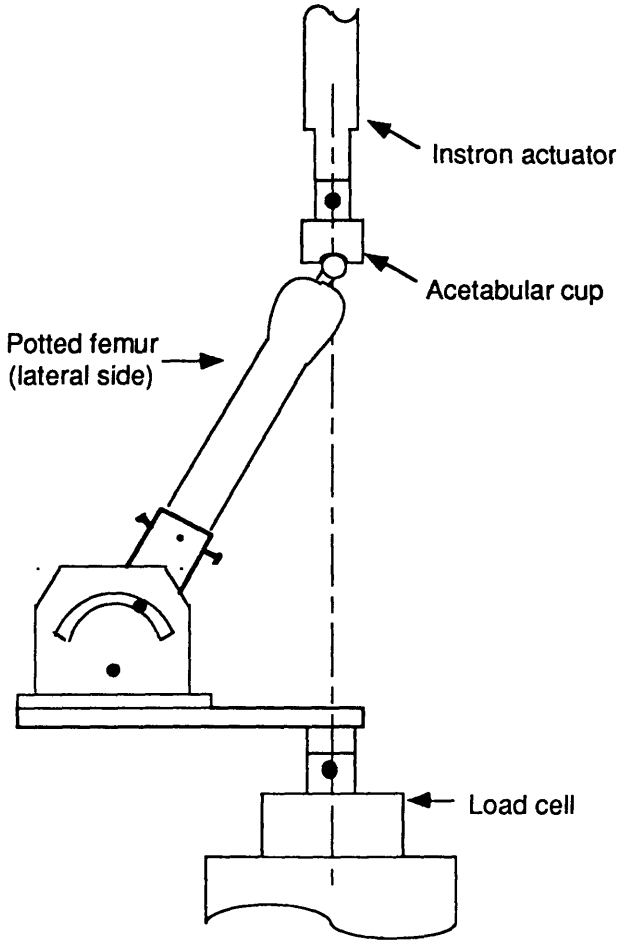

Figure 2.9 - Loading apparatus to simulate stair climb position.

LabView software (National Instruments Corp., Austin, TX). These data were sampled, filtered, reduced and stored to disk at an effective sampling rate of 0.5 Hz.

2.5 PROSTHESIS BONDING AND REMOVAL

To test a single bone under a variety of bonding conditions, methods were developed to: (i) simulate porous or HA coating by bonding a portion of the stem to the bone; and (ii) de-bond the stem from the bone without ruining the bone for further implantation. A cyanoacrylate gel (SuperBonder 409, Loctite Corp., Newington, CT) was used to bond the stem to the bone. Because of its high viscosity, the gel maintained its distribution on the stem after application. This provided a method by which the bonding distribution could be controlled.

Removal of the stem was accomplished in two stages. The first was to place the bone in boiling water until the cyanoacrylate deconstituted, and the stem could be removed (typically 30 to 60 minutes). The cortical shell of the synthetic femur was unaffected by this procedure. However, the polyurethane foam became hydrated or was removed along with the stem. In order to restore the "trabecular bone", any remaining foam was removed and the bone was filled with new foam. The new foam was then reamed, using the original "cortex" as a guide to implant the prosthesis.

2.6 EXPERIMENTAL DESIGN

A Latin square design was originally to be employed in this study (Cochran and Cox 1957). This design was selected because of its ability to statistically eliminate the effects of two extraneous sources of variability; in this experiment, the extraneous sources of variability with the potentially greatest effect were the variation between bones and the variation within a bone due to the repeated bonding and removal of the stem.

However, only three of the original six bones were tested. Nonetheless, the treatments were randomized and therefore will fit the Latin square design when the remaining three bones are tested. An additional test was done with bone 6 and its original treatment (100% bonding). This provided an indication of repeatability and variability introduced by the test procedure and order.

Six treatments were applied to each bone in a randomized order (Table 2.1). The treatments (as percentage of stem length with coating, measured from the proximal end) were 0%, 21%, 36%, 65%, 81% and 100% bonded. These lengths were selected to match those used in the finite-element model. Two identical tests were run for each bone in each loading configuration with each bonding condition. This was required because only nine LVDT's were available and a total of eighteen displacement measurements were required for each loading case.

Table 2.1 - Experimental Design

	B2	B5	B6
T1	21%	81%	100%
T2	65%	0%	21%
T3	36%	100%	0%
T4	100%	36%	65%
T5	0%	65%	81%
T6	81%	21%	36%
T1a	-	-	100%

Entries in table represent percentage of length of stem coated (measured from the proximal end).

B - Bone number; T - Test number

2.7 DATA ANALYSIS

2.7.1 Strain data

The local principal strains (ε_I and ε_{II}) and angle from the long axis of the bone to the major principal axis (ϕ) were calculated using the data from each rosette (ε_1, ε_2 and ε_3) and the strain-transformation relationship (Dally and Riley 1978):

$$\varepsilon_{I,II} = \frac{\varepsilon_1 + \varepsilon_3}{2} \pm \frac{1}{\sqrt{2}}\sqrt{(\varepsilon_1 - \varepsilon_2)^2 + (\varepsilon_2 - \varepsilon_3)^2} \tag{2.1}$$

$$\phi = \frac{1}{2}\tan^{-1}\left(\frac{2\varepsilon_2 - \varepsilon_1 - \varepsilon_3}{\varepsilon_1 - \varepsilon_3}\right) - 45^\circ \tag{2.2}$$

From these data, the local axial (ε_{zz}) and hoop (ε_{hoop}) strains were calculated (Dally and Riley 1978):

$$\varepsilon_{zz} = \frac{\varepsilon_I + \varepsilon_{II}}{2} + \frac{\varepsilon_I - \varepsilon_{II}}{2}\cos(2\phi) \tag{2.3}$$

$$\varepsilon_{hoop} = \frac{\varepsilon_I + \varepsilon_{II}}{2} - \frac{\varepsilon_I - \varepsilon_{II}}{2}\cos(2\phi) \tag{2.4}$$

In order to compare bonding cases, the local axial and hoop strains for six rosettes were compared. The rosettes used for comparison were (rosette identification numbers in parentheses): proximally, the anterior-medial (0) and posterior (6) rosettes; at the mid-stem level, the medial (1) and posterior-lateral (7) rosettes; and at the distal level, the medial (2) and posterior-lateral (8) (Figure 2.6).

As well, the maximum tensile and compressive strains for each cross-section were computed. In general the axial strain ε_{zz} can be expressed at any point (x,y) in a cross-section by (Gross *et al.* 1992):

$$\varepsilon_{zz}(x,y) = a + bx + cy \tag{2.5}$$

Using equation 2.5, the cross-sectional axial strain profile was calculated using the local axial strains measured at each of the three gauge locations in a cross-section to solve for the three unknown parameters, a, b, and c. The gauge locations were determined from cross-section contours digitized from the CT images using custom image processing software and automated edge detection algorithms. Strains were calculated for each digitized point on the contour and the peak strain magnitudes and locations were determined. These calculations were done for each of the three strain planes per bone. It should be noted that because of the point load on the proximal plane (the abductor force inserts on the lateral side), this linear interpolation is not strictly valid for the proximal cross-section in single leg stance.

All strain data were subjected to inclusion criteria which were designed to objectively eliminate obviously erroneous data. These criteria were necessary because, on occasion, a gauge would malfunction before or during a test and this malfunction was not obvious at the time of testing. The criteria were established based on the expected linear behavior of the strains with increasing load, with no strain before loading. The latter criterion should have been met in all cases; the gauges were tarred before loading. The strains were considered to be linearly increasing with load if a regression analysis yielded a correlation coefficient (r^2) greater than 0.75 ($r^2 > 0.75$). The exception to this criterion was strains that had poor correlation but had magnitudes that could be attributed to noise alone. For the six rosettes selected for comparison, a total of 432 measurements

were made; seven of these measurements did not meet the criteria and were excluded from the analyses.

2.7.2 Relative motion data

In order to compare bonding cases, uniaxial-axial site-specific motions were compared. The LVDT's were selected to provide an indication of a component of motion - subsidence, rotation or toggle. The LVDT's used for comparison are summarized in Table 2.2. However, due to the limitations of uni-axial measurements, these data were only used for comparisons of different bonding conditions and not to completely characterize the motion.

Table 2.2 - LVDT's used for uniaxial motion comparisons

Component	LVDT (refer to Figure 2.5)
Proximal axial	Lat-Ant (5), Medial (8)
Proximal rotation	Medial (7)
Proximal AP toggle	Lat-Ant (6)
Proximal ML toggle	Medial (9)
Distal axial	Anterior (5), Medial (8)
Distal rotation	Medial (7)
Distal AP toggle	Lateral (3), Anterior (6)
Distal ML toggle	Medial (9)

In order to extrapolate these data to interfacial relative motion, a rigid body analysis was performed on a single bone for illustrative and comparative purposes. In general, the motion of any point on a rigid body, from an initial position vector, $\mathbf{X}^{\mathbf{initial}}$, to a final position vector, $\mathbf{X}^{\mathbf{final}}$, can be decomposed into a rotation matrix, **R**, and a translation vector, v, and can be described by:

$$\mathbf{X}^{\text{final}} = \mathbf{R}\ \mathbf{X}^{\text{initial}} + \mathbf{v} \tag{2.6}$$

This description can provide a complete characterization of the translational and rotational motions of the prosthesis relative to the bone. With the appropriate measurements, the rotation matrix and translation vector for each of the two micromotion planes can be determined. The solution assumes that a thin transverse cross-section behaves essentially as a rigid body. The solution applies to the cross-section alone and cannot be extrapolated to describe the motion of the entire implant.

The three-dimensional motion of the three targets in a plane (2 planes per bone - proximal and distal) was measured. This provided the displacement vectors for three points on the rigid body. The initial position vectors were determined from digitized CT contours of the prosthesis with the targets attached. A global coordinate system was defined and, for each target, the measured motions were transformed from the target coordinate system to the global coordinate system. The final position vectors were calculated as the sum of the transformed displacement vectors and the initial position vectors:

$$\mathbf{X}_{\text{global}}^{\text{final}} = \mathbf{X}_{\text{global}}^{\text{initial}} + \mathbf{X}_{\text{global}}^{\text{displacement}} \tag{2.7}$$

To solve for **R** and **v**, a least-squares algorithm was applied (Veldpaus *et al.* 1988). This algorithm provides an estimation for the translation vector and rotation matrix from measurements of the spatial coordinates of at least three non-collinear markers on a rigid body. It does so in an optimal manner by employing an unweighted least-squares approach. It also avoids some of the numerical difficulties with other methods, such as eigenvalue calculations and large systems of non-linear equations. The

solution is relatively simple, requiring the solution of a system of two well-behaved non-linear equations using the Newton-Raphson method.

Displacements were calculated for each point on the digitized prosthesis contour and peak interfacial micromotions were determined. The distal peak micromotions were decomposed into axial, tangential and radial components. These calculations were done for the distal micromotion plane of a single bone (Bone 5).

The motion data were subjected to inclusion criteria which were designed to objectively eliminate obviously erroneous data. These criteria were necessary because, on occasion, the LVDT bracket or target would not be firmly fixed and would move. This happened frequently with the proximal-lateral LVDT bracket which interfered with the abductor cable in bones 2 and 5. The criteria were established based on the expected linear behavior of the motions with increasing load, with no change at a constant load and (partial) return to the zero load position on unloading. The motions were considered to be linearly increasing with load if a regression analysis yielded a correlation coefficient (r^2) greater than 0.70 ($r^2 > 0.70$). An exception was made to this criterion if the magnitude of the motion could be attributed to noise alone. If motion was observed at a constant load, or if the magnitude of the motion increased after unloading, it was attributed to faulty measurements. A total of 648 single LVDT measurements were made; 58 of those measurements did not meet the criteria and were excluded from the analyses.

2.7.3 Statistical analysis

Unpaired Student t-tests were performed to compare strain gauge, maximum strain and uniaxial motion data between bonding conditions.

2.8 FINITE ELEMENT ANALYSIS

One of the objectives of this study was to compare the experimental results to those of the finite element analyses performed by Ramamurti (1992), in order to validate the FEM. To better compare the results of the finite element model and the experimental data, some modifications were made to the model to better represent this experiment. The measured moduli for the reinforced epoxy and polyurethane foam of the synthetic bone were substituted in the model for the cortical and trabecular bone, respectively. Similar loading conditions to these experiments were applied to the FEM. There were two significant differences in the loading conditions: (1) In the model the insertion of the abductor muscle force was distributed over a series of nodes and in the experiment the insertion was concentrated where the screw was inserted; and (2) In the experiment the distal bone was constrained (by potting) along its length from levels 1 to 2, whereas the distal constraint in the model was only applied to the nodes at level 1. Bonding conditions of 21%, 65% and 100% of stem length were considered. By finite element analysis, the axial strains on the surface of the bone, the maximum tensile and compressive surface strains and the relative motion of the distal tip were computed and compared to the experimentally determined values.

2.8.1 Axial surface strains

In order to compare axial strains at specific gauge locations, the FEM contours were compared to the CT cross-sectional scans showing gauge locations and nodes corresponding to six rosette locations were identified (refer to Section 2.7.1). The strains at these nodes were used for comparison with experimental data. The maximum tensile and compressive axial surface strains also were identified for each of the three cross-sections (levels 4, 8 and 12) for comparison with the calculated maximum tensile and

compressive strains from the experimental data. Both the magnitude and location of the peak strains were identified.

2.8.2 Relative motion

In order to compare relative motion at specific locations on the prosthesis, the FEM contours were compared to the CT cross-sectional scans showing target locations and the nodes corresponding to six target attachment locations (Table 2.2) were identified for the bone and prosthesis. The relative motion of the prosthesis with respect to the bone was simply the difference between the two displacements. The relative interface motion in the FEA was defined with respect to a global coordinate system. In order to compare these displacements with the uniaxial LVDT measurements, the global displacements were transformed into the coordinate system of the LVDT target of interest.

It was not possible with this analysis to compare the magnitudes of relative motion because the displacements from the FEA were interfacial motions, whereas in the experiment the motion of the targets was measured. Nonetheless, the trends should be similar and a comparison between the FEA and experimental trends was made for each of the six LVDT's previously identified for comparison (refer to Section 2.7.2).

RESULTS

3.1 SYNTHETIC BONE MODEL VALIDATION

3.1.1 Bond strength

The bond strength of a titanium alloy prosthesis to cortical bone was tested using five cadaveric bone specimens, with a total number of 19 trials. The mean maximum tensile strength was 14.75 ± 5.15 (SD) MPa (Table 3.1). Despite the wide variation, all trials yielded a maximum tensile strength of greater than or equal to 9.45 MPa.

Three fiber reinforced epoxy specimens were tested once each. The bond strength for the epoxy specimens (3.88 ± 1.09 (SD) MPa) was lower than for the cadaveric samples.

Table 3.1 - Maximum tensile bond strength for cortical bone (cadaveric or synthetic) bonded to a prosthesis with cyanoacrylate gel.

Sample	Number of trials	Mean of maximum tensile strength (MPa)	Standard Deviation of max. tensile strength
1 - cadaveric	5	11.88	1.18
2 - cadaveric	7	19.85	5.27
3 - cadaveric	1	12.02	-
4 - cadaveric	1	9.45	-
5 - cadaveric	5	12.08	1.55
Total - cadaveric	**19**	**14.75**	**5.15**
1 - synthetic	1	3.46	-
2 - synthetic	1	5.12	-
3 - synthetic	1	3.07	-
Total - synthetic	**3**	**3.88**	**1.09**

3.1.2 Compressive modulus and strength

The modulus of the polyurethane foam and fiber reinforced epoxy was measured in compression. Eight cylindrical foam specimens and six fiber reinforced epoxy specimens were tested. The modulus and yield strength was determined for all fourteen samples (Table 3.2). For the foam, the average compressive modulus was 16.8 ± 3.85 (SD) MPa and the average yield strength was 0.923 ± 0.097 (SD) MPa. For the fiber-reinforced epoxy, the average compressive modulus was 1.18 ± 0.6 (SD) GPa, and the average yield strength was 66.9 ± 11.0 (SD) MPa.

Table 3.2 - Compressive modulus of polyurethane foam and fiber-reinforced epoxy

Sample	Height (mm)	Dia. (mm)	Modulus (MPa)	Yield Strength (MPa)
Foam - 1	7.00	6.50	14.84	.975
Foam - 2	6.96	6.53	26.16	.885
Foam - 3	6.25	6.48	15.14	.900
Foam - 4	6.78	6.53	16.41	.990
Foam - 5	7.52	6.50	16.79	.855
Foam - 6	7.11	6.45	15.67	1.065
Foam - 7	6.07	6.53	14.46	0.750
Foam - 8	6.10	6.50	15.25	0.960
Foam Mean ± SD	-	-	**16.84 ± 3.85**	**0.923 ± 0.097**
Epoxy - 1	5.095	6.50	1103	68.1
Epoxy - 2	5.23	6.28	1058	66.3
Epoxy - 3	5.65	6.55	1365	51.7
Epoxy - 4	9.065	6.32	2255	59.6
Epoxy - 5	4.41	6.49	732.2	84.0
Epoxy - 6	4.44	6.58	579.1	71.9
Epoxy Mean ± SD	-	-	**1182 ± 595**	**66.93 ± 11.0**

3.1.3 Coefficient of friction

To determine the coefficient of friction between a titanium alloy prosthesis and the foam, a total of three titanium specimens were tested. A variety of lubrication treatments were considered. Two specimens were tested with four treatments and one was tested with only three treatments. The lubricant that yielded the lowest coefficient of friction was the solvent (Table 3.3). However, there was no statistically significant difference between any pair of treatments ($p>0.18$).

Table 3.3 - Coefficient of friction between titanium alloy and foam with a variety of lubrication treatments

Sample No.	No lubricant	Silicone	Solvent	Re-silicone
1	0.335	0.319	0.183	0.180
2	0.225	0.167	0.136	N/A
3	0.218	0.209	0.209	0.232
Mean ± SD	**0.259 ± 0.066**	**0.231 ± 0.079**	**0.176 ± 0.037**	**0.206 ± 0.037**

3.1.4 Bone-prosthesis contact

Serial transverse CT scans were taken of bone 2 from the level of the mid-stem gauge to just distal to the stem tip. This region was identified as the most likely to have gaps between the bone and stem. Proximal contact was evaluated using the transverse CT scans of the proximal LVDT window and strain gauge locations. Proximally, the stem was in complete circumferential contact with the foam (Figure 3.1a). Below the mid-stem gauge (level 7) there was a small medial-posterior gap, but the majority of the stem circumference was in direct apposition to foam or reinforced epoxy (Figure 3.1b). Further distally, there was no contact between the prosthesis and the bone (Figure 3.1c).

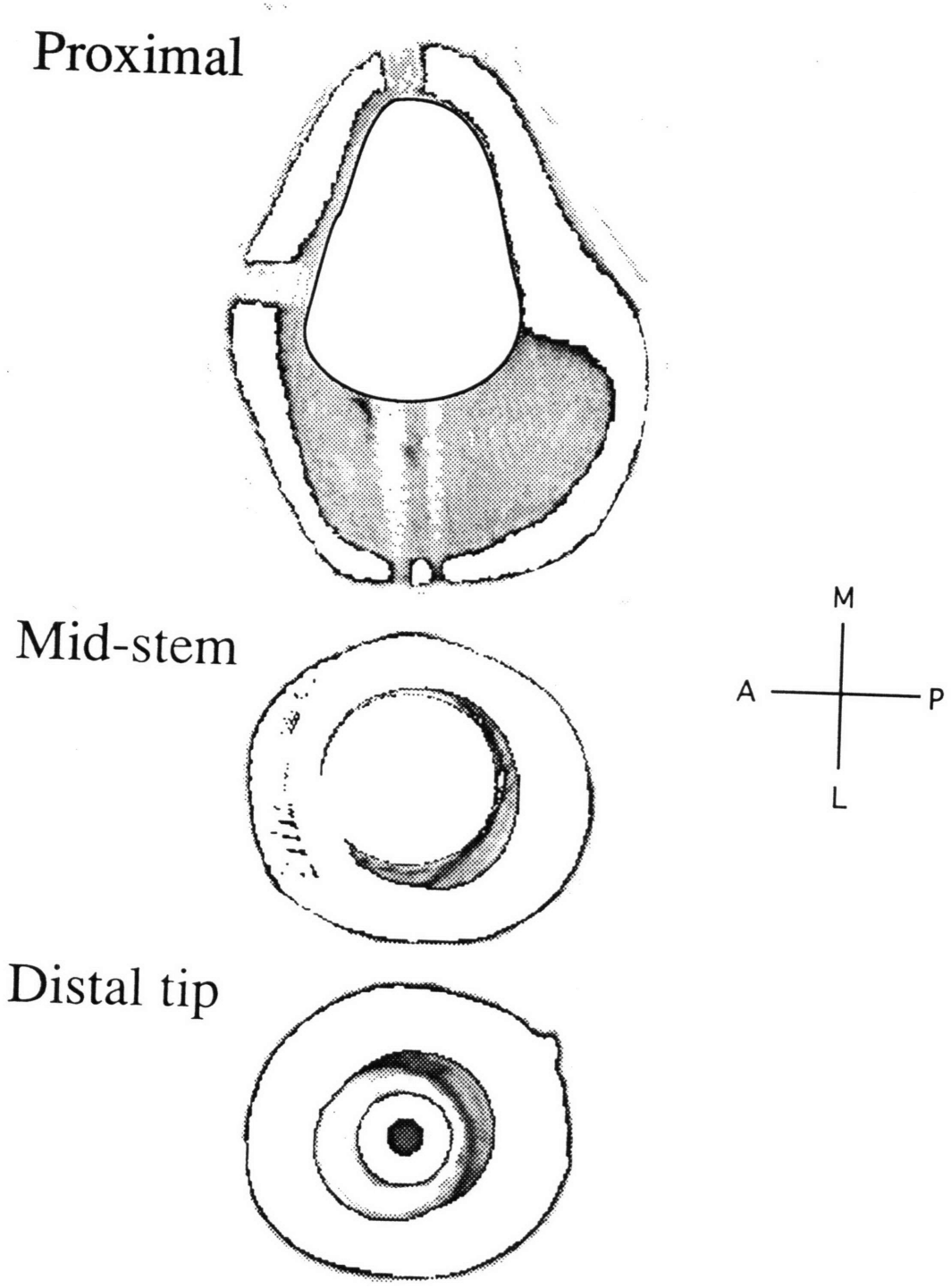

Figure 3.1 - Transverse CT scans of bone 2 showing bone-prosthesis contact at the (a) proximal (level 13), (b) mid-stem (level 7), and (c) distal tip (level 5) levels.

Four radiographs of bone 2 were taken - one each of the medial-lateral (ML) and anterior-posterior (AP) views as well as two from intermediate views (from the medial-anterior side (MA-LP) and from the medial-posterior side). It was not possible to determine the extent of the reamed canal on the radiographs and therefore, gaps could not be identified. However, the demarcation between the foam and the fiber reinforced epoxy was evident and it was possible to determine the areas of stem apposition to the epoxy.

Apposition of the prosthesis to the epoxy was evident in the ML and the MA-LP radiographs at the level of the mid-stem gauge (level 8) on the posterior and medial surfaces (Figure 3.2b and 3.2c). Proximally, at the level of the proximal gauge (level 12), there appeared to be only a small gap or possibly contact on the anterior and medial surfaces (Figures 3.2a and 3.2b). In general, the stem was positioned fairly centrally in the bone, with the stem curvature in the AP plane causing small areas of contact between the prosthesis and the fiber reinforced epoxy. This pattern of contact is probably generally consistent across bones, although there will be differences between bones due to variations in initial implant position. A scout view of bone 3 (not tested in this study, but prepared in the same manner) confirms that there was some variation in the implanted stem position (Figure 3.2d).

3.1.5 Simplified model

The relative motion of the distal target was measured by three orthogonal LVDT's. The LVDT's were oriented so that each gave an indication of one component of motion - axial, medial-lateral toggle or rotation. For any one bonding condition, the magnitude of the motion increased with load (Figures 3.3a, b and c). After unloading, there was some permanent motion in all three cases. In general, the rod primarily subsided with slight rotation and toggle to the lateral side. The greatest motion for all three components was observed with the 1/3 bonding case (Figure 3.4). As the extent of bonding increased, the

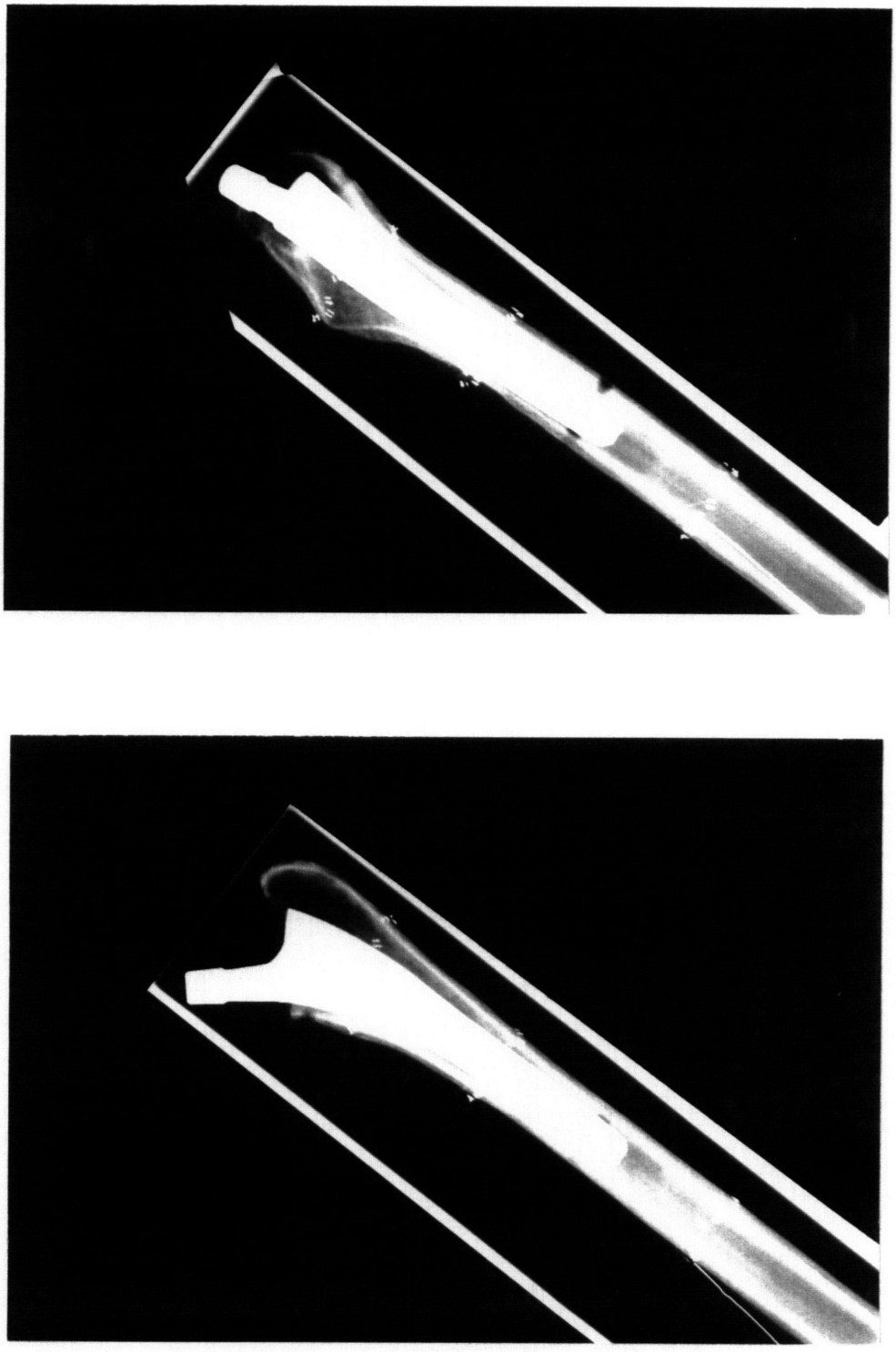

Figure 3.2 - Radiographs showing the position of the prosthesis in bone 2 from (a) medial-lateral and (b) anterior-posterior views.

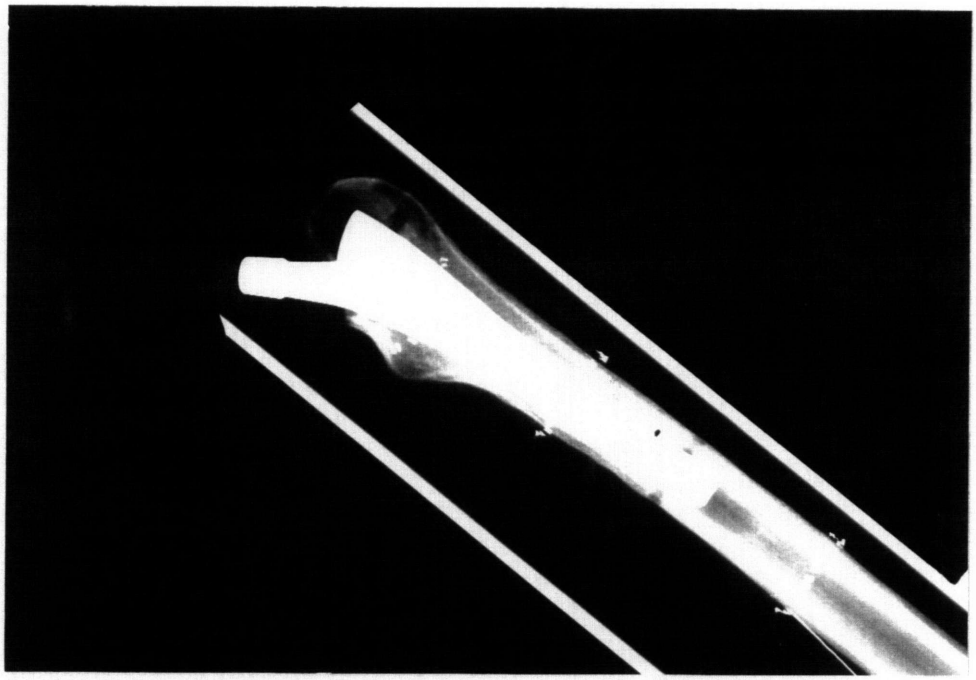

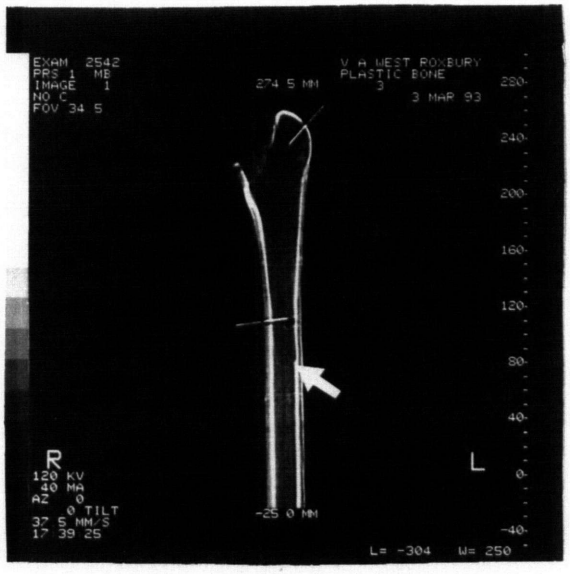

Figure 3.2 (continued) - (c) Radiograph showing the position of the prosthesis in bone 2 from the medial-anterior side; (d) Radiograph showing position of the prosthesis in bone 3. Note the difference in distal stem position from bone 2 (Fig. 3.2b).

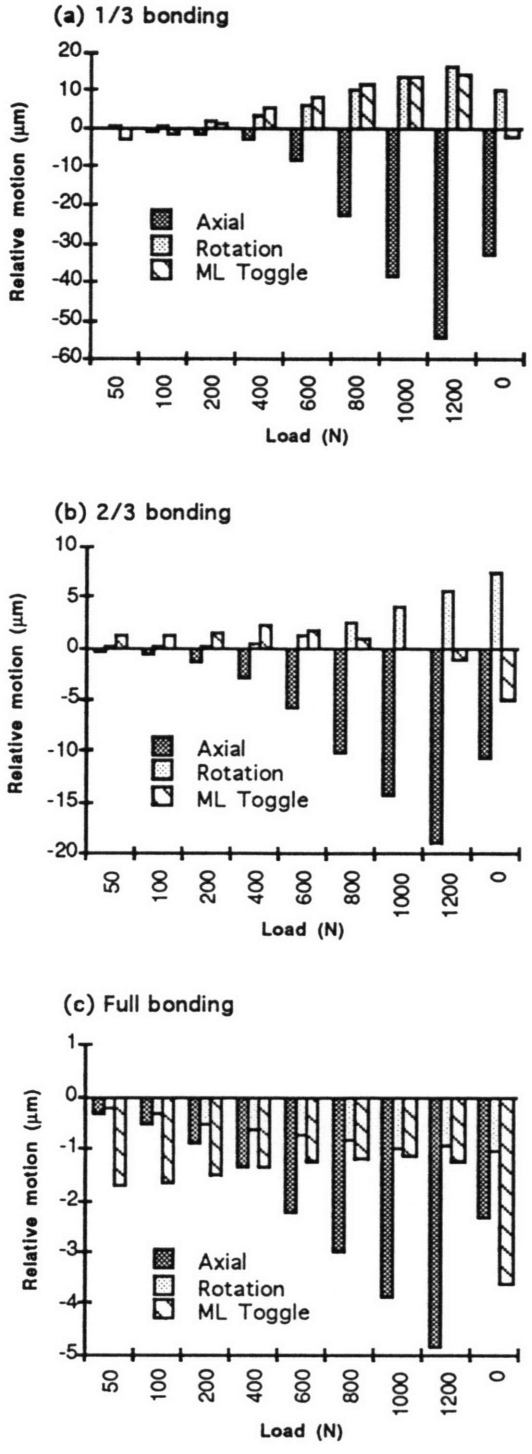

Figure 3.3 - Relative motion between the rod and tube with (a) 1/3 bonding, (b) 2/3 bonding, and (c) full bonding as a function of applied load.

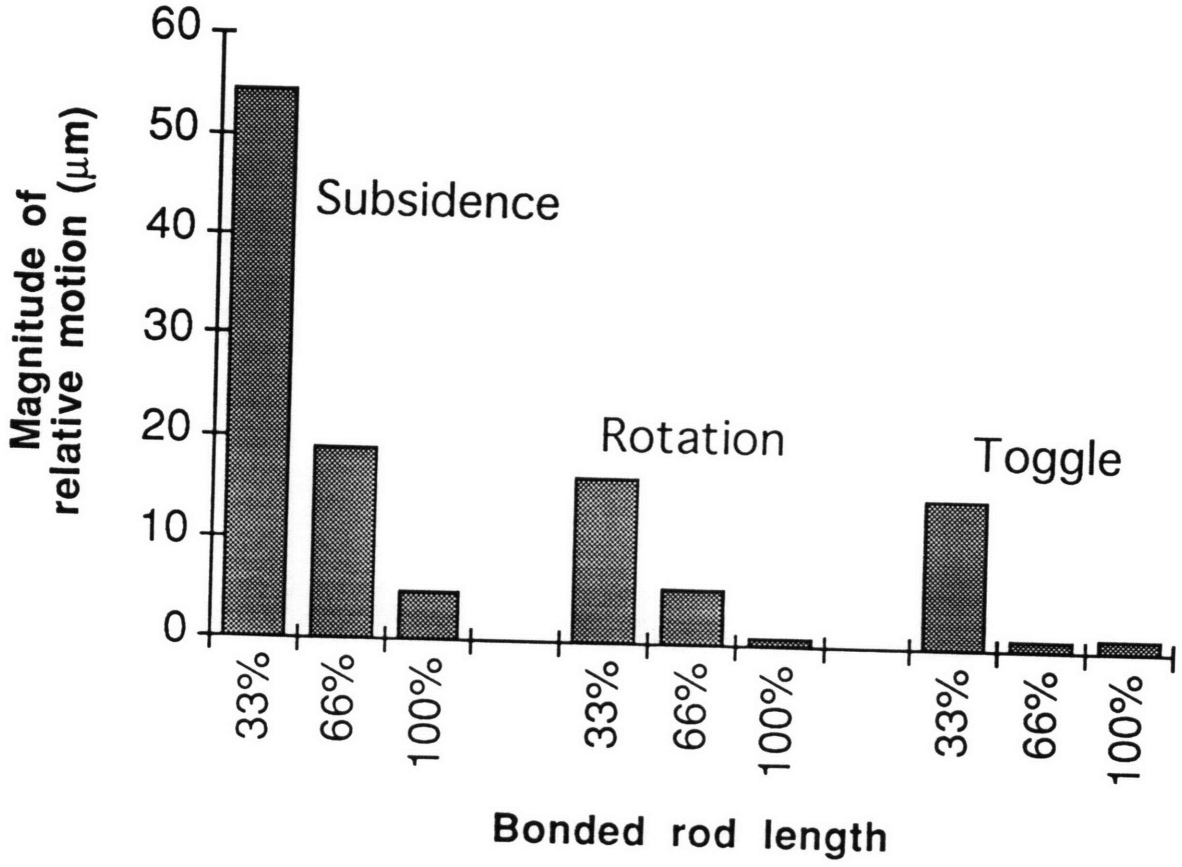

Figure 3.4 - Three components of the relative motion between the rod and the tube at maximum load (1200 N) as a function of bonding distribution.

magnitude of the motion of each of the components decreased. With full bonding, the motion was less than 5 micrometers for any component.

The extent of bonding was observed after removal of the rod, as evidenced by glue and/or foam residue on the rod. For all three cases, glue was confined to the desired region and provided complete coverage. The amount of foam remaining on the stem correlated with the degree of bonding. With 1/3 bonding, there was no foam left on the stem, whereas with 2/3 bonding there was some foam at the proximal end and with full bonding the proximal 2 cm were covered with a layer of foam around the entire circumference. This suggests that there was better proximal bonding to the foam when a greater volume of glue was applied to the rod.

3.2 STRAIN DATA

In order to investigate the effect of varying bonding distribution on stress shielding, surface strain measurements were made at proximal, mid-stem and distal levels of the bone. Axial and hoop surface strains at the gauge locations were measured. From these data, calculations of the magnitudes and locations of the maximum axial surface strains were made. Very few significant differences ($p<0.5$) were noted, probably due to the small sample size. Therefore, the results are presented without any reference to statistical significance with the understanding that only general trends were observed and more samples are required before statistically significant conclusions can be made.

3.2.1 Local axial strain

The trends in the variation of axial strain magnitudes with bonding distribution were consistent for both loading cases. Distally, there was little variation in axial strain with different bonding conditions on either the medial or posterior-lateral side (Figures 3.5c, 3.6c). At the mid-stem and proximal levels, however, the axial strain did vary with

different bonding conditions. In general, as the bonded surface was extended more distally, from 21% to 65% of stem length bonded, the axial strain magnitudes decreased (Figures 3.5a,b, 3.6a,b). The axial strains were minimal when there was 65% coating. With 81% and 100% coating, the axial strain magnitudes typically remained the same or increased from the when there was 65% coating.

The press-fit case did not consistently follow these trends. For single leg loading, the distal axial strains were similar to those for the other bonding cases. Proximally, the axial strains were the highest at both rosette locations. However, at the mid-stem level, the axial strains for the press-fit case were lower than those when there was 21% bonding and similar to the strains with 36% bonding. With stair-climb loading, similar trends were observed at the distal and mid-stem levels. Proximally, the axial strain magnitudes were the lowest for the press-fit case.

Consistent with single leg stance loading, the medial axial strains were compressive and the lateral axial strains were tensile at the distal and mid-stem levels (Figure 3.5). When loading in stair climb, the axial strains were compressive on the medial and posterior-lateral surfaces at the mid-stem and distal levels, as expected (Figure 3.6). Proximally, the behavior changed for both loading cases due to the influence of the prosthesis. In single leg stance, both the anterior-medial and posterior strains were compressive; the abductor muscle also played a role in the proximal strain distribution. In stair climb the anterior-medial axial strains were tensile and the posterior axial strains were compressive.

In stair climb load the distal strain magnitudes were higher than when loaded in single leg stance. For instance, the distal maximum strains (normalized to the magnitude of the resultant head load) were over 3 times greater in stair climb. At the mid-stem level, the strains were approximately equal with each loading case. Proximally, the strains were higher in single leg stance, probably in part due to the abductor. The variation in strain along the length of the bone was more prominent with the stair climb loading. For

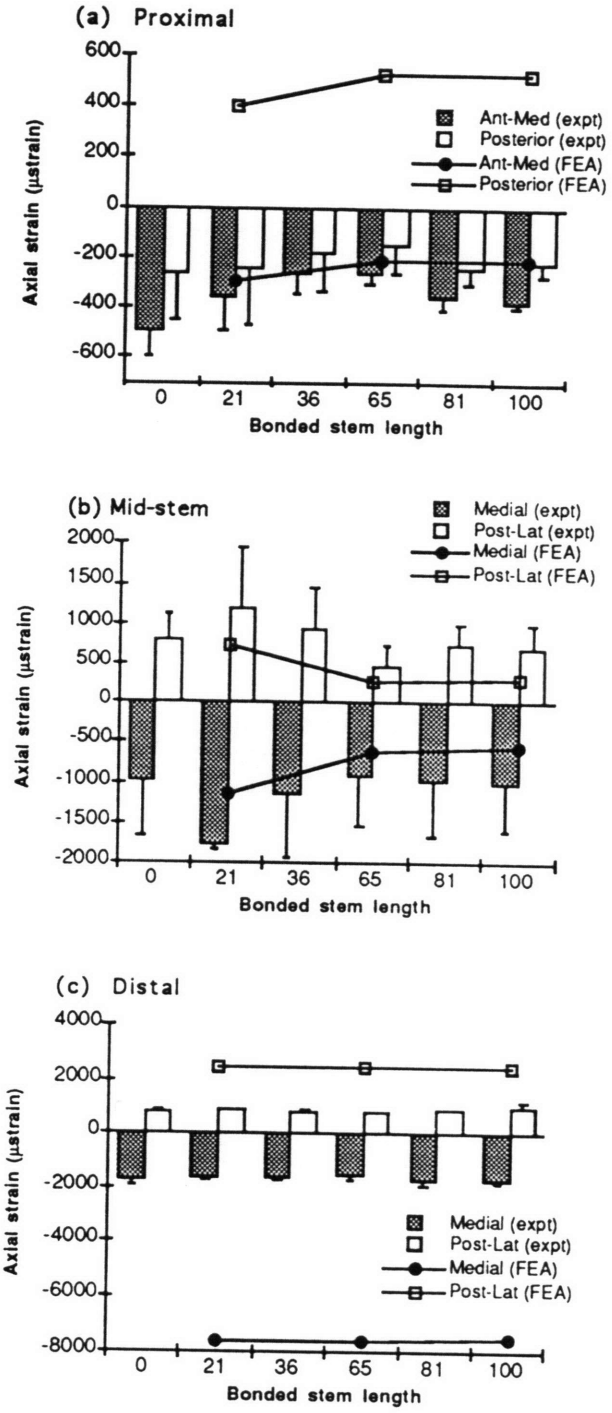

Figure 3.5 - Experimental and FEA axial surface strains at (a) proximal, (b) mid-stem, and (c) distal rosette locations as a function of bonding distribution (Single leg stance, 650 N BW)

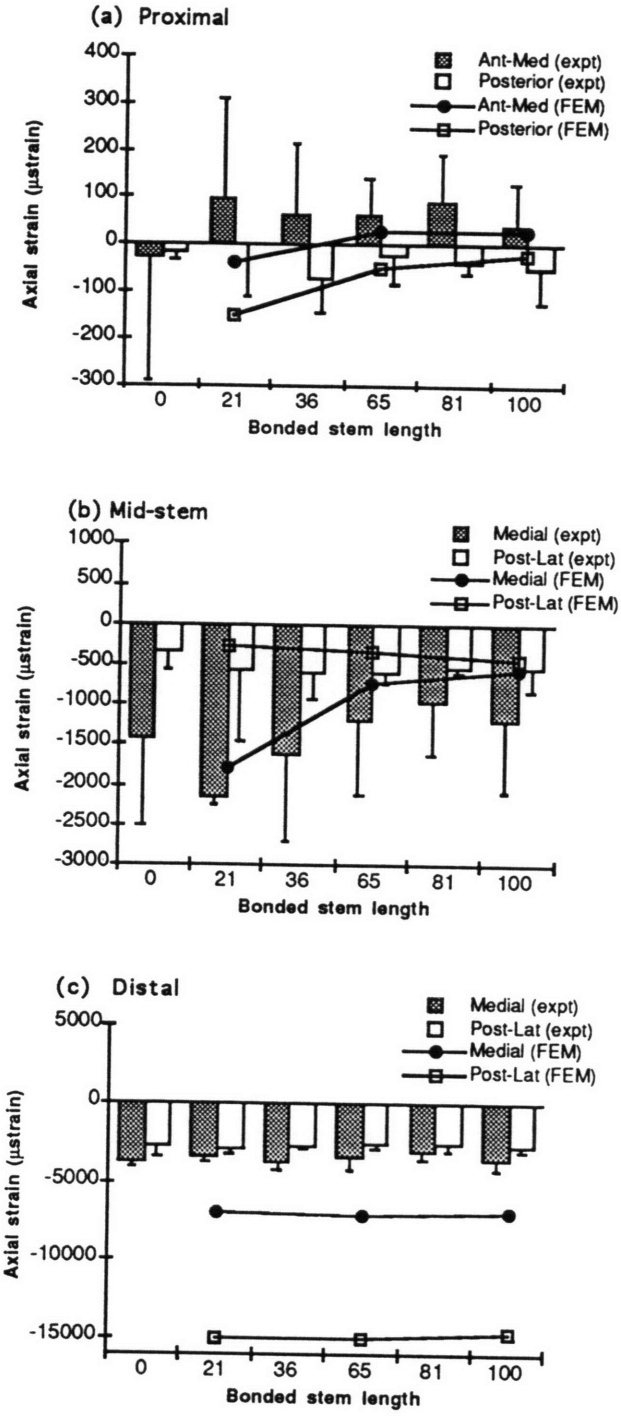

Figure 3.6 - Experimental and FEA axial surface strains at (a) proximal, (b) mid-stem, and (c) distal rosette locations as a function of bonding distribution (Stair climb stance, 1000 N)

instance, the maximum strains decreased by a factor of more than 10 from the distal to proximal level. However, with single leg loading the maximum strains decreased slightly from distal to mid-stem level, but not at the proximal level (again due to the abductor).

3.2.2 Local hoop strain

Some of the trends observed for the hoop strain magnitude variations are similar to those for axial strain magnitudes. For instance, in both loading cases the hoop strain magnitudes at the distal level remained approximately constant regardless of bonding condition (Figures 3.7c, 3.8c). Proximally, the hoop strains decreased in magnitude as coating was extended distally from 21% to 65% of stem length (Figures 3.7a, 3.8a). As was observed with axial strain, with 81% and 100% coating the hoop strain magnitudes typically remained the same or increased slightly from the strains when there was 65% coating. This trend was observed at the mid-stem level as well, except for the posterior-lateral hoop strains under stair-climb loading (Figures 3.7b, 3.8b). At this rosette, the hoop strains increased slightly with more distal coating.

As with the press-fit axial strains, the press-fit hoop strains did not follow the trends. Distally, they were similar to those for the other bonding cases. For both loading cases, at the proximal and mid-stem levels the hoop strain magnitudes were less than those for 21% coating, and similar to the strains for the 36% or 65% coating cases.

3.2.3 Axial strain contours and maximal strains

The maximal axial strains calculated from the axial strain contours follow similar trends to the local axial strains (as expected). Distally there is little variation in the magnitude of maximal tensile or compressive strains (Figures 3.9c, 3.10c). At the mid-stem and proximal levels, the maximal strains decreased as the coating was extended distally to a minimum, usually at 65% coating (Figures 3.9a,b, 3.10a,b). With more distal

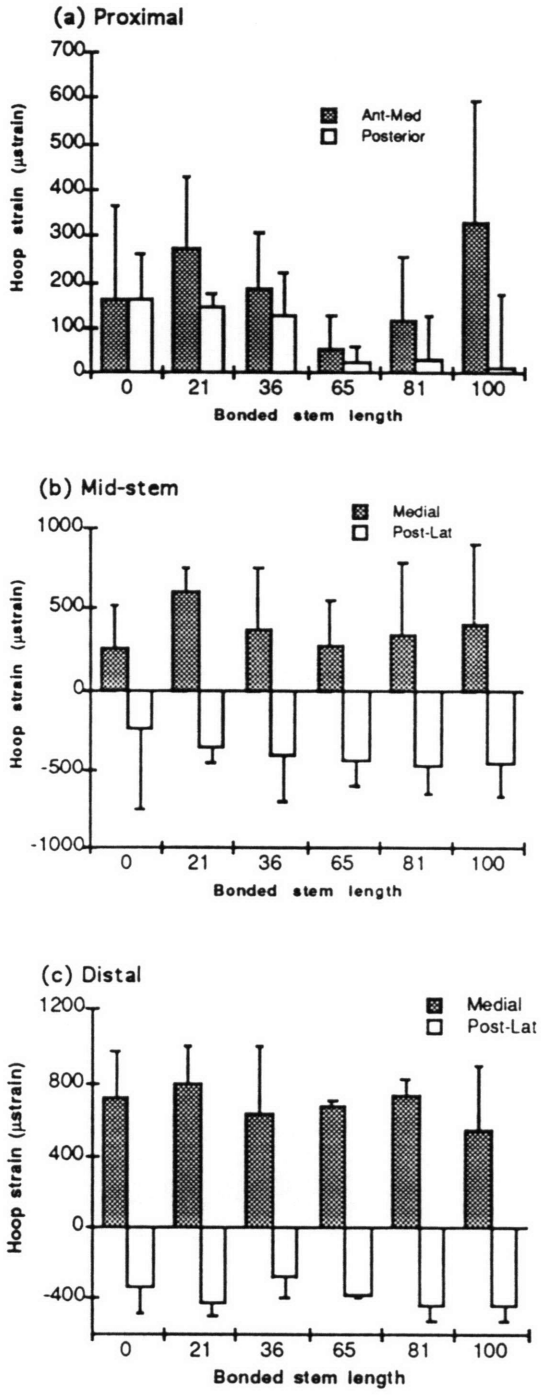

Figure 3.7 - Experimental hoop surface strains at (a) proximal, (b) mid-stem, and (c) distal rosette locations as a function of bonding distribution (Single leg stance, 650 N BW)

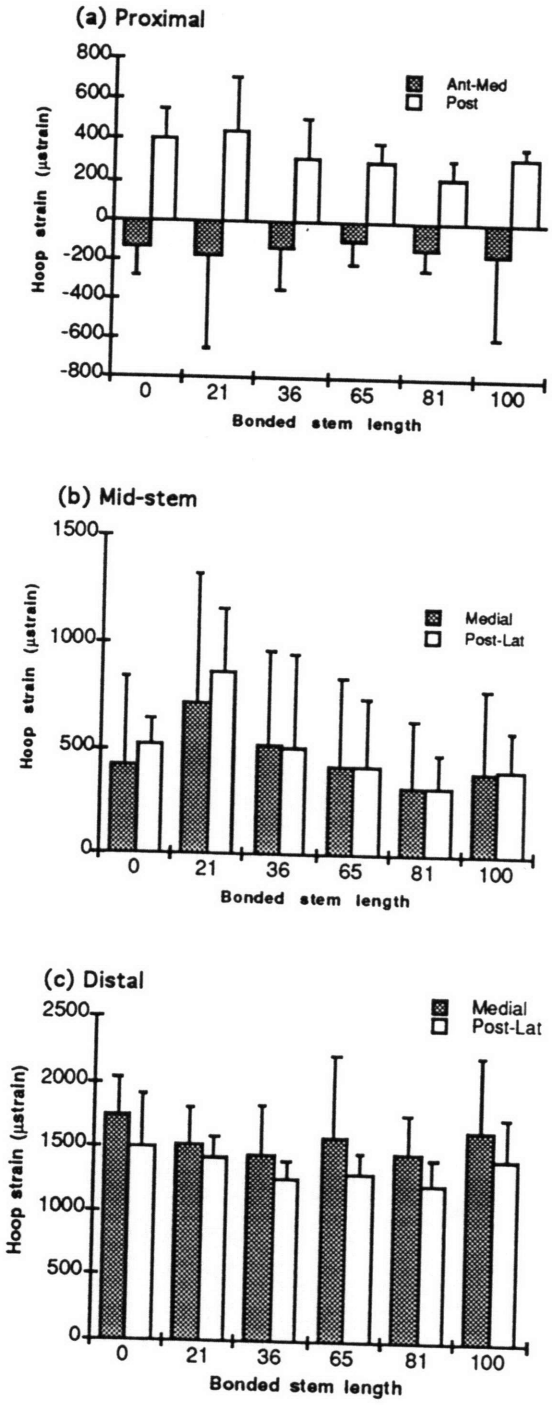

Figure 3.8 - Experimental hoop surface strains at (a) proximal, (b) mid-stem, and (c) distal rosette locations as a function of bonding distribution (Stair climb stance, 1000 N)

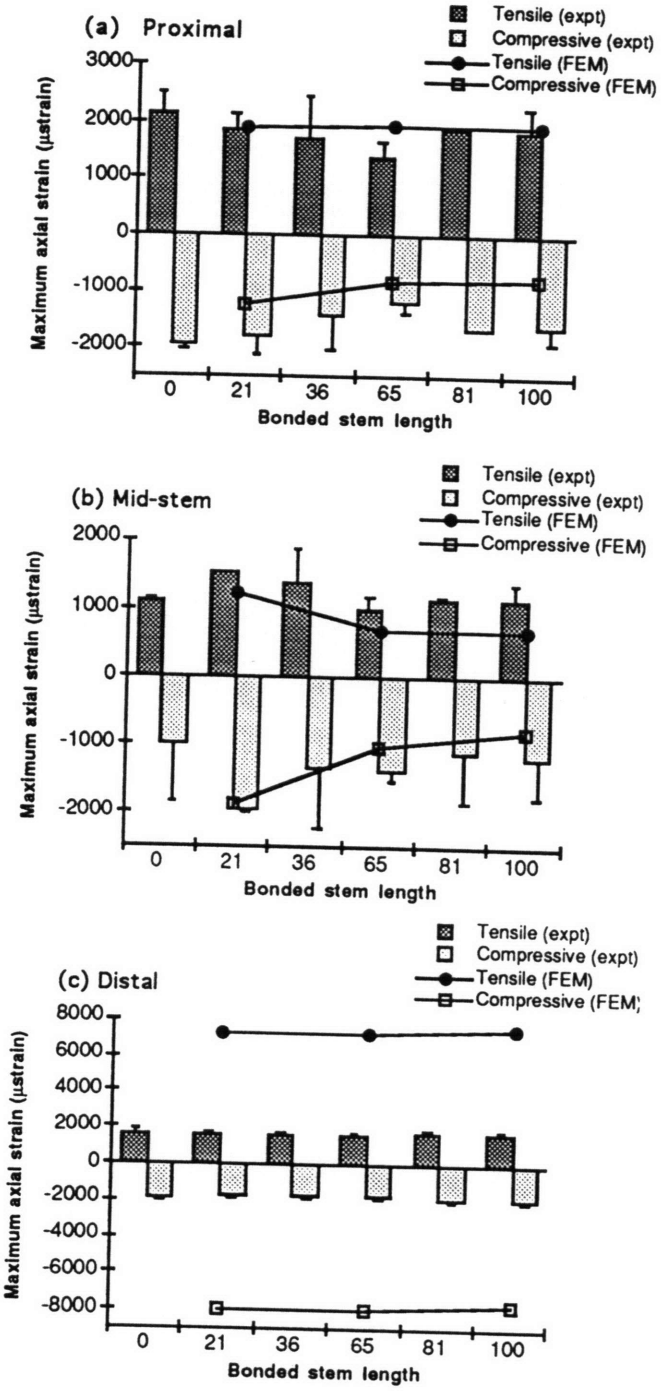

Figure 3.9 - Experimental and FEA maximum axial surface strains at (a) proximal, (b) mid-stem, and (c) distal rosette locations as a function of bonding distribution (Single leg stance, 650 N BW)

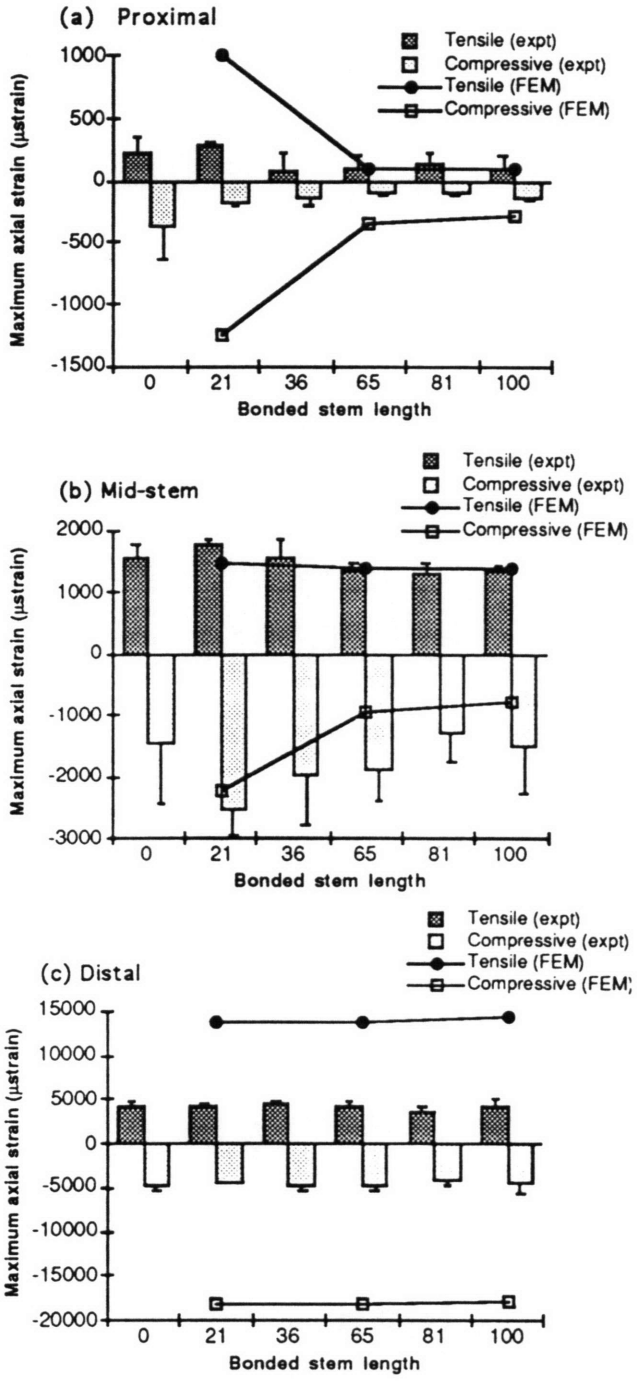

Figure 3.10 - Experimental and FEA maximum axial surface strains at (a) proximal, (b) mid-stem, and (c) distal rosette locations as a function of bonding distribution (Stair climb stance, 1000 N)

coating, the strains remained approximately the same or increased from the minimum at 65% coating.

The locations of the distal maximum strains were consistent with the loading configurations (Figures 3.11 and 3.12). Further indication of the influence of the prosthesis proximally was the change in the position of the maximum strains from the distal to mid-stem and, in particular, from the mid-stem to proximal levels. In single leg stance, the locations of the maximum strains at a particular level was fairly consistent, regardless of the bonding condition. The variation between bones was also minimal. In stair climb stance, however, there was a lot of variation at the proximal level both with bonding condition and between bones. The large variation may in part be attributable to the low strain magnitudes which are more vulnerable to small variations and experimental error.

3.3 RELATIVE MOTION DATA

The effect of varying the bonding distribution on relative motion was determined by measuring the relative motion between the bone and a target attached to the prosthesis at proximal and distal stem levels. Measurements of the target motion from single LVDT's (uni-axial motion) were used for comparisons. Very few significant differences were noted, probably due to the small sample size. Therefore, the results are presented without any reference to statistical significance with the understanding that only general trends were observed and more samples are required before statistically significant conclusions can be made.

Calculation of the interface motion from the target motion was made for a single bone (bone 5).

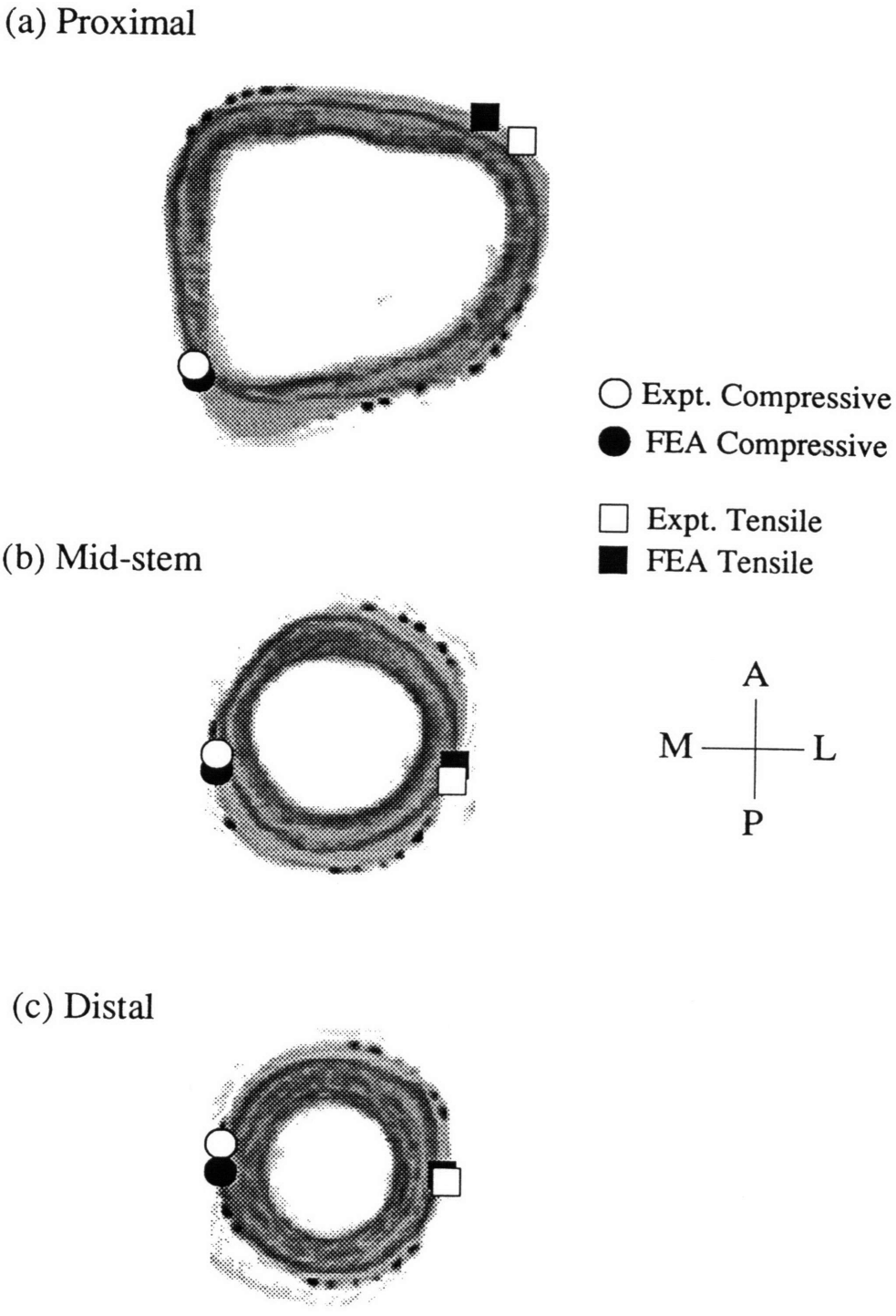

Figure 3.11 - Experimental and FEA locations of maximum axial surface strains at (a) proximal, (b) mid-stem, and (c) distal rosette levels for single leg stance (650 N BW, 65% bonding)

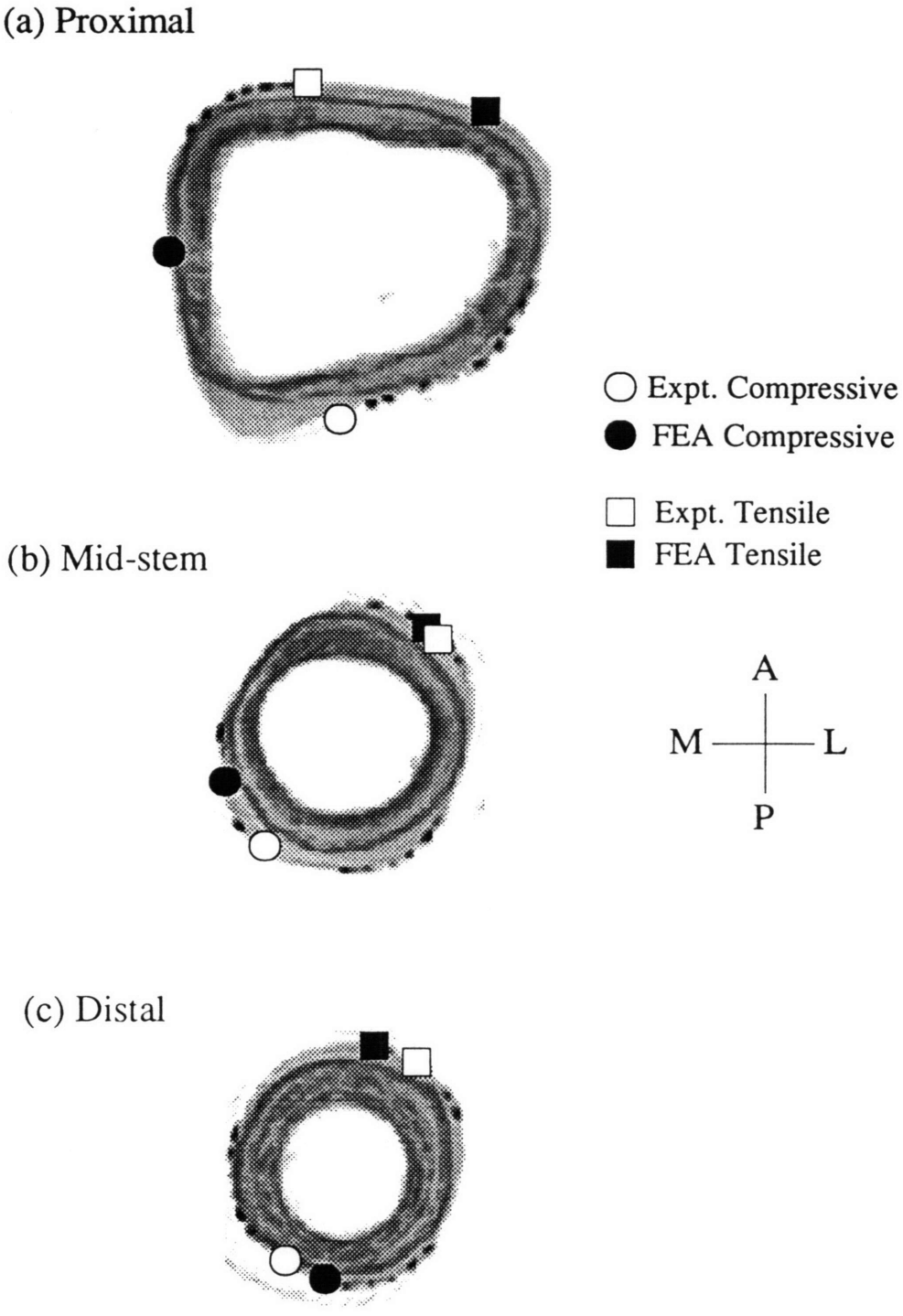

Figure 3.12 - Experimental and FEA locations of maximum axial surface strains at (a) proximal, (b) mid-stem, and (c) distal rosette levels for stair climb stance (1000 N, 65% bonding)

3.3.1 Uni-axial measurements

Despite the large variability in the motion measurements some general, but not entirely consistent trends were apparent. Proximally, for the most of the bonded cases (21% to 100%), the target moved 10 μm on average, with a maximum of 20 μm (Figures 3.13, 3.14). However, there were some cases where significant motion did occur, indicating that the prosthesis moved despite the bond or that the LVDT and/or bracket was dislodged. Accordingly, the average motion of the three bones for these bonding conditions is artificially high; this is reflected in the standard deviations which are much greater than the means.

There tended to be a decrease in motion at the distal tip when the bond was extended more distally (Figures 3.15, 3.16). The rate of decrease in motion with more distal bonding was usually not linear. Instead, the tendency was for the motion to decrease sharply from 21% to 36% or 36% to 65% bonding and decrease only slightly as the bond was extended more distally (similar to a decaying exponential). For instance, the rate at which the motion decreased from 21 to 36% bonding was over 21 times the rate of decrease from 65% to 81% bonding for the LVDT measuring ML toggle in stair climb stance (Figure 3.16d). In some cases with full bonding, this trend was not followed as the axial component of motion tended to increase relative to 81% bonding. Since no motion would be expected for the fully bonded case, this suggests that the distal end of the prosthesis may not have been adequately bonded to the bone. In those cases where the motion did not increase with distal bonding, the decrease relative to the neighboring bonding condition was minimal, which follows the trend observed for more proximal bonding conditions.

The press-fit prostheses experienced large motions when loaded initially and then less motion for the subsequent similar loading case (Figure 3.17). In fact, the motion measured by all the LVDT's (other than 7 and 8) was maximal with the initial single leg stance load, even when compared with the stair climb loading cases (Figure 3.17b). With

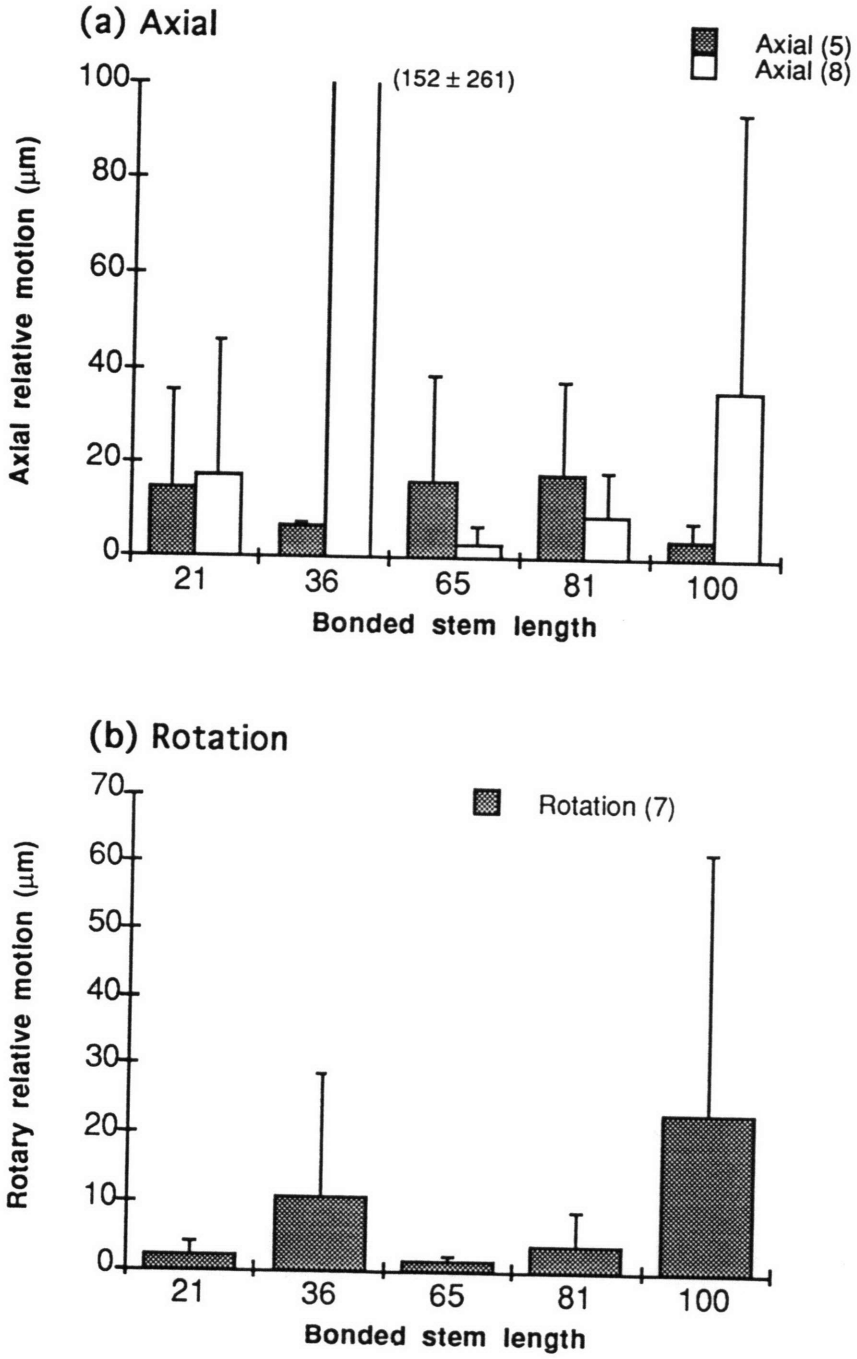

Figure 3.13 - Magnitude of (a) axial and (b) rotation components of proximal relative motion as a function of bonding distribution (Single leg stance, 650 N BW)

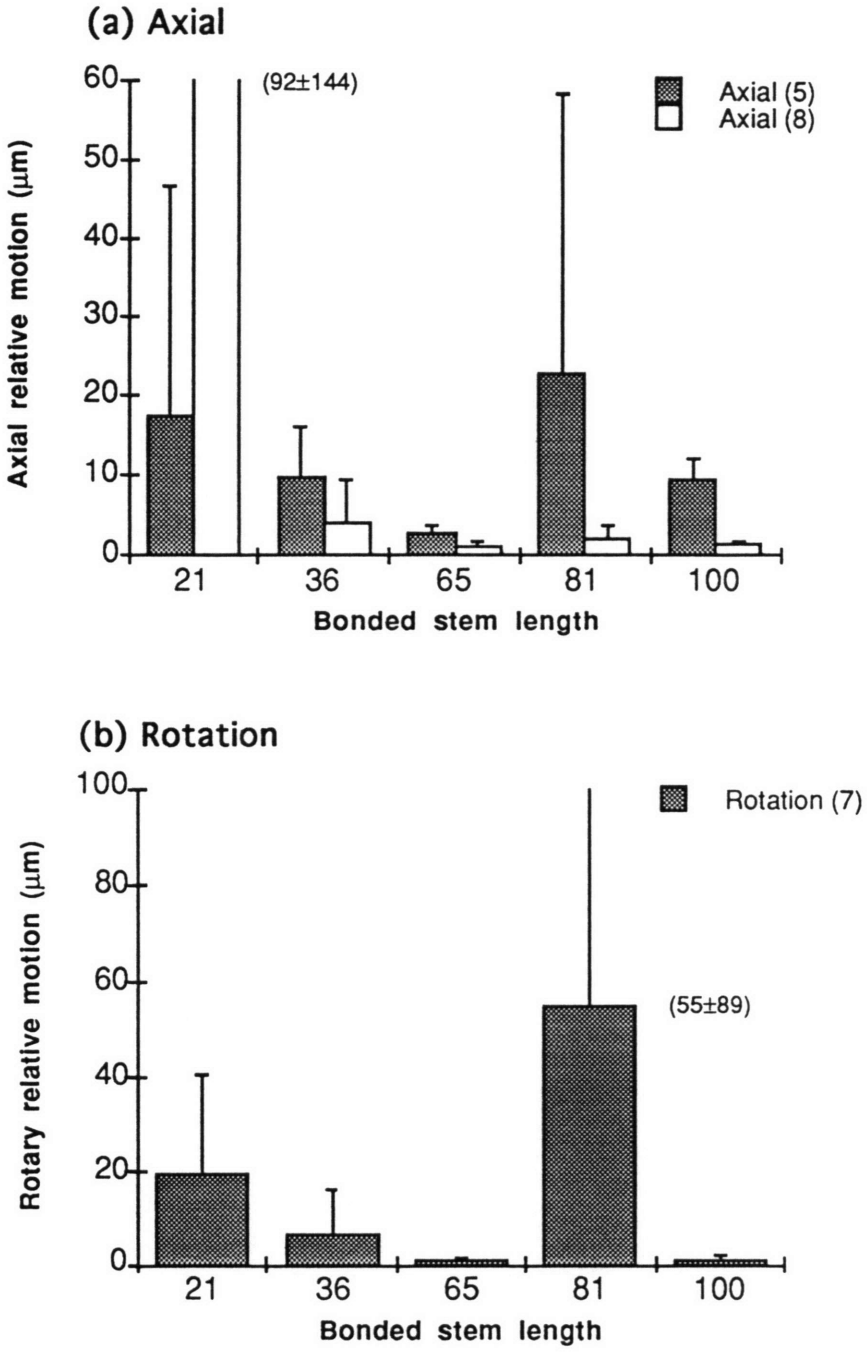

Figure 3.14 - Magnitude of (a) axial and (b) rotation components of proximal relative motion as a function of bonding distribution (Stair climb stance, 1000 N)

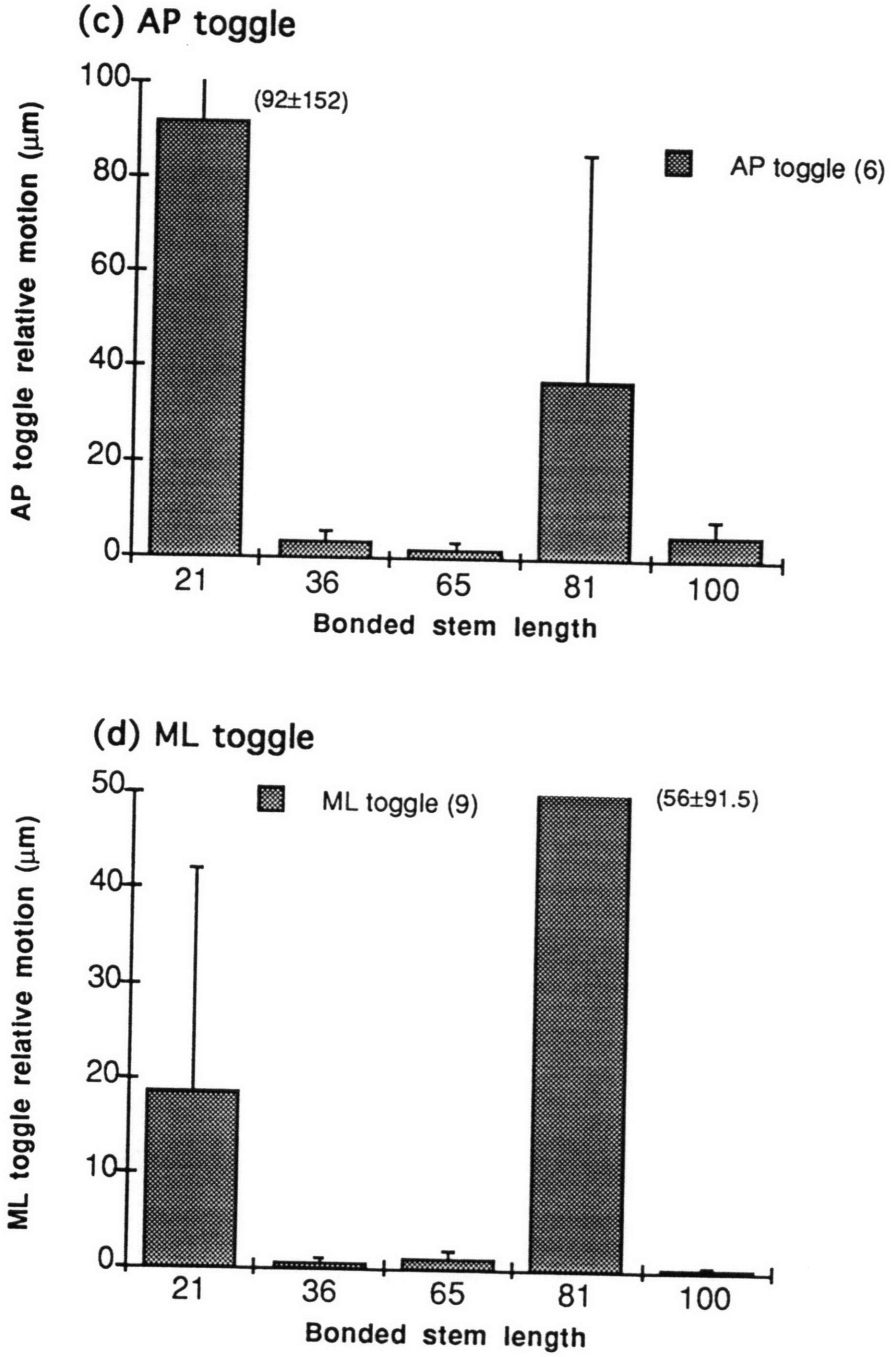

Figure 3.14 (continued) - Magnitude of (c) AP toggle and (d) ML toggle components of proximal relative motion as a function of bonding distribution (Stair climb stance, 1000 N)

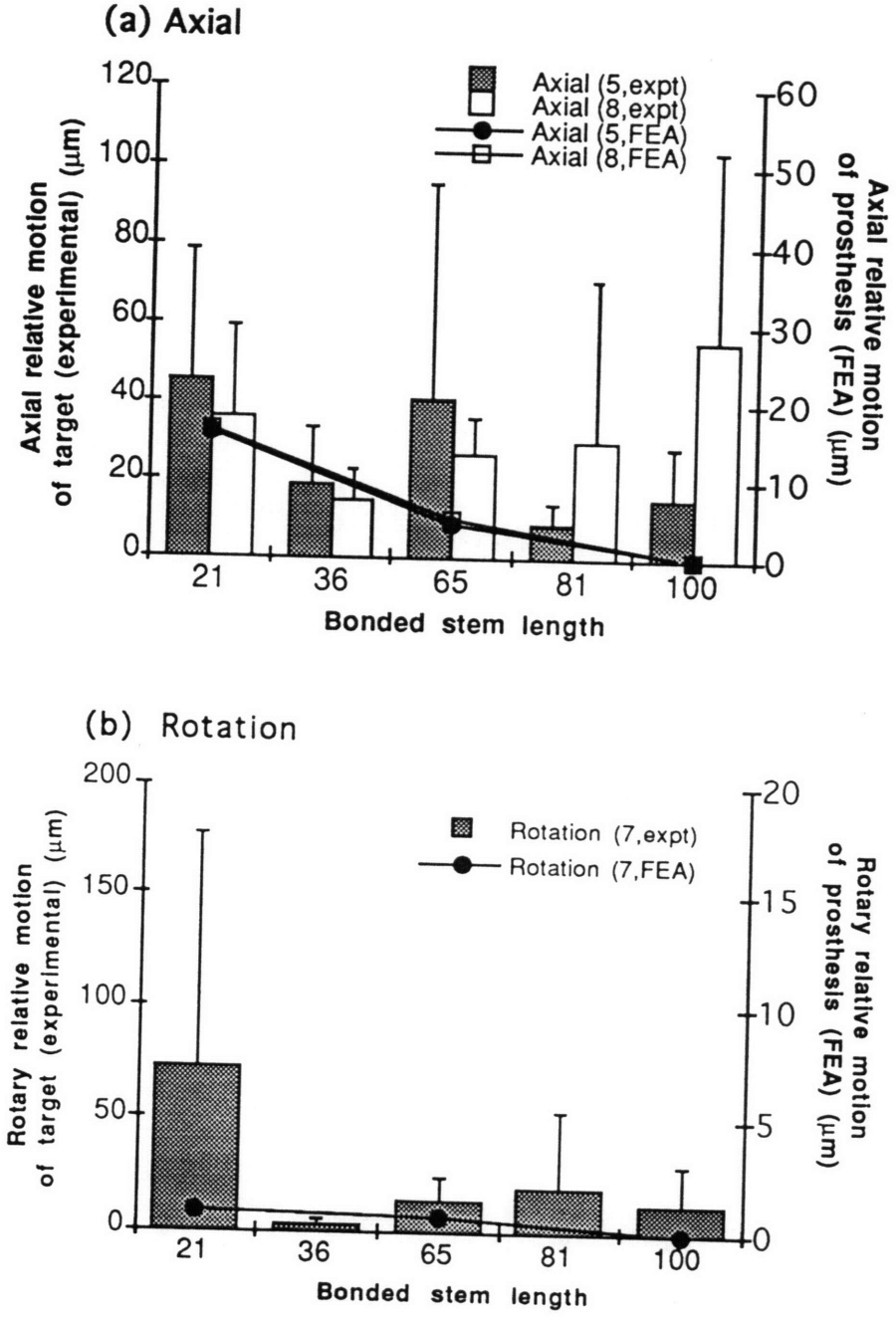

Figure 3.15 - Magnitude of (a) axial and (b) rotation components of distal relative motion as a function of bonding distribution (Single leg stance, 650 N BW)

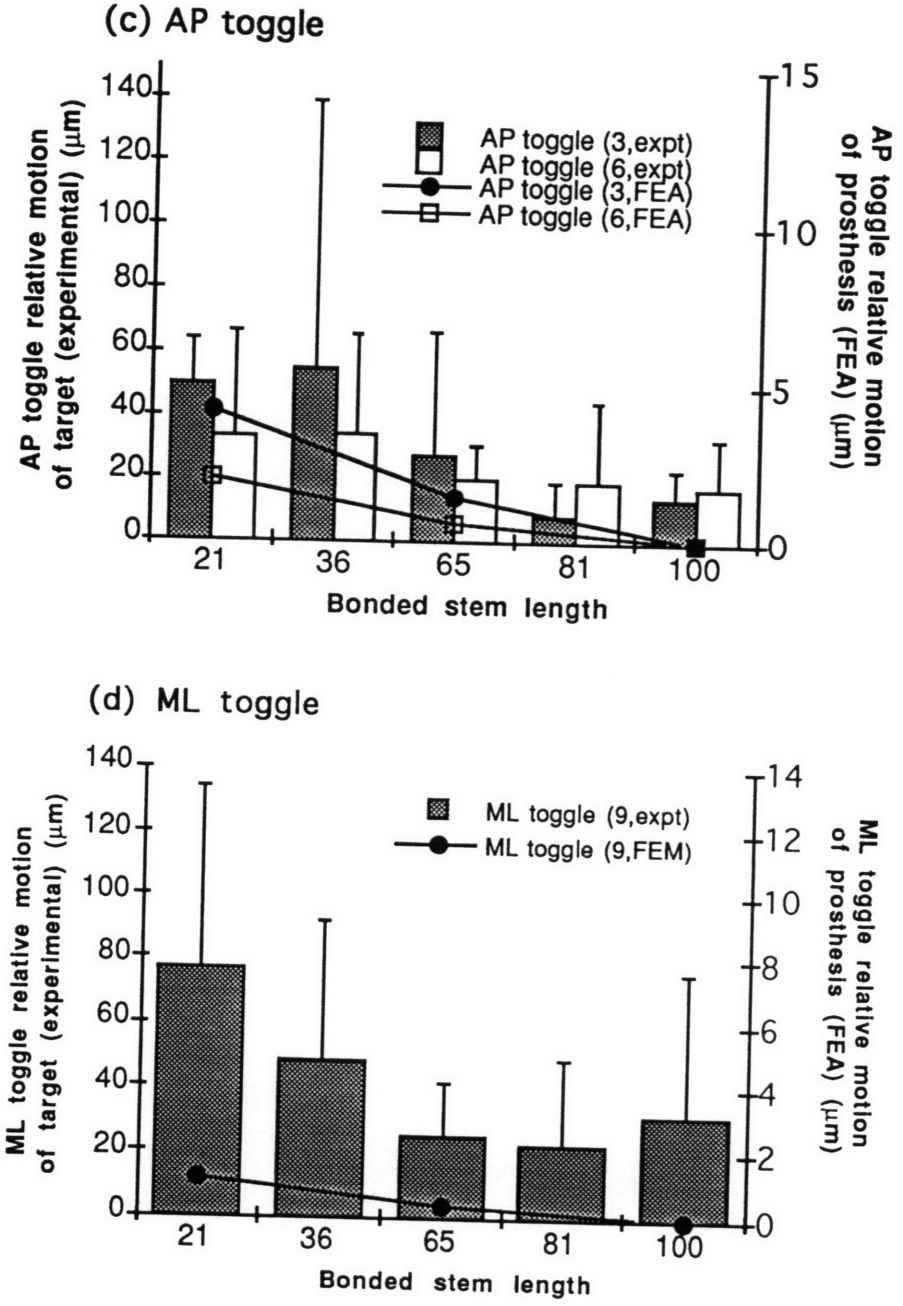

Figure 3.15 (continued) - Magnitude of (c) AP toggle and (d) ML toggle components of distal relative motion as a function of bonding distribution (Single leg stance, 650 N BW)

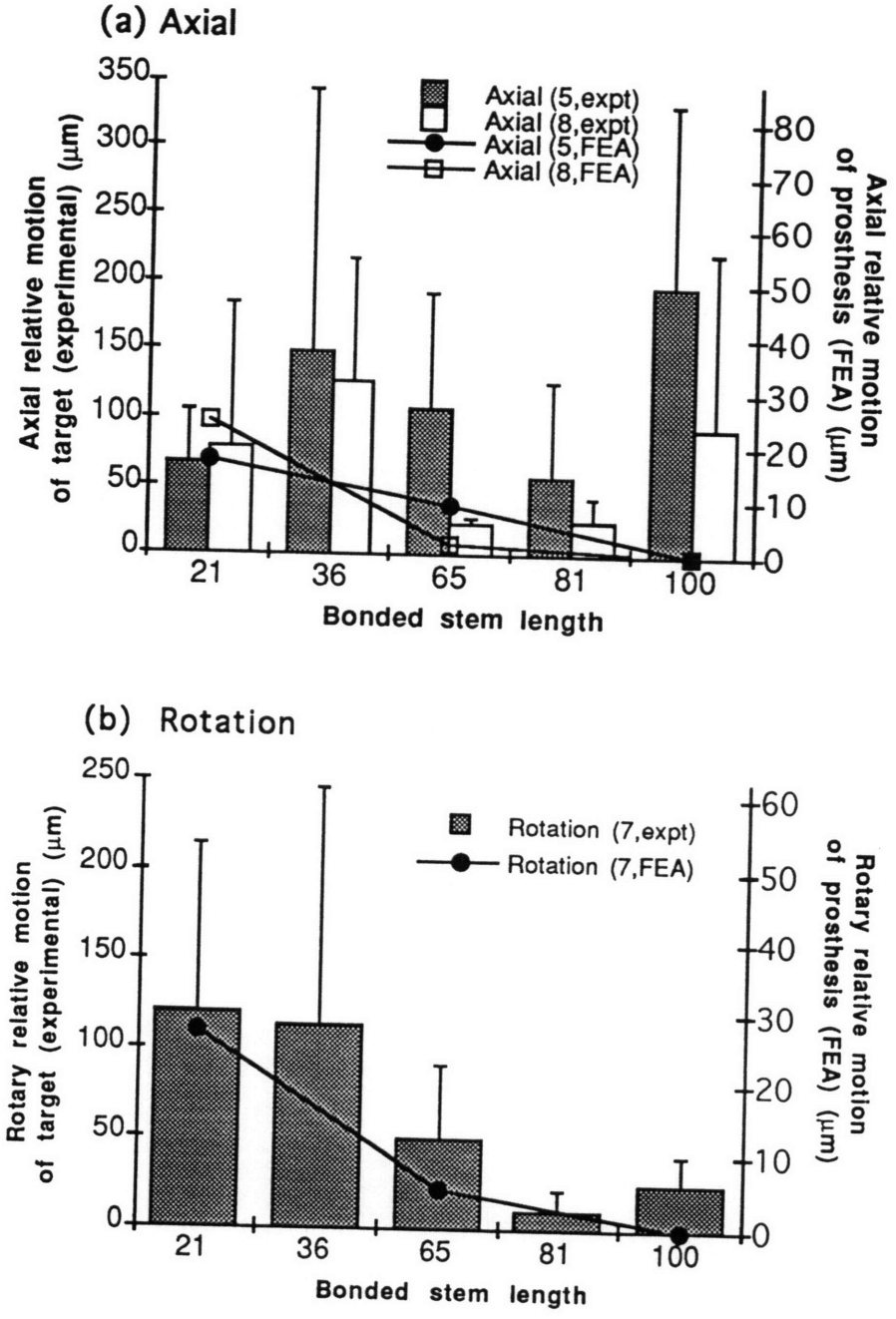

Figure 3.16 - Magnitude of (a) axial and (b) rotation components of distal relative motion as a function of bonding distribution (Stair climb stance, 1000N)

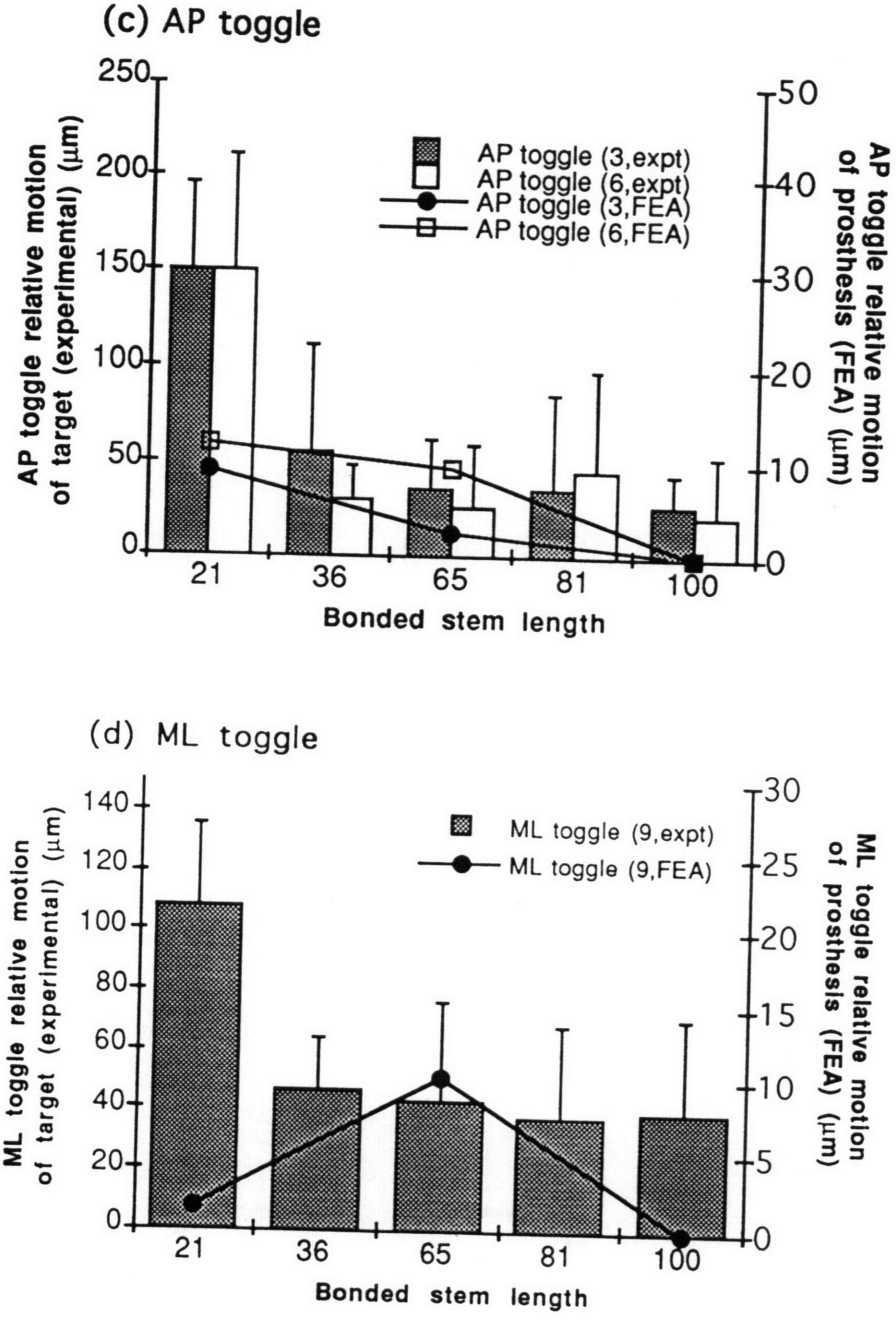

Figure 3.16 (continued) - Magnitude of (c) AP toggle and (d) ML toggle components of distal relative motion as a function of bonding distribution (Stair climb stance, 1000 N)

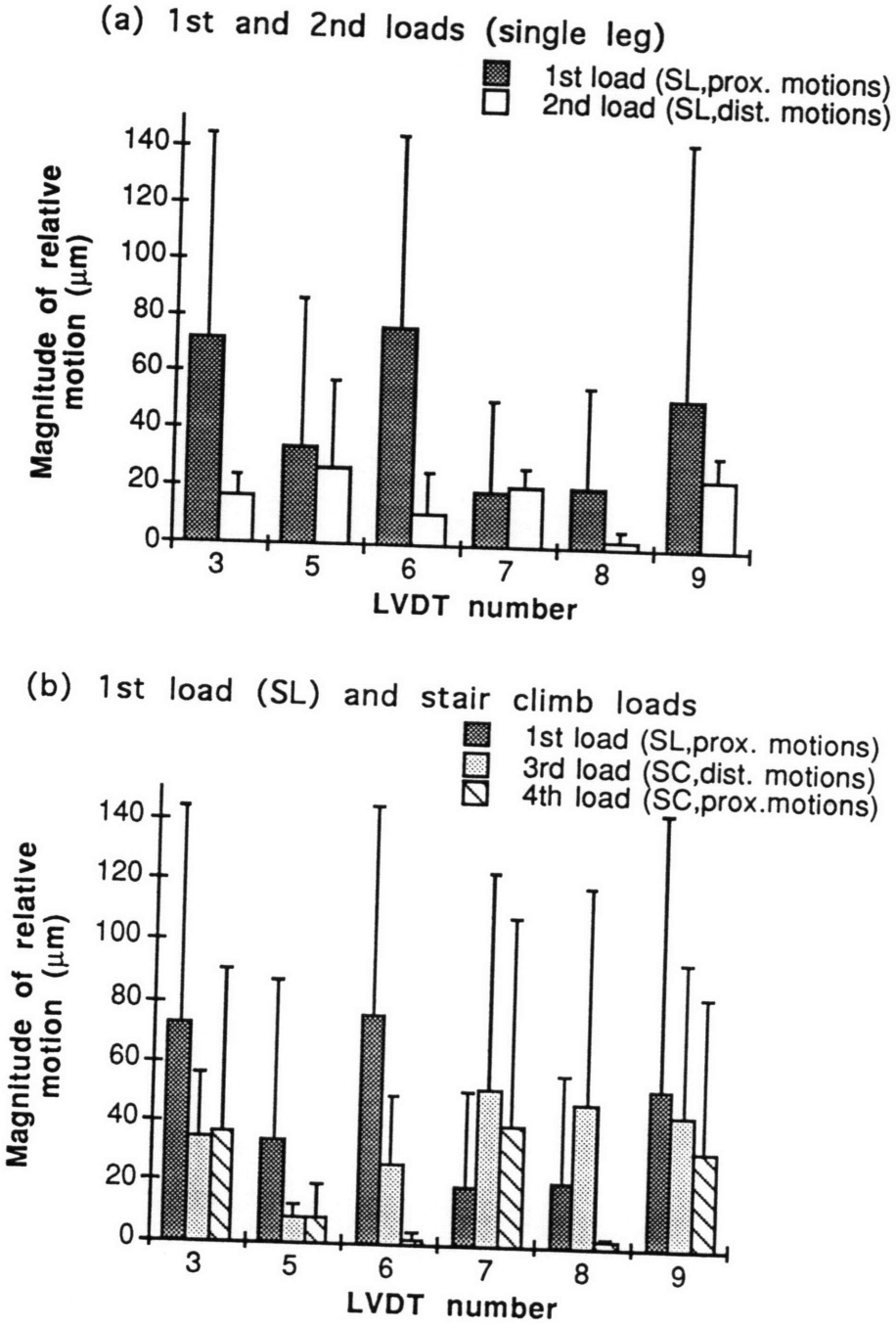

3.17 - Settling and wedging of the press-fit prostheses illustrated by a comparison of relative motions between (a) first and second loads in single leg stance, and between (b) the initial single leg stance load and subsequent stair climb loads.

bonded prostheses, however, the largest motions were observed with stair climb loads and at the distal end. The fact that the proximal motions in single leg stance are the greatest for the press-fit stems suggests that settling occurred during first loading cycle providing a fit that was better than could be achieved by hand. In effect, the press-fit prostheses had a better fit for the final three loading cases than did the most proximally bonded prostheses, due to the large initial motion which would tend to wedge the prostheses in the medullary canal.

The largest motions were observed with stair climb loads which produced large motions for all the components - axial, rotation and toggle (AP and ML) (Figure 3.16). Single leg stance loads, however, did not produce much rotary or ML toggle motion (Figures 3.16b,d) consistent with the in-plane loading. However, the relatively large AP toggle motions suggest that the loading was not isolated to the plane or that the complicated geometry of the prosthesis was creating a moment about the ML axis.

3.3.2 Interface motion

Calculation of the interface motion from the target motion required a complete set of data (all 9 LVDT's). Because some data was excluded, these calculations were not performed for all the bones. Instead, the interface motion for a single bone (bone 5) was determined and the target and interface motions were compared.

As expected, the maximum target motions were 1.5 to 3.4 times greater than the maximum interface motions (Figure 3.18a). The fact the maximum motions trends were somewhat different between the target and the interface indicates the complexity of the motion and the inadequacy of uni-axial site-specific target motions to completely characterize the movement. Comparison of the axial and tangential components of the interface motion to the uni-axial motions measured by LVDT's 7, 5 and 8 confirmed that the uni-axial measurements were coupled and, therefore, did not accurately describe the relative motion at the interface (Figure 3.18b,c).

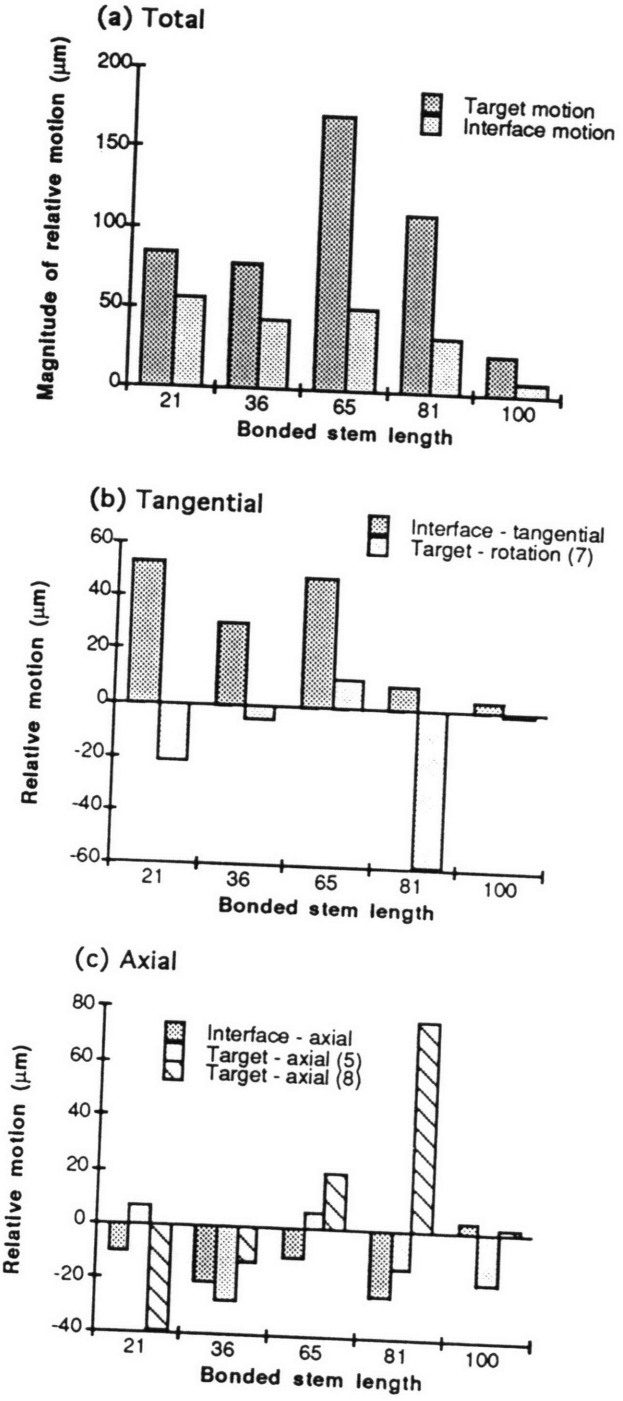

Figure 3.18 - Comparison of the measured target motion and the calculated interface motion: (a) magnitudes of motion vector; (b) tangential components; and, (c) axial components (Single leg stance, 650 N BW).

3.4 REPEATED TEST RESULTS

A single test was repeated (Bone 6, 100% bond) to get an indication of repeatability of the tests. In both loading cases there was good agreement between the axial surface strains for the original and repeated tests (Figure 3.19). In general for the original test, the strains were slightly higher in single leg stance and slightly lower in stair climb stance, although the differences were minor.

However, there was much more variation in the motion measurements between the original and repeated tests (Figure 3.20). The repeated test experienced large motions, even in the proximal region despite full bonding. A time history of the loading showed that there was a large permanent initial movement (particularly proximal AP toggle), after which the trend and magnitudes of the motion with increasing load were similar to the first trial. Although radiographs were not taken, it was evident during implantation that the position of the prosthesis was not consistent with previous trials; this may explain some of the differences between trials.

3.5 FINITE ELEMENT ANALYSIS

The finite element model (Ramamurti 1992) was modified to match the experimental conditions and the analyses repeated for comparison with the experimental data. The purpose of this comparison was to validate the FEM. Local axial surface strains and the magnitudes and locations of maximum axial surface strains were compared. Trends in relative motion were compared. However, magnitudes were not compared since the FEA predicted interface motion and the target motion was measured in the experiment.

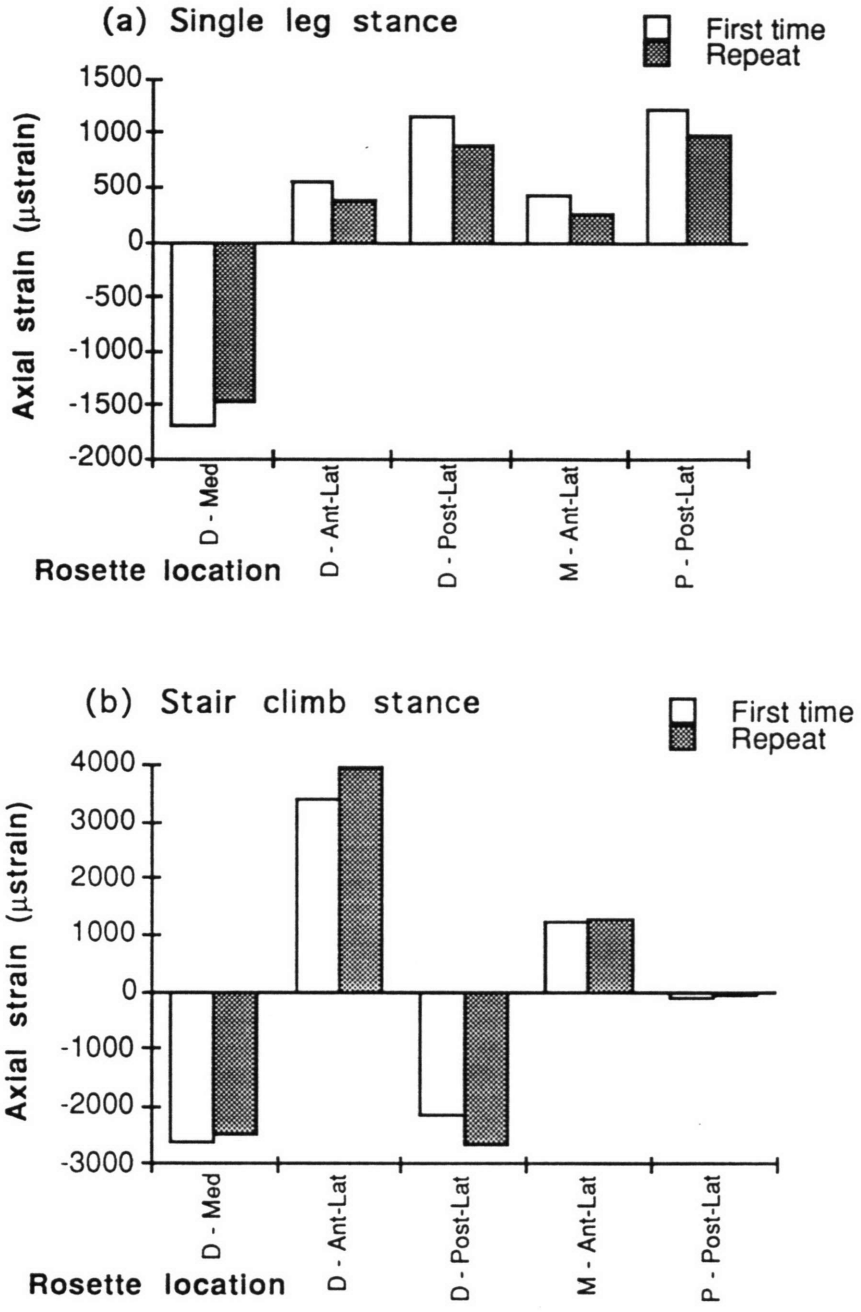

Figure 3.19 - Axial surface strains at various rosette locations with (a) single leg loading (650 N BW) and (b) stair climb loading (1000 N) for the repeated test (bone 6, 100% bond).

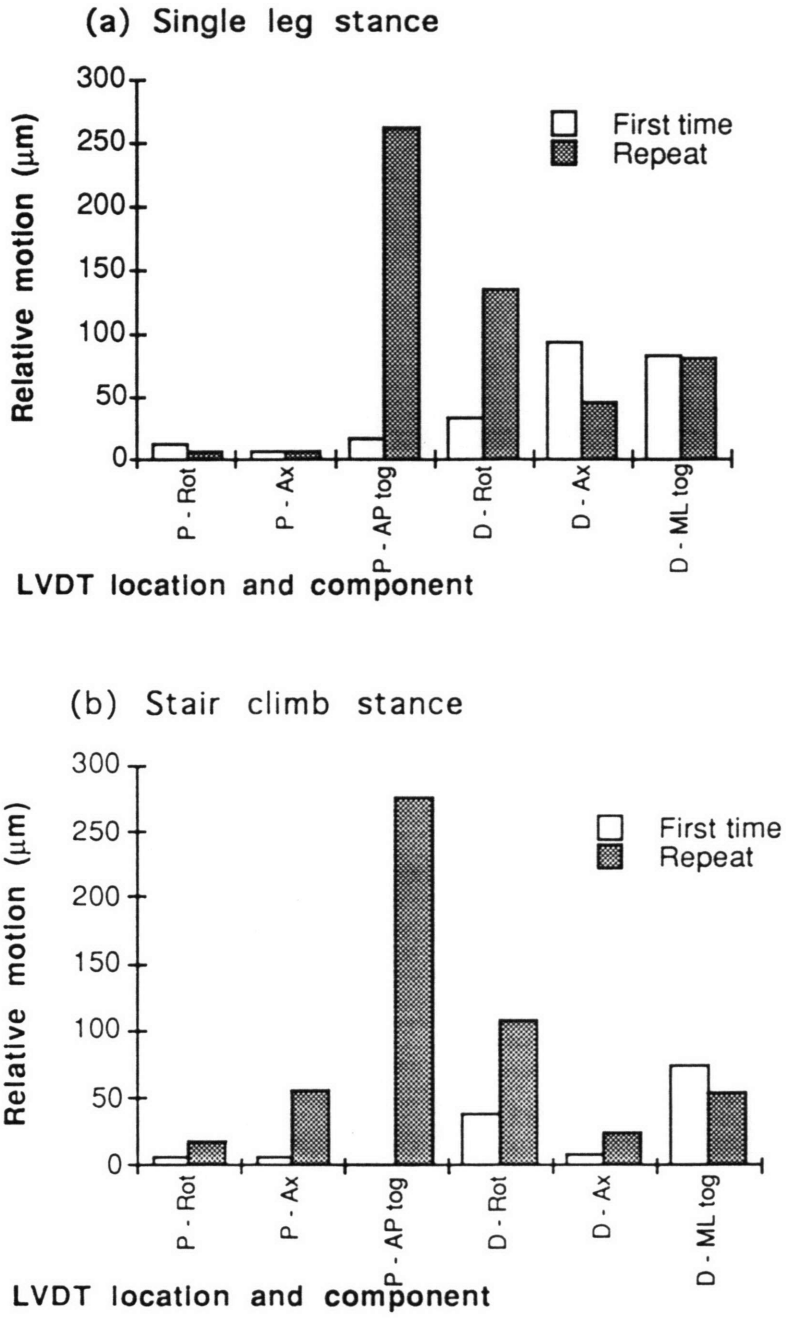

Figure 3.20 - Magnitude of various components of relative motion with (a) single leg loading (650 N BW) and (b) stair climb loading (1000 N) for the repeated test (bone 6, 100% bond).

3.5.1 Local axial surface strain

At the distal level, the FEA predicted little variation in axial strain with different bonding conditions (Figures 3.5c, 3.6c). This was observed in the experiment as well. There was a large discrepancy in the strain magnitudes between the FEA and the experiment, indicating that the modulus for the fiber-reinforced epoxy in the diaphysis of the synthetic bones was much higher than that used for the FEA. The value used in the FEA came from the compressive tests on samples taken from the distal condyles.

At the mid-stem level, there was a significant change in strain magnitude with different bonding conditions. In single leg stance, the strain magnitude decreased significantly at both gauge locations when bonding was increased from 21% to 65% (Figure 3.5b). With further bonding (to 100%) there was little or no change in axial surface strain. In stair climb stance, the same trend was observed at the site of the medial gauge (Figure 3.6b). The strain at posterior-lateral gauge site was compressive and did not change with changes in bonding distribution. All these results compare well with the experimental data, both in magnitude and change with bonding condition. The exception is with full bonding which produced the minimum strain in the FEA (although in single leg stance the strain did not change as the bond was extended beyond 65%). Experimentally, the minimum strain was observed with 65% bonding and the strains typically increased slightly with more distal bonding.

Proximally, the strain varied with different bonding conditions. However, like the mid-stem strains, the change in strain magnitude beyond 65% bonding was minimal. In single leg stance, the anterior-medial strains agree well with the experimental results, except at full bonding. Posteriorly, the FEA and experimental strains are different in sense, but do follow similar trends. The difference in sense (tensile for the FEA and compressive for the experimental) was due to the action of the abductor and the difference in the location of muscle insertion between the FEM and the experiment. In stair climb stance, the posterior

strains were in good agreement with the experimental data, although the same discrepancy with full bonding existed. The anterior-medial strains show the same discrepancy.

As in the experiment, the distal strains were higher in stair climb load than in single leg stance. However, at the mid-stem level the two loading cases produced similar strains and proximally, the strains were higher in single leg stance probably due to the abductor. This also agrees with the experimental observations. The variation in FEA strain along the length of the bone was more prominent in stair climb load than in single leg stance, which had little variation between mid-stem and proximal levels. Again, this was observed in the experiment, although the variation in stair climb load was more dramatic in the FEA.

3.5.2 Axial strain contours and maximal strains

The magnitudes of the maximum strains at the distal contour were much higher in the FEA than in the experiment. This indicates that the epoxy modulus in the diaphysis was probably much higher than the value used in the FEA, which came from the compressive tests of distal condylar samples. However, the trends were comparable; both the experiment and FEA showed no change in distal strain magnitude with a change in bonding condition (Figures 3.9c, 3.10c). This indicates that the distal contour is far enough removed from the stem so that it is not influenced by changes in proximal interface conditions.

For the strain magnitude at the mid-stem, the FEA and experimental results agreed well for 21% and 65% bonding. The trend was similar to that of the axial strains (as would be expected). With more distal bonding the maximum strains decreased, with only a small decrease in strain when bonding was extended distal to 65% (Figures 3.9b, 3.10b). Conversely, the minimum strain occurred at 65% or 81% bonding in the experiment with a small increase at 100% bonding.

At the proximal section, there were some differences between the model and experiment. With stair climb loading, the FEA and experimental strains varied in the same

manner as at the mid-stem section (Figure 3.10a). However, the rate of change in strain from 21% to 65% bonding was magnified in the FEA compared with the measured rate of change. In single leg stance, the abductor force complicated the strain field. The maximum tensile strain from the FEA varied little with bonding condition because of the overwhelming influence of the abductor muscles (Figure 3.9a). The compressive strains, however, followed the pattern that was typical at the mid-stem level. The experimental results were similar for bonding cases up to 65% bonding, after which the strain increased as was typical at the mid-stem level.

As in the experiment, the location of the maximum strains in the FEA changed along the length of the bone (Figures 3.11 and 3.12) and was the most consistent with the loading configuration at the distal level where the influence of the prosthesis was negligible. The bonding condition also slightly influenced the position of the neutral axis, but not to the same degree as the longitudinal position. The locations agreed well with the experimental results, except for the proximal level with stair climb loading for which there was a lot of variation in the experimental data.

3.5.3 Relative motion

In general, as the bonding was extended distally, the relative motion at the distal tip decreased (Figures 3.15, 3.16). The one exception was the medial-lateral toggle LVDT for stair climb - the magnitude of the displacement increased when the bonding was changed from 21% to 65% (Figure 3.16d). Otherwise, the maximum displacement occurred with 21% bonding and, usually the decrease in motion from 21% to 65% bonding was greater than the decrease from 65% to 100%. This agrees well with the general trend observed experimentally. There was no relative motion with 100% bonding in the FEA; this was a boundary condition of the model. Experimentally, the distal tip moved even when fully bonded and, in some cases, moved more than it did for more proximal bonding conditions. Again, this discrepancy between the experimental results and both the model and the

boundary condition imposed by true full bonding suggests that bonding of the distal tip was not adequate.

The motions were typically greater for the stair climb load, particularly the out-of-plane components (rotation and AP toggle) (Figure 3.16b,c). As in the experiment, the rotary and ML toggle motions in single leg stance were minimal (Figures 3.15b,d). However, there was also very little AP toggle in the FEA, consistent with in-plane loading.

For any one target, the motion at the interface predicted by the FEA was 4 to 10 times less than the measured motion of the target. The interface motions calculated using the rigid body techniques were only 1.5 to 3.4 times less than the target motion. This indicates that the FEM prosthesis was better fixed than the experimental prosthesis. Overall, there was not much relative motion of the modeled prosthesis; the greatest motion was only 27 μm (a rotary displacement in stair climb load).

DISCUSSION

4.1 EXPERIMENTAL MODEL

Validation of the experimental model was required before the effects of varying the surface coating distribution could be investigated. The experimental model, consisting of the synthetic bone and cyanoacrylate gel as the bonding agent, was found to be a reasonable model for this study. However, there are limitations and some improvements could be made; these will be outlined in the following sections.

4.1.1 Synthetic bone model

To compare the synthetic bone to fresh bone on a material basis, the modulus of elasticity and coefficient of friction were selected as the most important material properties. The moduli of the polyurethane foam (16.8±3.85 (SD) MPa) and the fiber reinforced epoxy (1.18±0.6 (SD) GPa) were low, although the foam was within the published ranges for human trabecular bone (Table 4.1). It would be desirable, however, to use materials which are more representative of the mean. One alternative to the standard polyurethane foam supplied by Pacific Research Labs, Inc., is Daro foam (Daro Products, Butler, Wisconsin). This polyurethane foam has been shown to have a modulus more comparable with human trabecular bone (Szivek *et al* 1993). In addition, the modulus and strength of the foam are dependent on the composition of the foam mixture and therefore can be controlled. It may be possible to modify the composition of the Pacific Research foam to produce a higher modulus material that more accurately represents human trabecular bone. The modulus of the fiber reinforced epoxy samples was much lower than expected. These samples were taken from the distal condyles and not the diaphysis. The fiber orientation in the condylar region is fairly random, which would explain the variability in the modulus measurement. Furthermore, the fibers in the diaphyseal region may be aligned so as to

increase the modulus. Szivek *et al.* (1991) showed that synthetic bones were only 30% less stiff than cadaveric bones and therefore, a higher modulus than what was measured here would be expected. If the discrepancies between the experimental and FEA distal surface strains are due to a low estimation of the epoxy modulus in the FEM, then the results suggest that the acutal diaphyseal epoxy modulus is higher than that measured by 300% to 450% (Figures 3.9c, 3.10c).

Table 4.1 - Published values for the elastic modulus of human trabecular and cortical bone

Type	Source	n	Mean (MPa)	SD	Range
Trabecular	Lindahl (1976)	32 (male)	55.6	-	1.1 - 139.1
Trabecular	Lindahl (1976)	32 (female)	35.1	-	5.2 - 103.6
Trabecular	Carter (1977)	50	54	37	-
Trabecular	Wixson (1989)	134	152	104	-
Cortical	Reilly (1974)	196	17.1 GPa	3.15 GPa	-

The cyanoacrylate solvent provided the lowest coefficient of friction (0.176) and was selected as the lubricant for two reasons. First, it compares well with published values for the friction coefficient of titanium on bone and titanium on soft tissue. Hayes and Perren (1972) measured the friction characteristics of the interface between a titanium compression plate and a bone segment from a sheep femur. They found an average static friction coefficient of 0.37 ± 0.057 (SD). Rancourt *et al.* (1990) measured the friction coefficients between human trabecular bone and smooth titanium samples. Their measurements ranged from 0.28 to 0.32 and were invariant with displacement rate. Lilley *et al.* (1992) measured the friction coefficient between articulate soft tissue and titanium in a serum bath. This is similar to the long-term *in vivo* situation, in which synovial-like

fibrous tissue surrounds the smooth, unbonded portions of a prosthesis. They found that at low sliding speeds the friction coefficient ranges from 0.14 to 0.20, depending on the applied load. Using solvent as a lubricant produces friction coefficients very close to those measured by Lilley, and similar to the simple bone-metal interface measurements of Hayes and Rancourt. The second reason that the solvent was selected was that it produced frictional properties most closely resembling the finite element model which assumed frictionless contact in unbonded areas. Analytical studies have demonstrated that stresses and micromotion are dependent on the friction coefficient at the interface (Keaveny and Bartel 1993; Rubin *et al.* 1993). In order to approximate the model, the friction coefficient was minimized in the experiment. The friction coefficient between the fiber reinforced epoxy and the prosthesis was not determined. However, the surface of the epoxy is much smoother than the foam and therefore, the friction coefficient of the stem on the epoxy is probably lower.

The gross mechanical behavior of the synthetic bone model has previously been shown to be appropriate for intercomparison studies (Szivek and Gealer 1991). On a material basis, this study confirmed that the model is an adequate representation of fresh cadaveric bone. The model could be improved, however, by replacing the standard foam with a foam with a higher modulus by either using an alternate foam or modifying the foam composition. The effect of increasing the foam modulus only about four times is unclear and may be minimal. Parametric analytical or experimental studies would be required to determine the influence of the foam modulus on the stem mechanics. The modulus of the epoxy component appeared to dependent on location in the bone and fiber orientation. The modulus of the diaphyseal epoxy is probably higher than that measured here, although still less than that of human cortical bone.

4.1.2 Simulated bonding

There are two requirements to get strong, consistent bonding: The first is that there must be adequate contact for the bond to be formed and the second is that the bond must be strong enough to withstand the loading it encounters. The tensile strength test data demonstrated that the cyanoacrylate gel provided adequate strength at the titanium - fiber reinforced epoxy interface, based on the expected interface stresses. During loading, the implant-bone interface was subjected to predominantly shear forces. The tensile strength of the bond was measured but not the shear strength. However, previous tests with a similar cyanoacrylate used to bond a steel-steel interface yielded similar bond strengths in tension and shear (Loctite Corporation, personal communication, 1994).

Although the bond strength of the titanium-foam interface was not determined, the cyanoacrylate gel appeared to be an adequate bonding agent to simulate bony ingrowth or attachment to the foam since portions of the stem had foam still glued to them after removal from the bone. Therefore, the foam was failing before the bond, and the bond strength exceeded the strength of the foam.

Instead of quantitatively determining the contact between the stem and bone using fit and fill measurements, a qualitative assessment of gaps and bone-stem apposition was made using transverse CT scans. Since the gel can only fill gaps of less than 0.5 mm wide, any regions of the stem that were coated with glue but not close enough to the endosteal surface may not have bonded. The transverse CT scans demonstrated that proximally there was complete contact between the foam and the stem, and presumably, full circumferential bonding. Further distally, there was no contact between the distal tip and the bone. Furthermore, the size of the titanium prosthesis is overestimated in CT scans (Robertson *et al.* 1988b) and therefore the gaps are wider than they appear and no bonding can be expected distally. Only the proximal 2/3 of the stem had sufficient contact to guarantee bonding; distal to that point the contact area and, therefore, the opportunity for adequate bonding, was negligible. Furthermore, distally the majority of the endosteal

surface is fiber reinforced epoxy (cortical bone) and the radiographs showed cortical contact only proximal to level 8 (51% of stem length).

The rod-in-tube model eliminated the complex geometry of the synthetic bone model. When there were no gaps between the stem and endosteal surface, the bonding was complete and controlled, as evidenced by the decrease in relative motion with more distal bonding and the extent of the glue residue on the removed rod. This suggests the absence of distal bonding of the prosthesis to the synthetic bone can be attributed to the gaps and not to the bonding ability of the glue.

In summary, the cyanoacrylate gel provided adequate strength and the synthetic bone model permitted bonding and de-bonding. For the proximal two-thirds of the prosthesis there was substantial contact between the stem and the bone and, therefore, consistent bonding. However, the large gaps distal to that point caused incomplete and, probably, inadequate bonding, especially at the tip of the prosthesis. It should be noted that the gaps were due to the geometry of the prosthesis and the reamed canal. Presumably this would occur *in vivo* as well and is unavoidable using the Profile prosthesis and standard surgical techniques with the current synthetic bone geometry. Distal bonding may be obtained artificially by plugging the distal gaps with a filling material, such as bone cement or the polyurethane foam, after implantation. Another option for this study would be to modify the bone geometry to improve the distal fit. However, these are not viable solutions for the *in vivo* situation. In order to get distal bonding *in vivo*, a prosthesis which is designed to have a good distal fit (such as the AML) should be used.

4.2 OPTIMAL SURFACE COATING DISTRIBUTION

Due to the limitations of the experimental model and the small sample size, it is not possible to make any conclusive statements on the optimal surface coating distribution. However, some general trends were observed which suggest the effect that bonding

distribution has on surface strains and the relative motion of the prosthesis. In addition, comparisons with the finite element analysis can be made, although they do not entirely validate the model. With the limitations of the model and sample size in mind, the trends and comparisons are discussed in the following sections.

4.2.1 Effect of bonding distribution on surface strains

The surface strains, both axial and hoop, varied with the bonding distribution in the mid-stem and proximal regions. Excluding the press-fit case, the minimum strain typically occurred with 65% bonding, with an increase or plateau at 81% and 100% bonding. It is counter-intuitive that a fully bonded prosthesis would behave similarly to a proximally bonded prosthesis and does not agree with previous studies (Huiskes *et al.* 1989; Huiskes 1990; Engh *et al.* 1992; Ramamurti 1992). The evaluation of the synthetic bone model suggested that bonding of the distal 1/3 of the prosthesis could not occur because of inadequate contact. Furthermore, the rod-in-tube experiment demonstrated that with more distal coating (i.e., more glue on the rod) there was stronger and more extensive proximal bonding possibly due to the excess glue being forced into the foam in the proximal region. If the same phenomenon was occurring with the prosthesis in the synthetic bone, it is possible that bonding of the distal stem could not occur, but there was better bonding of the proximal regions from the excess glue. As a result, one would expect more load transfer proximally, similar to a prosthesis with 2/3 or more proximal bonding. This was observed with the 81% and 100% bonded cases. Although this explanation is supported by the strain data and supplementary experiments, it is speculation and needs to be confirmed through further testing. Nonetheless, there is strong evidence that controlled distal bonding could not occur; this is further supported by the strain (and relative motion) data.

The maximum axial surface strains in the mid-stem and proximal regions decreased as bonding was increased from 21% to 65% of the stem length. With such limited data it is difficult to estimate the rate of decrease of strain with increased bonding, but it appears that

the decrease was less rapid as the bond was extended more distally. This suggests that the reduction in proximal stress shielding is minimal as the bonding distribution is extended distally beyond a point somewhere between 36% and 65% bonding.

The magnitudes of the maximum strains at the mid-stem level compare well with the results of Engh *et al.* (1992) who measured surface strains of 33%, 80% and 100% coated stems in single leg stance. Proximally, they recorded medial axial strains ranging from -14 to -463 microstrain which is much lower than the maximum proximal compressive strains measured in this study. However, their gauge was located more proximally and the strain they reported was the strain at the rosette location and, therefore, not necessarily the maximum. Furthermore, the synthetic bone is up to 30% less stiff than cadaveric bone (Szivek and Gealer 1991) and therefore higher strains would be expected. Distally, Finlay *et al.* (1991) recorded tensile strains of approximately 1100 microstrain and compressive strains of about 1200 microstrain with embalmed cadaveric bone loaded in single leg stance (but with a lower joint reaction force than in this study). Considering the difference in loading, the maximum distal axial strains recorded with the synthetic bone of around ±1700 microstrain are reasonable. Unfortunately, Engh *et al.* (1992) have not reported their strain data for stair climb loading.

The press-fit cases were difficult to interpret. The main reason is that the prosthesis was not well seated after implantation and hence, settling occurred during the first trial for each load case. Therefore, for a single loading case the prosthesis was positioned differently for each of the two trials (one measuring proximal motion, one measuring distal motion). In order to ensure that the prosthesis is seated, either the stem should be tested for stability before loading (Berzins *et al.* 1993) or it should be subject to pre-condition loading (Walker *et al.* 1987).

The influence of the loading condition was expected. With out-of-plane loading (stair climb) the distal strain magnitudes were much higher than with in-plane loading and the reduction of the proximal strains was more marked. This is consistent with the results

of previous studies (St. Ville *et al.* 1991; Rubin *et al.* 1993). The abductor played a dominant role in the proximal strain distribution in single leg stance and was in part responsible for reducing the degree of proximal strain shielding. The importance of muscle simulation has previously been demonstrated (Finlay *et al.* 1991) in single leg stance and presumably would be important in any loading configuration. If a better comparison between loading cases was desired, then the stair climb configuration should be modified to include the dominant musculature.

The repeated test confirmed that similar loading of the bone and stress transfer to the bone could be achieved after testing, removal and re-insertion of the prosthesis with the same bonding conditions.

Finally, the variation in the location of the maximum strains emphasizes the importance of the strain instrumentation. It is not possible to predict *a priori* the location of the maximum strains, especially proximally, nor is it possible to predict the orientation of the principal strains on a post-arthroplasty femur. Therefore, determination of the maximum strains requires a minimum of three rosettes for each cross-section of interest.

4.2.2 Effect of bonding distribution on relative motion

There was much greater variation in the relative motion measurements than was observed in the strain measurements. There are several possible explanations for the large variability. The most important factor is the sample size. For any one bonding condition, there was only one measurement of relative motion at each level for each bone, whereas there were two measurements of strain. Therefore, the already small sample size was effectively halved for relative motion measurements. Furthermore, the inclusion criteria eliminated obviously erroneous data (due to experimental errors) and further reduced the number of samples.

A secondary source of variation is the inherent sensitivity of micromotion measurements to interface conditions. Unlike surface strains, which are measured

relatively far from the bone-stem interface and, therefore, are less sensitive to small changes in interface conditions, relative motion of the prosthesis with respect to the bone is directly dependent on the interface condition. This has been demonstrated analytically by Rubin *et al.* (1993) who demonstrated that micromotion and interfacial shear stresses were strongly dependent on the coefficient of friction at the interface, but surface strains were not. The dependency of relative motion on interface conditions was also suggested by the results of Ramamurti (1992). The repeated test results for this experiment showed similar surface strains between the original and repeated tests, but significantly different relative motions (Figures 3.18 and 3.19). There are several factors that would influence the interface conditions in this study, including: i) the likelihood that distal bonding did not occur; (ii) the possibility that more complete proximal bonding occurred when there was a greater volume of glue on the prosthesis (i.e., for more distal bonding conditions); and, (iii) the likelihood of slight variations in the position of the prosthesis in the bone between tests. However, with the synthetic bone model, bone geometry and material properties are not as variable as they would be with cadaveric bone. This suggests that despite the limitations of the model, it should produce less variable results for relative motion than would a cadaveric model.

Despite the large variability, some general, but not entirely consistent trends were apparent. Proximally, there was less than 20 μm of target motion for the bonded cases. Engh *et al.* (1992) measured less than 40 μm of interfacial relative motion in areas of porous ingrowth. Distally with the fully bonded rod-in-tube model, the maximum target motion was less than 5 μm. Although both studies show minimal motion, the magnitudes are different. The discrepancy can be attributed to the difference in bonding between the synthetic bone model and the autopsy-retrieved specimens. With the synthetic bone there was complete circumferential bonding proximally, whereas *in vivo* specimens commonly have irregular and incomplete circumferential bonding. Thus the proximal motion measurements are lower limits, which are probably unattainable *in vivo*. There were some

cases with much larger proximal motion, indicating that the prosthesis moved or that the LVDT's and/or bracket was bumped or dislodged. However, the prostheses seemed well bonded proximally as evidenced by the difficulty of removal and by the residue of the foam and glue on the proximal stem. The rod-in-tube model demonstrated that with fully controlled bonding, the rod moved as hypothesized and therefore, the system to measure the motion was functioning well. Nonetheless, more stable LVDT brackets and more stable fixture of the bones to the loading apparatus would prevent some of the experimental errors.

The large relative motions for the first loading of the press-fit stems provided further evidence that the prostheses were not well seated after implantation. After settling, the magnitudes of the motions were comparable to the proximally bonded cases indicating that the prostheses were firmly wedged in the medullary canal.

Distally, the relative motion varied with the bonding condition and usually, the least motion occurred with 81% bonding. With full bonding, there was typically a slight increase in motion although none was expected. If there was full distal bonding, then motions of the same magnitude as the proximal motions would be expected at the distal tip. However, the magnitude of many of the components of distal motion were greater than 20 μm; this can be explained by the apparent absence of distal bonding. The increase in the axial component of the motion from 81% to 100% bonding is more difficult to explain and requires further investigation. It may be due to changes in the interface condition or may simply be an artifact of the small sample size. Nonetheless, for the other three components of motion, there was little change from 81% to 100% bonding. This is consistent with the trend observed for the more proximal bonding conditions, namely that the decrease in motion is less rapid as the bond is extended distally. This suggests that the reduction in distal relative motion is minimal as the bonding distribution is extended distally beyond a point around 65% to 81% bonding. The inverse relation between distal relative motion and

extent of bonding was also demonstrated by Engh *et al.* (1992), although their study did not permit them to predict the rate of change.

It is difficult to compare the uniaxial motion measurements with those of previous studies because (i) the motions measured are target motions, not interface motion; (ii) the target placement is not consistent between studies; and, (iii) relative motion is sensitive to small changes in interface conditions, which include the prosthesis and bone geometry. In addition, the only experimental study to measure micromotion with coated prostheses is that of Engh *et al.* (1992). However, from their data it appears that the prostheses in this study were comparatively more stable. With 33% coating, they measured up to 200 μm of distal relative motion in single leg stance. With 80% coating, the maximum distal motion in single leg stance was approximately 85 μm and when fully coated, the maximum distal motion was about 10 μm. Using the synthetic bone model and the Profile prosthesis, the maximum relative motions of the target (which were shown to overestimate the interface relative motion by up to 3.4 times) averaged less than 60 μm for 36% bonding, and less than 30 μm for 81% bonding.

Generally, the distal axial and rotary components of relative motion were greater when loaded in stair climb stance than single leg stance, although the difference was minimal with distal bonding conditions. Torsional loading has been shown cause much greater motion in press-fit prostheses by numerous authors (Gebauer *et al.* 1989; Nunn *et al.* 1989; Sugiyama *et al.* 1989; Phillips *et al.* 1990; Burke *et al.* 1991; Hayes *et al.* 1992; Berzins *et al.* 1993). However, Engh's data suggest that for bonded prostheses the increase in distal relative motion is not substantial or consistent. Nonetheless, the data from this study suggest that stair climb loading is an important load case to consider because of its effect on the axial and rotational (or tangential) components of relative motion.

Finally, the calculated interface motions for bone 5 illustrated that uni-axial site-specific motion measurements may be adequate for comparisons between bonding conditions, but cannot be used to characterize the motion at the interface.

4.2.3 Comparison with FEA

A secondary goal of this study was to validate the FEM (Ramamurti 1992). Although every attempt was made to approximate the FEM and experimental model, there were some differences which could not easily be eliminated, such as bone geometry. Therefore, a correlation in trends, and not exact magnitudes, was considered sufficient for validation of the FEA.

The trends observed experimentally are general and obviously not statistically significant, and therefore, complete validation of the FEA with these results is not possible. Nonetheless, some indication of the validity of the FEA can be made by comparison with the experimental data. There was generally good agreement between the FEA and the experiment for the trends in surface strain and relative motion. When the differences between the FEM and experimental model (distal constraint, muscle action and material properties) were accounted for, there was good agreement for the surface strain magnitudes. The magnitudes of the relative motion are difficult to compare since the FEA produces interfacial relative motion and the motion of the targets was measured experimentally. However, for bone 5, the calculated interface motions were about three times greater than the FEA motions, indicating that fixation in the experiment was not "ideal". In the FEA, ideal bonding (i.e., zero motion at the bonded interface) is the boundary condition imposed on elements of the prosthesis which contact bone. As demonstrated by these data and those of Engh *et al.* (1992), however, there is some motion, even in bonded regions, and sporadic bonding is more likely than complete, ideal bonding.

The most significant discrepancy between the analytical and experimental data that cannot be attributed to obvious differences between the models (i.e. bone geometry and materials, distal constraint and the location of the muscle force) is the trends of the strain with 81% and 100% coating distributions and the relative motion with 100% coating. The discrepancy is not surprising since the experimental evidence suggests that distal bonding was not occurring; the FEA results further support this claim. The FEA results also confirm that the trends that were inferred by the experimental data (for bonding distributions from 21% to 65%) can be extended to the more distal bonding distributions.

The fact that the magnitudes of the surface strains agree so well illustrates the insensitivity of surface strains to small changes in interface condition, in this case the difference in bone geometry between the analytical and experimental models. Furthermore, both the experiment and model predicted a notable decrease in proximal surface strains when the bonding distribution was extended from proximal to mid-stem levels, where surface strain was used as a relative measure of strain shielding. Ramamurti (1992) used a different indicator for stress shielding, namely the peak von Mises stress for the femoral elements at the level of the lesser trochanter (level 11), and found that the degree of stress shielding was relatively insensitive to the bonding distribution. For a optimization problem, the formulation of the objective function will strongly influence the solution. When a parameter that cannot be measured directly (such as stress shielding) is part of the objective function, then the selection of the indicator for that parameter will also influence the solution. It is likely that the indicator for stress shielding used by Ramamurti is more appropriate than the surface strains, considering that bone resorption is observed clinically on the endosteal, not periosteal, surface and that surface strains appear to be relatively insensitive to small changes in interface conditions. However, surface strain measurements are the best experimental indicator available and, from these data and that of others, are obviously sensitive to gross changes in load transfer. Since stress shielding is the result of

changes in load transfer, surface strains measurements can be used to indicate the degree of stress shielding, although they are not the ideal measure.

4.2.4 The optimization problem

Due to the limitations of the experimental model and the small sample size, it is not possible to make any conclusive statements on the optimal surface coating distribution. Presumably with more samples, and possibly improvements to the model, the data would be less variable and a statistically significant optimum could be determined. Nonetheless, from these data some comments on the procedure and trends can be made.

The optimal surface coating distribution will minimize relative motion and stress shielding. Numerically, this can be represented by an objective function that is composed of a measure of relative motion and a measure of strain shielding. For instance, similar to the methods used by Ramamurti (1992), the peak value of relative motion at the interface and the peak values of tensile and compressive axial surface strains (relative to an intact femur) could be normalized and summed over the two loading conditions to produce the objective function. The bonding distribution with the minimum value for the objective function would therefore be the optimum. This study has all the tools required to solve this problem, although an intact femur would have to be tested in order to quantify the reduction in proximal strain post-arthroplasty. The experimental objective function would differ from that used by Ramamurti in the FEA because (i) the indicator of stress shielding differs between the two; (ii) the loading conditions are different; and, (iii) shear stresses at the bone-stem interface were not measured and therefore, cannot be included in the experimental objective function.

Based on this objective function and the general trends in the experimental data, it qualitatively appears that the optimum surface coating distribution is to coat somewhere between the proximal 65% and 81% of the stem length. A sample optimization is shown in Figure 4.1; it shows the competing trends in proximal stress shielding and distal relative

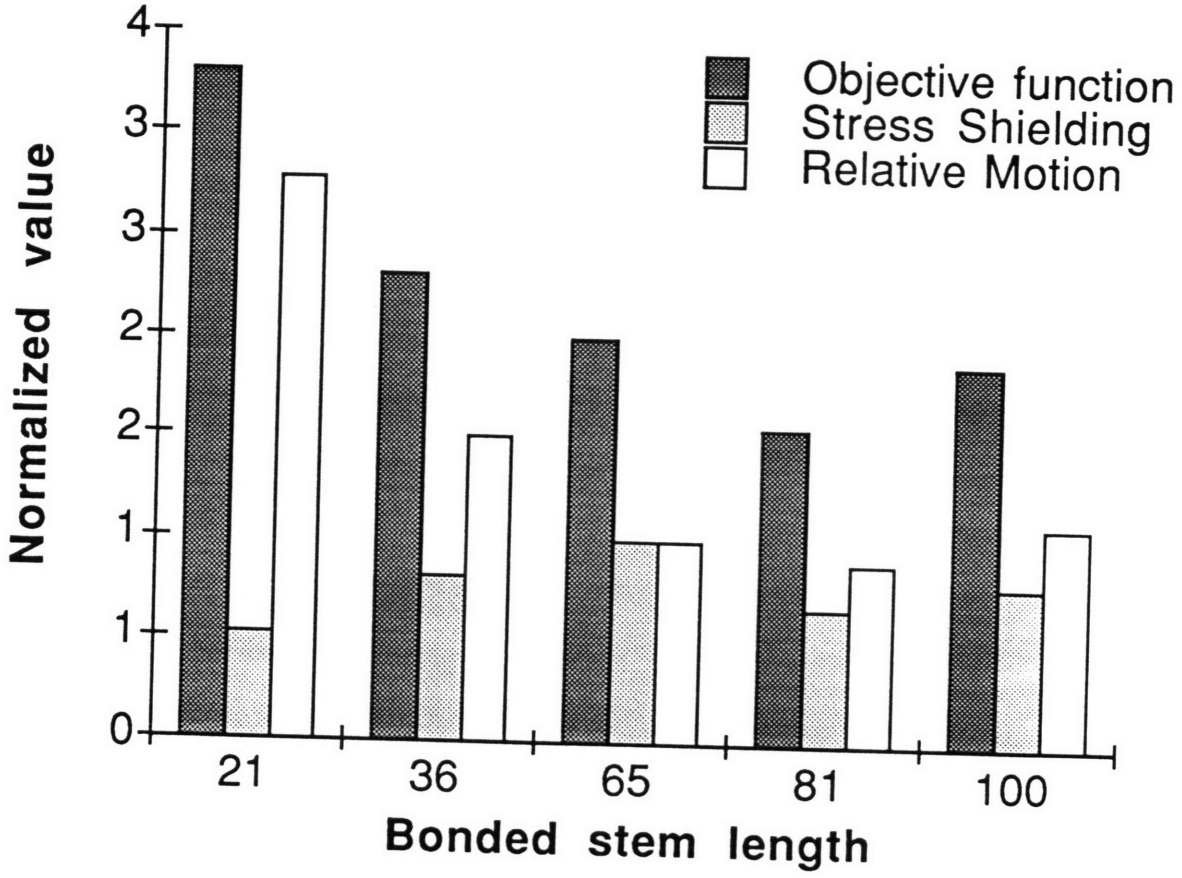

Figure 4.1 - Sample optimization plot showing competing trends of proximal stress shielding and distal relative motion. For the purposes of this example, stress shielding was defined as the expected proximal strain for an intact bone divided by the maximum measured proximal strain. The distal ML toggle motion component was used as a measure of distal relative motion. The average value for the two loading cases was plotted, after normalization to the 65% bonding value. The objective function was simply defined as the sum of stress shielding and relative motion.

motion. The optimal distribution is based on a reasonable compromise between the proximal stress shielding and distal relative motion. The optimization performed by Ramamurti (1992) predicted that coating the proximal 51% of the stem length was optimal. The solutions, however, are very dependent on the formulation of the objective function, as well as the type of prosthesis (geometry and material), the bone anatomy, and the loading conditions. Therefore, this solution is specific to this particular prosthesis, bone geometry and this formulation of the objective function. Reformulation of the objective function or application of these methods to a different prosthesis and/or different bone could result in a different optimal bonding distribution.

It is interesting to note that variations in bonding distribution have a stronger effect on relative motion than on stress shielding (based on the formulation in Figure 4.1). In the finite element analysis, Ramamurti (1992) observed a similar dependency, although their measure of stress shielding was less sensitive to variations in bonding distribution. For patients with cementless THA, thigh pain (probably resulting from distal tip motion) is the most symptomatic and debilitating problem. The results of this study suggest that surface coating distribution is a design variable which can significantly reduce relative motion, with the trade-off being a small increase in stress shielding. Because of its strong influence on relative motion, the surface coating distribution can play an important role in the reduction of thigh pain. However, it's influence on stress shielding cannot be ignored and therefore, an optimization approach is necessary.

Since the bonding distribution was varied in an incremental manner and the only strategy for bonding was to remove (or add) distal coating, it is possible these methods would produce a local minimum in the objective function. However, this strategy is the most common current design trend and other design trends (such as removing coating at high stress regions and adding distal fixation to a proximally coated stem) proved less optimal in the FEA (Ramamurti 1992). To better determine the optimal extent of coating, more distributions within the optimal region could be tested experimentally. However, it

would be more efficient to use these experimental methods and data to validate the FEA and then use the FEA to determine the exact bonding distribution.

CONCLUSIONS AND RECOMMENDATIONS

The objective of this study was to develop and apply methods to experimentally determine the optimal surface coating distribution for a femoral prosthesis. The coating distribution has previously been shown to be an important design parameter that, if optimized, could potentially reduce some of the clinical problems with cementless prostheses by minimizing the likelihood of failure at the bone-prosthesis interface. However, there is not a clear consensus on the optimal distribution. This study was, therefore, motivated by the need to experimentally address the optimization problem and to validate the finite element solution of the same problem.

Although the small sample size and limitations of the experimental model prevent a statistically significant solution to the optimization problem, the data suggest certain trends and the following conclusions and recommendations are made:

1) The experimental model, consisting of the synthetic bone and cyanoacrylate to simulate bonding, was found to a reasonable model for this study. The synthetic bone, however, is suitable only for intercomparison studies because it is more flexible than real bone; the synthetic bone could be improved to better approximate real bone by using a higher modulus polyurethane foam and fiber reinforced epoxy. The friction between the unbonded prosthesis and synthetic bone was similar to the friction that occurs *in vivo*.

The cyanoacrylate provided adequate strength in bonded areas. However, it appears that bonding could not occur in certain areas, particularly on the distal 1/3 of the stem, because of large gaps between the stem and bone. These gaps were due to the geometries of the bone and prosthesis and presumably would occur *in vivo* as well. In order to get distal bonding in this experiment, the gaps could be artificially plugged using a filling material such as bone cement or the foam. Otherwise, the anatomy of the synthetic bone could be modified to improve the distal fit of the Profile stem. In order to

get a good distal fit *in vivo*, a prosthesis that was designed with that objective (such as the AML) would have to be used.

2) The proximal and mid-stem surface strains varied with bonding distribution. The maximal axial surface strains tended to decrease as the extent of bonding was increased to 65% of the stem length. This corresponds to an increase in stress shielding with more distal bonding. The rate of decrease in strain was less rapid as the bond was extended distally, sugggesting that the reduction in proximal stress shielding is minimal as the bonding distribution is extended distally beyond a point somewhere between 36% and 65% bonding. Slight increases in the the strain with 81% and 100% bonding can probably be attributed to the lack of distal bonding and possibly, better proximal bonding. However, this is speculation and requires further testing for confirmation. The press-fit stem was not well seated after implantation and therefore, the two trials for a single load case produced different results. In the future, the press-fit stems should be tested for initial stability before testing.

In order to reduce the variability, more tests should be conducted. Completion of the Latin square would not only increase the sample size, but would permit statistical determination of the variability introduced by using different bones and by the test order.

3) Proximally, in the bonded areas the relative motions between the targets and the bones were typically less than 20 μm. Distally, the motion decreased with more distal bonding distributions, with the least motion occurring with 81% bonding. The decrease in relative motion was less rapid as the bond was extended distally, suggesting that the reduction in distal relative motion is minimal as the bonding distribution is extended distally beyond between 65% and 81% of the stem length. With 100% bonding, some relatively large motions were recorded which is consistent with the absence of distal

bonding. Settling of the press-fit prostheses was evident during the initial loading. Calculated interface motions were 1.5 to 3.4 times less than target motions.

The relative motion data were much more variable than the strain data due to a smaller sample size and the inherent sensitivity of the prosthesis motion to interface conditions. To increase the sample size, more tests with more bones need to be conducted. To address the sensitivity, and to prevent data from being lost to experimental errors, more stable LVDT brackets and more stable fixture of the bones to the loading apparatus would be beneficial.

4) There was generally good agreement between the trends observed experimentally and those predicted by the finite element analysis. As well, there was surprisingly good agreement in the magnitudes of the surface strains. The most obvious discrepancies between the FEA and experiment were the differences in strain and motion with full bonding. This is not surprising since all the experimental evidence suggested that distal bonding was not occuring; the FEA further supported this claim. The finite element analyses also demonstrated that the trends predicted experimentally with proximal distributions can be extended to more distal bonding distributions.

5) Due to the small sample size and limitations of the experimental model, a conclusive statement on the optimal bonding distribution could not be made. With further tests and improvements to the model, a statistically significant optimal bonding distribution could be determined. The methods of this study provide all the tools necessary to solve the optimization problem. Qualitatively, the trends in the data suggest that the optimal distribution (which minimizes the combination of stress shielding and relative motion) is to coat somewhere between the proximal 65% and 81% of the stem length.

These conclusions support many design principles for cementless prostheses that are based on clinical, analytical and experimental studies. This study is unique, however, in (i) its development of an experimental model for studying the variation in surface coating distribution; and in (ii) its experimental demonstration of the complicated interaction between relative motion and surface strains with variation in bonding distribution. The conflicting effects of varying the surface coating distribution on these two parameters confirm that an optimization approach is necessary to determine the most suitable coating distribution, where the optimal solution corresponds to a compromise between the parameters.

BIBLIOGRAPHY

Andriacchi, T. P., Andersson, B. J., Fermier, R. W., Stern, D. and Galante, J. O. (1980) A study of lower-limb mechanics during stair-climbing. *J Bone Joint Surg [Am]* **62,** 749-757.

Berzins, A., Sumner, D. R., Andriacchi, T. P. and Galante, J. O. (1993) Stem curvature and load angle influence the initial relative bone-implant motion of cementless femoral stems. *J. Orthopaedic Research* **11,** 758-769.

Bobyn, J. D., Pilliar, R. M., Binnington, A. G. and Szivek, J. A. (1987) The effect of proximally and fully porous-coated canine hip stem design on bone modeling. *J. Orthop. Res.* **5,** 393-408.

Borchers, R. E. and Gibson, L. J. (1992) Effects of storage and heating on the mechanical properties of bovine trabecular bone. *38th Annual Meeting, Orthopaedic Research Society* 554.

Burke, D. W., O'Connor, D. O., Zalenski, E. B., Jasty, M. and Harris, W. H. (1991) Micromotion of cemented and uncemented femoral components. *J. Bone and Joint Surgery* **73-B,** 33-37.

Callaghan, J. J., Dysart, S. H. and Savory, C. G. (1988) The uncemented porous-coated anatomic total hip prosthesis. Two-year results of a prospective consecutive series. *J Bone Joint Surg [Am]* **70,** 337-46.

Cameron, H. U., Pilliar, R. M., Yoneda, B. T. and Macnab, I. (1973) The effect of movement on the bonding of porous metal to bone. *J Biomed Mat Res* **7,** 301-311.

Carter, D. R., Vasu, R., Spengler, D. M. and Dueland, R. T. (1981) Stress fields in the unplated and plated canine femur calculated from *in vivo* strain measurements. *J Biomech* **14,** 63-70.

Carter, D. R. and Hayes, W. C. (1977) The compressive behavior of bone as a two-phase porous structure.*J Bone Joint Surg [Am]* **59,** 954-962.

Chandler, H. P., Reineck, F. T., Wixson, R. L. and McCarthy, F. C. (1981) Total hip replacement in patients younger than thirty years old. *J Bone Joint Surg [Am]* **63,** 1426-1434.

Cheal, E. J., Spector, M. and Hayes, W. C. (1992) Role of loads and prosthesis material properties on the mechanics of the proximal femur after total hip arthroplasty. *J. Orthop. Res.* **10,** 405-422.

Cochran, W. G. and Cox, G. M. (1957) *Experimental Designs*. John Wiley & Sons, Inc., New York.

Collis, D. K. (1984) Cemented total hip replacement in patients who are less than fifty years old. *J Bone Joint Surg [Am]* **66,** 353-9.

Crowninshield, R. D., Pederson, D. R. and Brand, R. A. (1980) A measurement of proximal femur strain with total hip arthroplasty. *J Biomech Eng* **102,** 230-233.

Dally, J. W. and Riley, W. F. (1978) *Experimental Stress Analysis*. McGraw-Hill, New York.

Diegel, P. D., Daniels, A. U. and Dunn, H. K. (1989) Initial effect of collarless stem stiffness on femoral bone strain. *J Arthroplasty* **4,** 173-8.

Djerf, K. and Gillquist, J. (1987) Calcar unloading after hip replacement. A cadaver study of femoral stem designs. *Acta Orthop Scand* **58,** 97-103.

Dorr, L. D., Takei, G. K. and Conaty, J. P. (1983) Total hip arthroplasties in patients less than forty-five years old. *J Bone Joint Surg [Am]* **65,** 474-9.

Engelhardt, J. A. and Saha, S. (1988) Effect of femoral component section modulus on the stress distribution in the proximal human femur. *Med. & Bio. Eng. Comput.* **26,** 38-45.

Engh, C. A., O'Connor, D., Jasty, M., McGovern, T. F., Bobyn, J. D. and Harris, W. H. (1992) Quantification of implant micromotion, strain shielding, and bone resorption with porous coated Anatomic Medullary Locking femoral prostheses. *Clin. Orthop.* **285,** 13-29.

Engh, C. A. and Bobyn, J. D. (1988) The influence of stem size and extent of porous coating on femoral bone resorption after primary cementless hip arthroplasty. *Clin. Orthop.* **231,** 7-28.

Engh, C. A., Bobyn, J. D. and Glassman, A. H. (1987) Porous-coated hip replacement. The factors governing bone ingrowth, stress shielding, and clinical results. *J. Bone Joint Surg. [Br]* **69,** 45-55.

Evans, F. G. (1973) Preservation effects. *Mechanical properties of bone* (Edited by Burdi, A. R.), pp. CC Thomas, Springfield.

Field, R. E. and Rushton, N. (1989) Proximal femoral surface strain gauge analysis of a new epiphyseal prosthesis. *J. Biomed. Eng.* **11,** 123-129.

Finlay, J. B., Chess, D. G., Hardie, W. R., Rorabeck, C. H. and Bourne, R. B. (1991) An evaluation of three loading configurations for the in vitro testing of femoral strains in total hip arthroplasty. *J. Orthop. Res.* **9,** 749-759.

Finlay, J. B., Rorabeck, C. H., Bourne, R. B. and Tew, W. M. (1989) In vitro analysis of proximal femoral strains using PCA femoral implants and a hip-abbductor muscle simulator. *The Journal of Arthroplasty* **4,** 335-345.

Gebauer, D., Refior, H. J. and Haake, M. (1989) Micromotions in the primary fixation of cementless femoral stem prostheses. *Arch. Orthop. Trauma Surg.* **108,** 300-307.

Gross, T. S., McLeod, K. J. and Rubin, C. T. (1992) Characterizing bone strain distributions in vivo using three triple rosette strain gages. *J. Biomechanics* **25,** 1081-1087.

Harris, W. H. and Sledge, C. B. (1990) Total hip and total knee replacement (Second of Two Parts). *N. Engl. J. Med.* **323,** 801-807.

Hayes, D. E. E., Jr., Bargar, W. L., Paul, H. A. and Taylor, J. K. (1992a) Three dimensional micromotion of femoral prostheses. *Orthopaedic Research Society* **17,** 380.

Hayes, D. E. E., Jr., Sharkey, N. A., Yerby, S. A. and Paul, H. A. (1992b) Implant stability and design: a correlation analysis using interfacial micromotions and fit, fill, and gap data. *Orthopaedic Research Society* **17,** 383.

Hayes, W. C. and Perren, S. M. (1972) Plate-bone friction in the compression fixation of fractures. *Clinical Orthopaedics* **89,** 236-240.

Hirano, S. K. (1986) Fit, strains and micromotion of a press-fit hip implant. *Massachusetts Institute of Technology S.M. Thesis*

Huiskes, R. (1990) The various stress patterns of press-fit, ingrown, and cemented femoral stems. *Clin. Orthop.* **261,** 27-38.

Huiskes, R., Weinans, H. and Dalstra, M. (1989) Adaptive bone remodeling and biomechanical design considerations for noncemented total hip arthroplasty. *Orthopedics* **12,** 1255-1267.

Jasty, M., Krushell, R., Zalenski, E., O'Connor, D., Sedlacek, R. and Harris, W. (1993) The contribution of the nonporous distal stem to the stability of proximally porous-coated canine femoral components. *J. Arthroplasty* **8,** 33-41.

Kavanagh, B. F., Ilstrup, D. M. and Fitzgerald, R. H. J. (1985) Revision total hip arthroplasty. *J Bone Joint Surg [Am]* **67,** 517-26.

Keaveny, T. M. and Bartel, D. L. (1993) Effects of porous coating and collar support on early load transfer for a cementless hip prosthesis. *J. Biomechanics* **26,** 1205-1216.

Lilley, P., Walker, P. and Blunn, G. (1992) Wear of titanium by soft tissue. *4th World Biomaterials Congress* 277.

Lindahl, O. (1976) Mechanical properties of dried defatted spongy bone. *Acta Orthop. Scand.* **47**, 11-19.

Lissner, H. R. and Roberts, V. L. (1966) Evaluation of skeletal impacts of human cadavers. *Studies on the anatomy and function of bone and joints* (Edited by Evans, F. G.), pp. Springer-Verlag, New York.

Longo, J. A., McTighe, T., Koeneman, J. B. and Gealer, R. L. (1992) Torsional stability of uncemented revision hip stems. *38th Annual Meeting, Orthopaedic Research Society* 308.

Lord, G. and Bancel, P. (1983) The madreporic cementless total hip arthroplasty. New experimental data and a seven-year clinical follow-up study. *Clin Orthop* **176,** 67-76.

Maistrelli, G., Fornasier, V., Binnington, A., McKenzie, K., Sessa, V. and Harrington, I. (1991) Effect of stem modulus in a total hip arthroplasty model. *J. Bone and Joint Surg.* **73-B,** 43-46.

Manley, M. T., Stern, L. S., Kotzar, G. and Stulberg, B. N. (1987) Femoral component loosening in hip arthroplasty. Cadaver study of subsidence and hoop strain. *Acta Orthop Scand* **58,** 485-90.

Maric, Z. and Karpman, R. P. (1992) Early failure of noncemented porous coated anatomic total hip arthroplasty. *Clin. Orthop. Rel. Res.* **278,** 116-120.

McElhaney, J., Fogle, J., Byars, E. and Weaver, G. (1964) Effect of embalming on the mechanical properties of beef bone. *Journal of Applied Physiology* **19,** 1234-1236.

McLeish, R. D. and Charnley, J. (1970) Abduction in the one-legged stance. *J. Biomechanics* **3,** 191-209.

Nunn, D., Freman, M. A. R., Tanner, K. E. and Bonfield, W. (1989) Torsional stability of the femoral component of hip arthroplasty. Response to an anteriorly applied load. *J. Bone joint surgery* **71-B,** 452-455.

O'Connor, D. O., Burke, D. W., Sedlacek, R. C. and Harris, W. H. (1991) What effect does a collar have on reducing proximal cement strains in a cemented femoral total hip replacement in both gait and stairclimbing? *17th annual meeting of the Society for Biomaterials* 206.

Oh, I. and Harris, W. H. (1978) Proximal strain distribution in the loaded femur. An in vitro comparison of the distributions in the intact femur and after insertion of different hip-replacement femoral components. *J Bone Joint Surg* **60A,** 75-85.

Phillips, T. W., Messieh, S. S. and McDonald, P. D. (1990) Femoral stem fixation in hip replacement. *J. Bone and Joint Surg.* **72-B,** 431-434.

Pilliar, R. M., Lee, J. M. and Maniatopoulos, C. (1986) Observations on the effect of movement on bone ingrowth into porous-surfaced implants. *Clin. Orthop. Rel. Res.* **208,** 108-113.

Ramamurti, B. S. (1992) Optimization of porous coating distribution on a femoral prosthesis in hip arthroplasty. *Boston University M.S. Thesis.*

Ranawat, C. S., Atkinson, R. E., Salvati, E. A. and Wilson, P. D. J. (1984) Conventional total hip arthroplasty for degenerative joint disease in patients between the ages of forty and sixty years. *J Bone Joint Surg [Am]* **66,** 745-52.

Rancourt, D., Shirazi-Adl, A. and Drouin, G. (1990) Friction properies of the interface between porous-srufaced metals and tibial cancellous bone. *J. Biomedical Materials Research* **24,** 1503-1519.

Reilly, D. T., Burstein, A. H. and Frankel, V. H. (1974) The elastic modulus for bone. *J. Biomechanics* **7,** 271-275.

Robertson, D. D., Walker, P. S., Hirano, S. K., Zhou, X. M., Granholm, J. W. and Poss, R. (1988a) Improving the fit of press-fit stems. *Clin. Orthop. and Rel. Res.* **228,** 134-140.

Robertson, D. D., Weiss, P. J., Fishman, E. K., Magid, D. and Walker, P. S. (1988b) Evaluation of CT techniques for reducing artifacts in the presence of metallic orthopedic implants. *Journal of computer assisted tomography* **12,** 236-241.

Rohlmann, A., Mossner, U., Bergman, G. and Kolbel, R. (1983) Finite-element-analysis and experimental investigation in a femur with hip endoprosthesis. *J Biomech* **16,** 727-742.

Rothman, R. H. and Cohn, J. C. (1990) Cemented versus cementless total hip arthroplasty. *Clin. Orthop. and Rel. Res.* **254,** 153-169.

Rubin, C. T. and Lanyon, L. E. (1982) Limb mechanics as a function of speed and gait: A study of functional strains in the radius and tibia of horse and dog. *J. Experimental Biol.* **101,** 187-211.

Rubin, P. J., Rakotomanana, R. L., Leyvraz, P. F., Zysset, P. K., Curnier, A. and Heegaard, J. H. (1993) Frictional interface micromotions and anisotropic stress distribution in a femoral total hip component. *J. Biomechanics* **26,** 725 - 739.

Schneider, E., Kinast, C., Eulenberger, J., Wyder, D., Eskilsson, G. and Perren, S. M. (1989) A comparative study of the initial stability of cementless hip prostheses. *Clin Orthop* **248,** 200-9.

Sedlin, E. D. (1965) A rheological model for cortical bone: a study of the physical properties of human femoral samples. *Acta Orthop Scand Suppl* **83,** 1.

Soballe, K., Hansen, E. S., Rasmussen, H. B., Jorgensen, P. H. and Bunger, C. (1992) Tissue ingrowth into titanium and hydroxyapatite-coated implants during stable and unstable mechanical conditions. *J. Orthop. Res.* **10,** 285-299.

St. Ville, J. A., Ecker, J. A., Winget, J. M. and Berghauer, M. H. (1991) The anatomy of midthigh pain after total hip arthroplasty. *Johns Hopkins APL Technical Digest* **12,** 198-218.

Stauffer, R. N. (1982) Ten year follow-up study of total hip replacement with particular reference to roentgenographic loosening of the components. *J Bone Joint Surg [Am]* **64-A,** 983-990.

Sugiyama, H., Whiteside, L. A. and Kaiser, A. D. (1989) Examination of rotational fixation of the femoral component in total hip arthroplasty. A mechanical study of micromovement and acoustic emission. *Clin Orthop* **249,** 122-8.

Sutherland, C. J., Wilde, S. H., Borden, L. S. and Marks, K. E. (1982) A ten year follow up of 100 consecutive Muller curved-stem total hip arthroplasties. *J Bone Joint Surg* **64A,** 970.

Szivek, J. A., Thomas, M. and Benjamin, J. B.(1993) Characterization of selected mechanical properties of a synthetic foam as a model for human cancellous bone. *Submitted to J Applied Biomaterials.*

Szivek, J. A. and Gealer, R. L. (1991) Comparison of the deformation response of synthetic and cadaveric femora during simulated one-legged stance. *J. Applied Biomaterials* **2,** 277-280.

Turner, T. M., Sumner, D. R., Urban, R. M., Rivero, D. P. and Galante, J. O. (1986) A comparative study of porous coatings in a weight-bearing total hip-arthroplasty model. *J. Bone Joint Surg. [Am]* **68,** 1396-1409.

Veldpaus, F. E., Woltring, H. J. and Dortmans, L. J. M. G. (1988) A least-squares algorithm for the equiform transformation from spatial marker co-ordinates. *J. Biomechanics* **21,** 45-54.

Walker, P. S., Schneeweis, D., Murphy, S. and Nelson, P. (1987) Strains and micromotions of press-fit femoral stem prostheses. *J Biomech* **20,** 693-702.

Whiteside, L. A. and Easley, J. C. (1989) The effect of collar and distal stem fixation on on micromotion of the femoral stem in uncemented total hip arthroplasty. *Clinical Orthop. and Rel. Res.* **239,** 145-153.

Wixson, R. L., Elasky, N. and Lewis, J. (1989) Cancellous bone material properties in osteoarthritic and rhematoid total knee patients. *J. Orthop. Res.* **7,** 885-892.

Wright, T. M. and Hayes, W. C. (1979) Technical note: Strain gage application on compact bone. *J. Biomech.* **12,** 471-475.